U.S. Department
of Transportation
**Federal Railroad
Administration**

A Review of Rail Behavior Under Wheel/Rail Impact Loading

Office of Research and
Development
Washington DC 20590

D. R. Ahlbeck

Batelle Columbus Laboratories
505 King Avenue
Columbus, Ohio 43201-2693

DOT-FRA-ORD-86-01
DOT-TSC-FRA-85-5

April 1986
Final Report

This document is available to the Public through the National Technical Information Service, Springfield, Virginia 22161.

NOTICE

This document is disseminated under the sponsorship of the Department of Transportation in the interest of information exchange. The United States Government assumes no liability for its contents or use thereof.

NOTICE

The United States Government does not endorse products of manufacturers. Trade of manufacturers'names appear herein solely because they are considered essential to the object of this report.

Technical Report Documentation Page

1. Report No.	2. Government Accession No.	3. Recipient's Catalog No.
DOT-FRA-ORD-86-01		

4. Title and Subtitle	5. Report Date
A REVIEW OF RAIL BEHAVIOR UNDER WHEEL/RAIL IMPACT LOADING	April 1986
	6. Performing Organization Code: TSC/DTS-73
7. Author(s): D.R. Ahlbeck	8. Performing Organization Report No.: DOT-TSC-FRA-85-5
9. Performing Organization Name and Address: Batelle Columbus Laboratories, 505 King Avenue, Columbus, OH 43201-2693*	10. Work Unit No. (TRAIS): RR619/R6654
	11. Contract or Grant No.
12. Sponsoring Agency Name and Address: U.S. Department of Transportation, Federal Railroad Administration, Office of Research and Development, Washington, DC 20590	13. Type of Report and Period Covered: Final Report, January - March 1984
	14. Sponsoring Agency Code: RRS-31

15. Supplementary Notes: Under Contract to: U.S. Department of Transportation, Research and Special Programs Administration, Transportation Systems Center, Cambridge, MA 02142

16. Abstract

This report discusses several studies involving factors that significantly affect rail life, particularly wheel impact loads. Parameters that characterize the effect of wheel impact loads on rail behavior are examined in terms of system variables such as geometry, material properties, loads, and track conditions that affect stresses which in turn control the mechanism, probability, and mode of failure. Quantitative descriptions of wheel/rail load characteristics typically encountered were obtained from a review of the literature and results from recent laboratory and field measurements.

17. Key Words	18. Distribution Statement
Impact Loads, Surface Geometry, Rail Joints, Wheel Flats, Rail Surface Profiles	DOCUMENT IS AVAILABLE TO THE PUBLIC THROUGH THE NATIONAL TECHNICAL INFORMATION SERVICE, SPRINGFIELD, VIRGINIA 22161

19. Security Classif. (of this report)	20. Security Classif. (of this page)	21. No. of Pages	22. Price
UNCLASSIFIED	UNCLASSIFIED	102	

Form DOT F 1700.7 (8-72) Reproduction of completed page authorized

PREFACE

The research reported herein combines portions of several studies sponsored by the U.S. Department of Transportation's Federal Railroad Administration (DOT/FRA). Two of these programs that were managed by the FRA/Office of Research and Development (ORD) and the Transportation Systems Center (DOT/TSC) of Cambridge, MA, the "Characterization of Wheel/Rail Loads" and "Analysis of Service Stresses in Rails", were both conducted by Battelle's Columbus Laboratories. More recent work on impact loads has been conducted under Development of Safety Criteria for Evaluating Concrete Tie Track in the Northeast Corridor for the DOT/FRA Office of Research and Development.

Special thanks are given to Dr. Oscar Orringer of DOT/TSC and to Mr. Howard Moody of DOT/FRA for their contributions and suggestions over the course of these studies. Thanks also to Robert Prause, Dr. S.G. Sampath and Harold Harrison for their contributions and encouragement as project managers for Battelle.

METRIC CONVERSION FACTORS

Approximate Conversions to Metric Measures

Symbol	When You Know	Multiply by	To Find	Symbol
		LENGTH		
in	inches	*2.5	centimeters	cm
ft	feet	30	centimeters	cm
yd	yards	0.9	meters	m
mi	miles	1.6	kilometers	km
		AREA		
in^2	square inches	6.5	square centimeters	cm^2
ft^2	square feet	0.09	square meters	m^2
yd^2	square yards	0.8	square meters	m^2
mi^2	square miles	2.6	square kilometers	km^2
	acres	0.4	hectares	ha
		MASS (weight)		
oz	ounces	28	grams	g
lb	pounds	0.45	kilograms	kg
	short tons (2000 lb)	0.9	tonnes	t
		VOLUME		
tsp	teaspoons	5	milliliters	ml
Tbsp	tablespoons	16	milliliters	ml
fl oz	fluid ounces	30	milliliters	ml
c	cups	0.24	liters	l
pt	pints	0.47	liters	l
qt	quarts	0.95	liters	l
gal	gallons	3.8	liters	l
ft^3	cubic feet	0.03	cubic meters	m^3
yd^3	cubic yards	0.76	cubic meters	m^3
		TEMPERATURE (exact)		
°F	Fahrenheit temperature	5/9 (after subtracting 32)	Celsius temperature	°C

*1 in. = 2.54 cm (exactly). For other exact conversions and more detail tables see NBS Misc. Publ. 286, Units of Weight and Measures. Price $2.25 SD Catalog No. C13 10 286.

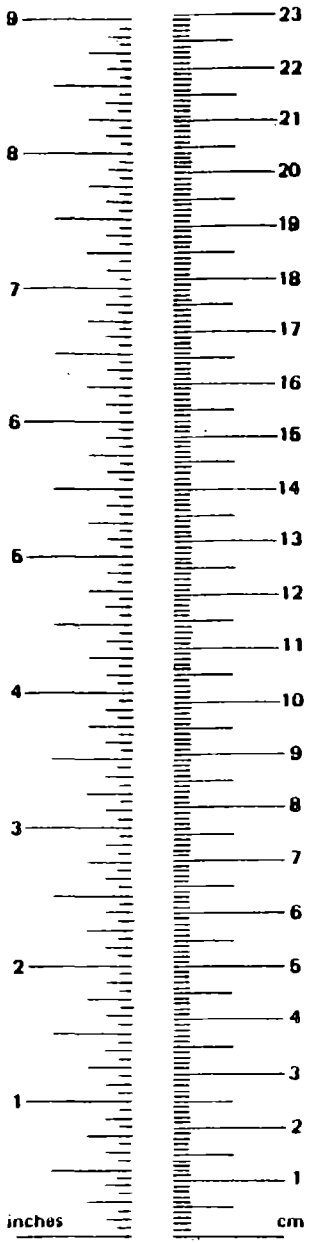

Approximate Conversions from Metric Measures

Symbol	When You Know	Multiply by	To Find	Symbol
		LENGTH		
mm	millimeters	0.04	inches	in
cm	centimeters	0.4	inches	in
m	meters	3.3	feet	ft
m	meters	1.1	yards	yd
km	kilometers	0.6	miles	mi
		AREA		
cm^2	square centimeters	0.16	square inches	in^2
m^2	square meters	1.2	square yards	yd^2
km^2	square kilometers	0.4	square miles	mi^2
ha	hectares (10,000 m^2)	2.5	acres	
		MASS (weight)		
g	grams	0.035	ounces	oz
kg	kilograms	2.2	pounds	lb
t	tonnes (1000 kg)	1.1	short tons	
		VOLUME		
ml	milliliters	0.03	fluid ounces	fl oz
l	liters	2.1	pints	pt
l	liters	1.06	quarts	qt
l	liters	0.26	gallons	gal
m^3	cubic meters	36	cubic feet	ft^3
m^3	cubic meters	1.3	cubic yards	yd^3
		TEMPERATURE (exact)		
°C	Celsius temperature	9/5 (then add 32)	Fahrenheit temperature	°F

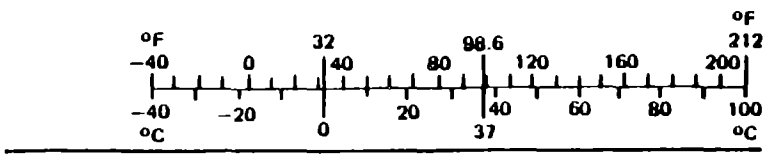

TABLE OF CONTENTS

LIST OF FIGURES

LIST OF FIGURES (CONT.)

LIST OF FIGURES (CONT.)

LIST OF TABLES

1. INTRODUCTION

In recognition of the need for improved track standards, the Federal Railroad Administration's Office of Research and Development (ORD) has been promoting research pertaining to better methods to evaluate and upgrade the safety and serviceability of railroad track. Such an objective has also been pursued by the Transportation Systems Center (TSC) for the FRA/ORD through participation in several studies, including some relating to rail integrity. These latter studies have included efforts to identify the factors that significantly affect rail life and to subsequently develop appropriate analytical and experimental models from which ways of reducing damage can be inferred and subsequently verified in field tests. This report discusses wheel impact loads, a factor affecting rail life that has been the subject of several studies.

The first step toward identifying causes of degradation of rails is to define the system variables which include geometry, material properties, loads, and track conditions, that is, those that affect stresses which in turn control the mechanism, probability, and mode of failure. A research project titled "Analysis of Services Stresses in Rails" was conducted at Battelle Laboratories toward analytically quantifying the track environment and fatigue damage in rails. This report is based on a portion of the work carried out during the course of the project. The subject of this report is the effects of parameters that characterize the effect of wheel impact loads on rail behavior. Quantitative descriptions of wheel/rail load characteristics typically encountered were obtained from a review of the literature and results from recent laboratory and field measurements.

Impact loads of wheels on the rail result primarily from anomalies in the running surface geometry of either the wheel or the rail. These are typically wheel flats, runout or surface spall on the wheel tread, or shelling, weld defects, crushed head, engine burns, or other defects of the rail running surface. Rail joints provide a special case of wheel/rail impact loads due to the joint gap, mismatch of the rail running surfaces and the gage face, the lower vertical track stiffness near the joint, and the tendency for the surface geometry to become "dipped" at the joint due to differential settlement. Impact loads also occur at special trackwork such as switch frogs and points, and crossings; however, sometimes these special structures are fabricated of high-strength

manganese steel and represent a special case. Impact loads can also result from gross dynamic misbehavior of the rail vehicle such as spring groups of a loaded freight car going solid during severe bounce response, or hard contact with side bearings during "rock 'n' roll". The two most important sources of impact loads, however, are wheel flats and rail joints.

The following sections of the report contain discussions about various aspects of impact loads on rails in the light of laboratory and field experiments and computer-based models.

2. BACKGROUND

2.1 RAIL JOINTS

Interest in defining impact loads at rail joints predates the availability of a suitable measurement system. The development of strain gage technology provided the needed capability. Measurements of joint impact loads from strain-gaged tie plates were taken during American Railway Engineering Association (AREA) tests on the Chicago and North Western Railway during the early 1950s[1]. It has been the work of British Rail, both in measurements and analysis, dating from the mid-1960s that has provided the best definition of rail joint impact loads.

Gilchrist[2] of British Rail has suggested that dipped rail joints form the most serious type of vertical track irregularity due to the repeated impact loading. A survey of data on rail joint loading conditions was performed by Prause and Harrison[3] in conjunction with an investigation of the mechanics of joint deterioration. This study summarized the findings of Jenkins, et al.[4] of British Rail which indicated two primary modes of dynamic loading to occur at rail joints. The first impact force, called the P_1 force peak, results from the wheel impacting the end of the rail onto which it is running. This P_1 force occurs 1/4 to 1/2 millisecond after the wheel crosses the gap in the rail ends. The second load impulse, called P_2, occurs 5 to 10 milliseconds later in the vicinity of the first running-on tie. The P_1 force has substantial high-frequency content in the range of 1000 to 2000 Hz and results primarily from the wheel/rail Hertzian contact stiffness and the rail mass. The P_2 forces are of lower frequency content in the range of 20 to 100 Hz and can be transmitted readily to the ties and ballast. Consequently, the P_1 force is associated with rail end batter, while the P_2 force is associated with the development of a depressed joint profile due to tie, ballast and subgrade deterioration.

Both test and analytical studies have been conducted, particularly by British Rail, to define the interrelationship of speed, static axle load, unsprung mass, and track dynamic modulus with impact force. In the paper by Jenkins, et al.[4], an analytical approach for the prediction of maximum values of P_1 and P_2 was presented. Maximum P_1 force is given by:

$$P_1 = P_o + 2 \alpha V \left(\frac{K_H M_e}{1+M_e/M_u} \right)^{1/2} \qquad [1]$$

where M_e = effective track mass (rail and tie)

M_u = vehicle unsprung mass

K_H = linearized Hertzian contact stiffness

P_o = static wheel load

α = rail dip angle at joint (from horizontal)

V = vehicle velocity.

This approximate equation assumes that the impact force, P_1, is resisted principally by the inertia of the rail and tie mass. Consequently the expression for the dynamic increment in load does not involve the compliance of the track foundation, but only the effective contact stiffness between the wheel and rail. According to Hertzian contact theory, the value of K_H varies with the applied load, P, and the resulting change in the contact zone. For example, the solution for two steel spheres in contact with each other, which case approximates wheel/rail contact, is given by[5]:

$$\delta = 0.775\left[P^2 \left(\frac{1}{R_1} + \frac{1}{R_2}\right) \left(\frac{1}{E_1} + \frac{1}{E_2}\right)^2\right]^{1/3} \qquad [2]$$

where

δ = the relative displacement in inches of two points on the contacting bodies which are removed from the contact patch

P = the applied load in pounds

E_1, E_2 = the elastic moduli of elasticity for each sphere (psi), and

R_1, R_2 = the radii of the spheres (inches).

The constant in Equation [2] is derived from the assumption that Poisson's ratio for both bodies is 0.3.

For this model, R_1 and R_2 are analogous to the wheel and rail effective radii, and P is analogous to the wheel load.

The stiffness, K_H, is defined as

$$K_H = P/\delta \; . \qquad [3]$$

By manipulating Equations [2] and [3], the following form is obtained:

$$K_H = C_1 \, P^{1/3} \qquad [4]$$

where C_1 is an empirically derived constant which is determined by the contact geometry and material properties. For example, for new (conical) wheel profiles, $C_1 \cong 3 \times 10^5$, and K_H has the units of lb/in.

Because K_H varies with P, the following iterative solution procedure is used to determine its value:

(1) Select a value of P, and calculate K_H from Equation [4]

(2) Calculate P_1 from Equation [1]

(3) Recalculate K_H from Equation [4], letting $P = P_1$

(4) Recalculate P_1 from Equation [1]

(5) Repeat Steps 3 and 4 until the change in K_H is quite small.

This procedure converges quite rapidly.

The maximum P_2 force is given by:

$$P_2 = P_o + 2\alpha V \left[\frac{M_u}{M_u + M_t}\right]^{1/2} \left[1 - \frac{C_t^2 \pi}{4K_t(M_u + M_t)}\right] \left[K_t M_u\right]^{1/2} \qquad [5]$$

in which M_t = effective track mass (rail, ties, ballast, subgrade)

K_t = track structural stiffness

C_t = track structural damping.

This equation must also be solved iteratively, because K_t is a function of load. In general, track stiffness measurements have shown that

$$K_t = C_2 P^{1/2} \qquad [6]$$

where C_2 is a function of the mean load, ballast and subgrade moduli, and rail size. For a 20,000-pound static wheel load and 140-pound rail on track with "average" charcteristics, $C_2 \approx 2760$ if P has the units of pounds and K_t is in pounds/inch. The procedure for calculating P_2 from Equations [5] and [6] is similar to that for calculating P_1.

Sensitivity of calculated maxima of P_1 and P_2 to variations in track and vehicle parameters has been derived from the above equations. As expected the P_1 force is insensitive to variations in track stiffness and only moderately

influenced by the range of typical unsprung vehicle masses. Neither the P_1 nor P_2 forces is dependent to any extent on vehicle suspension parameters. The P_2 force, however, is strongly influenced by the vehicle unsprung mass. Both forces are strongly dependent on the joint geometry (depth and angle of joint dip), the vehicle speed, and (of course) the static wheel load. Joint impact parameter effects are summarized in Table 2-1.

TABLE 2-1. PARAMETERS WHICH HAVE A MAJOR EFFECT ON RAIL JOINT LOADS

PARAMETER	JOINT LOADS	
	P_1	P_2
Vehicle Unsprung Mass	No*	Yes
Track Stiffness	No	Yes
Track Damping	No	Yes
Track Effective Mass	No	Yes
Rail Effective Mass	Yes	No
Primary Suspension	No	No**
Vehicle Speed	Yes	Yes
Joint Dip Angle/Joint Deflection	Yes	Yes
W/R Contact Stiffness	Yes	No
Static Wheel Load	Yes	Yes

*Except for very low mass.
**Only if very stiff.

The joint dip angle, α, used in both Equations [1] and [5] is defined by British Rail[4] for a representative low-joint geometry:

$$Z(x) = h\ [1 - \cos(2\pi x/d)]\ \text{for } 0 < x < d/4,$$
$$= h\ [1 - \cos(2\pi x/d + \pi)]\ \text{for } d/4 < x < d/2 \qquad [7]$$

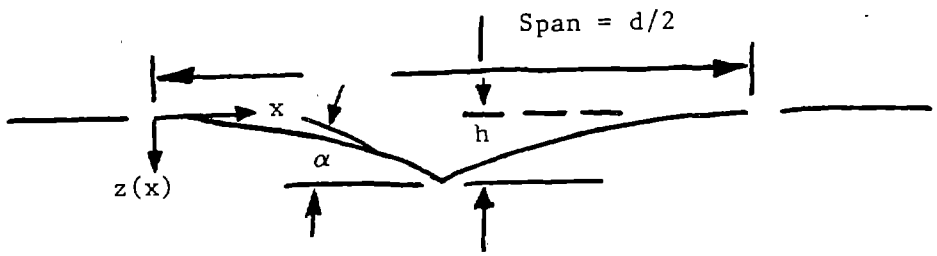

where $\alpha = 2\pi h/d$ for a symmetrical joint.

Typical values for high-speed track are given by British Rail as h = 0.5 in., d = 45 ft. The combination of dip angle and speed, then, becomes the "input" to Equation [1] and [5] to calculate peak impact loads.

Radford[6] has used these methods developed by Jenkins to estimate the vertical wheel/rail forces in high-speed railway operation, using typical North American locomotive, car and track parameter values. Two recent studies[7,8] have employed these equations to relate vehicle and track parameters, track geometry standards, and the resulting impact forces.

2.2 WHEEL FLATS

Wheel flats are the other most important source of vertical impact loads on the rail. Slid flats typically are formed when moving a car with the brakes still applied or during hard braking conditions with a lightly-loaded car. Impact loads due to wheel flats can be quite high -- over 400,000 N (90,000 lb) -- and can occur at any randomly-chosen point along the rail, including a joint or a rail flaw. A quantitative definition of these loads and the resulting stresses in both wheel and rail are therefore important in predicting safe operating limits.

Extensive tests were conducted by the Association of American Railroads (AAR) on the Chicago and North Western Railway during 1947, utilizing both track-side and on-board instrumentation[9]. From strain gages on the rail base, impact loads up to 400,000 N (90,000 lb) were estimated under a 111 kN (25,000 lb) static wheel load and a 114 mm (4.5 in.) flat length. Maximum rail flexural strains were noted in the 27 to 37 km/h (17 to 23 mph) speed range and were generally lower at speeds up to 145 km/h (90 mph). Similar results were reported by Satoh[10] from both analytical predictions and experimental measurements conducted by the Japanese National Railways in the 1960s. An increase in rail vertical bending strain of nearly three times the static strain was noted with a flat length of 125 mm (4.9 in.), with a speed-dependent maximum in the 20 to 30 km/h (12 to 18 mph) range. Rail vertical accelerations of 600 g and ballast accelerations of 45 g were measured under this length of wheel flat.

Frederick, et al.[11] have reported on both theoretical and experimental work by British Rail on wheel flat impact loads. A computer code was developed by Lyon[12] to model the wheel/rail system, considering the track as a beam on elastic foundation (BOEF) and using a nonlinear Hertzian contact stiffness between wheel and rail. Experimental measurements of tie plate load and dynamic strain in

the rail were made to check the validity of the model. Rather than using a flattened wheel with the attendant uncertainty of the precise location of an impact, the British Rail researchers used an analogous identation in the rail running surface to simulate a rounded 125 mm (4.9 in.) wheel flat. These experiments showed short-duration peaks in longitudinal (bending) and shear strains in the rail as bending and shear response waves were propagated away from the point of impact. The British Rail researchers[11] have concluded that these impact-induced strains will travel substantial distances along the rail with little attenuation, and that certain types of rail defects will be influenced by wheel flat loads regardless of impact location.

As a result of these experiments, the analytical model of the wheel/rail system has been expanded to represent a Timoshenko beam on discrete elastic supports, as reported by Newton and Clark[13]. Rail normal modes of vibration are handled as a Fourier series truncated at the frequency range of interest. This model is reported to provide the best comparison with the measured strain data.

One important aspect of the wheel flat is the actual shape. The wheel/rail geometry error of a freshly-slid flat can be described by the function:

$$e_z = -R_{wh1}(1-\cos\psi) \qquad [8]$$

where ...

ψ = arcsin (Vt/R_{wh1}) for $0 \leq Vt < L_f/2$

ψ = arcsin $[(L_f - Vt)/R_{wh1}]$ for $L_f/2 \leq Vt < L_f$

L_f = flat length

R_{wh1} = wheel tread radius

V = vehicle speed

t = time (zero as flat edge first contacts rail)

$\dot{e}_z = -V\sin\psi$ for $0 \leq Vt < L_f/2$

$\dot{e}_z = +V\sin\psi$ for $L_f/2 \leq Vt < L_f$

e_z and $\dot{e}_z$ = 0 for $Vt \geq L_f$.

This function results in a "cusped" geometry error somewhat analogous to a dipped joint. However, a slid flat is very quickly battered into a more rounded shape, as noted in the AAR experiments[9]. Lyon[12] has suggested a versine function as more realistic of a service-worn slid flat profile:

$$e_z = -0.5D_f [1 - \cos(2 \pi \ Vt/L_f)] \qquad [9]$$

$$\dot{e}_z = -(D_f \ V/L_f)\sin(2 \ \pi \ Vt/L_f) \qquad [10]$$

where $D_f = L_f^2 / 16R_{wh1}$, the effective flat depth.

The fundamental frequency of the wheel flat is dependent on both the effective length and the train speed; and the impact force may range in duration from a fraction of a millisecond (a small flat at high speed) to over 10 milliseconds (a large flat at low speed). Therefore, a wide range of rail and track structural resonant frequencies may be excited by wheel flat impact loads.

3. EXPERIMENTAL MEASUREMENTS

3.1 FIELD EXPERIMENTS

Extensive wheel/rail load data were gathered during a measurement program on the Union Pacific Railroad in February of 1978[14]. This measurement program utilized both wayside and on-board instrumentation. Two tangent-track sections on the California Division were chosen as test sites: one of bolted-joint rail (BJR), the other of continuous-welded rail (CWR) on wood ties and good ballast. Each section provided 5 km (3 mi) of relatively homogeneous track for test runs with an instrumented open-top 100-ton hopper car. The primary instrumentation on this car was a strain-gaged wheel for measuring vertical and lateral loads. Within each 5-km section of track, a 274-m (900 ft) subsection was instrumented with wayside transducers. Strain gage patterns were applied at seven randomly-chosen locations within each subsection to measure vertical and lateral loads, as shown in Figure 3-1. In addition, an "extended" vertical measurement zone was instrumented, combining the signals from rail strain gages and load cell tie plates (Figure 3-1) to provide a vertical load sample roughly 1 m (39 in.) in length. In one test section, this extended zone was located at a rail joint.

In addition to vertical and lateral loads on the rail under passing revenue traffic, one measurement site was chosen in each location for an array of longitudinal strain gages. These provided a sample of longitudinal strains in both bolted-joint (BJR) track and continuous-welded (CWR) track. Weldable strain gages approximately one inch in length were applied to the rail head fillet and rail base as sketched below, centered in the crib area between two ties. Each gage was monitored individually, using precision 120-ohm resistors to complete the bridge.

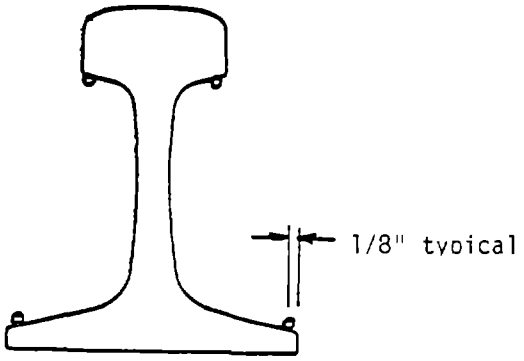

Locations of Longitudinal Strain Gages on Rail

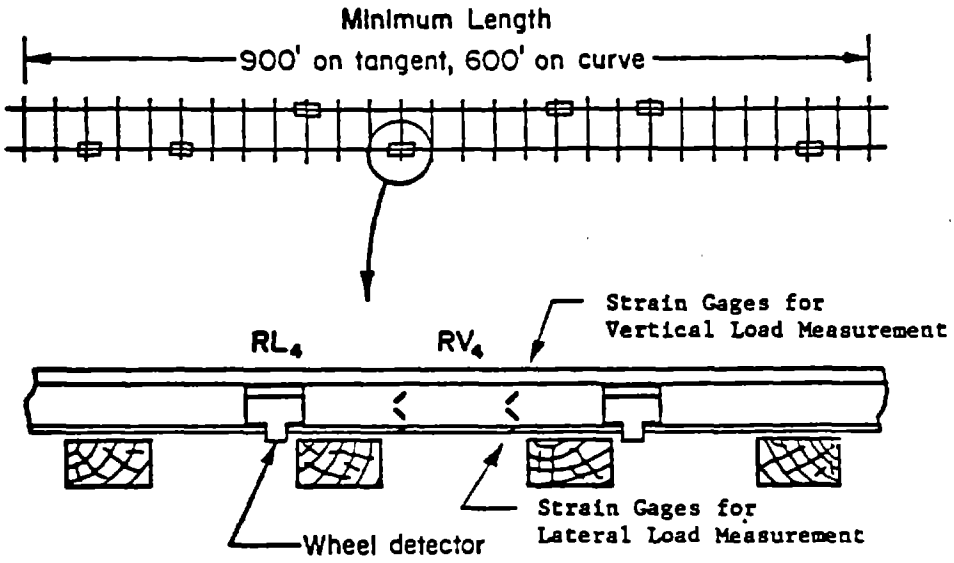

(a) RANDOMLY-SPACED LOAD MEASUREMENT SITES
(TRACK LOAD CATEGORIES I, II, III)

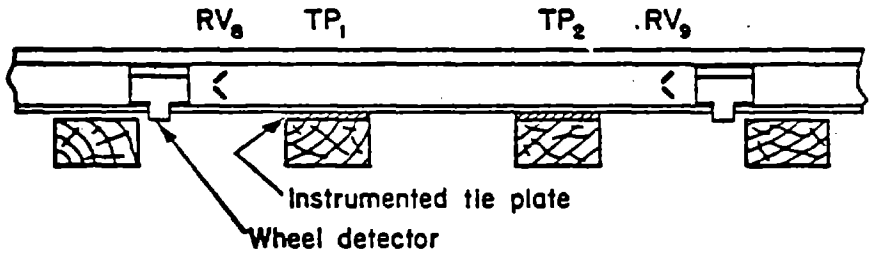

(b) CONTINUOUS VERTICAL WHEEL/RAIL LOAD MEASUREMENT ZONE
(TRACK LOAD CATEGORY II)

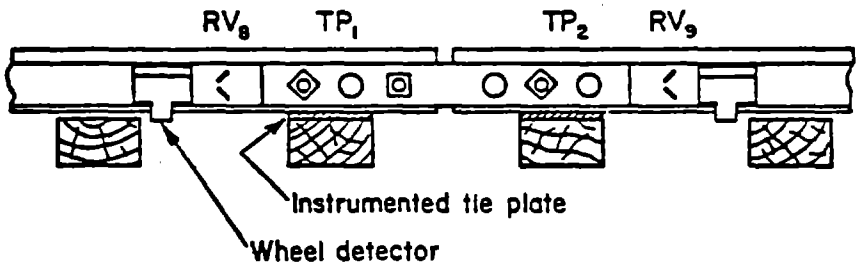

(c) VERTICAL WHEEL/RAIL LOAD MEASUREMENTS AT JOINT

FIGURE 3-1. LAYOUT OF WHEEL/RAIL LOAD TRANSDUCERS
FOR DIFFERENT WAYSIDE TEST SECTIONS

Each data channel was recorded by frequency-division multiplexing on a Sangamo Sabre VI Wide Band Group I tape recorder. For this study the data were recorded on a Honeywell Model 1858 fiber optic oscillograph at the full recording bandwidth of 2000 Hz.

Data from the instrumented wheel were analyzed for 50 consecutive rail joints in the BJR track section from constant-speed test runs from 24 to 105 km/h (15 to 65 mph) to characterize the joint impact loads. A direct comparison of track and wheel load measurements were provided at the instrumented rail joint. Wayside measurements were recorded for all revenue traffic over a 7-day period at each tangent-track location. Traffic included mixed-freight trains, both loaded and empty unit trains, and priority (TOFC/COFC) freight at speeds up to 127 km/h (79 mph). Data were measured for roughly 22,000 axles on the BJR track and 24,000 axles on the CWR track. During these tests, flat wheel impact loads up to 463 kN (104,000 lb) were recorded.

3.2 RAIL JOINT IMPACT LOADS

An extended vertical load zone was installed at the instrumented rail joint at Test Section 1 to measure wheel/rail loads in the vicinity of this joint. Although this rail joint was chosen initially because it was visually 1/4 to 3/8-inch low, the process of installing the instrumented tie plates (holding the tie up with a tamping bar while spiking) resulted in a nearly-flat joint. In fact, rail surface measurements from a taut string showed the joint to be 1.1 mm (0.04-in.) "proud" under no load. Due to mechanical tamping in the recent past, a number of rail joints in this track section appeared visually to be slightly high relative to the rail midspan region.

A typical example of vertical wheel loads through the joint region is shown in Figure 3-2 for the instrumented hopper car during a 105 km/h (65 mph) test run through the wayside instrumented track section. The classical "P_2" force peak, 10 to 12 milliseconds in duration, can be seen quite plainly, resulting in a wheel load roughly 25 percent higher than the nominal 115 kN (25,800 lb) load. In this illustration, a 300-Hz 4-pole Bessel filter has been employed; but the same data through 1000-Hz and 2000-Hz filter settings still showed no indication of the "P_1" short-duration impact load. This may be attributed to the essentially flat surface profile and small (~6 mm, 1/4 in.) rail gap at this point.

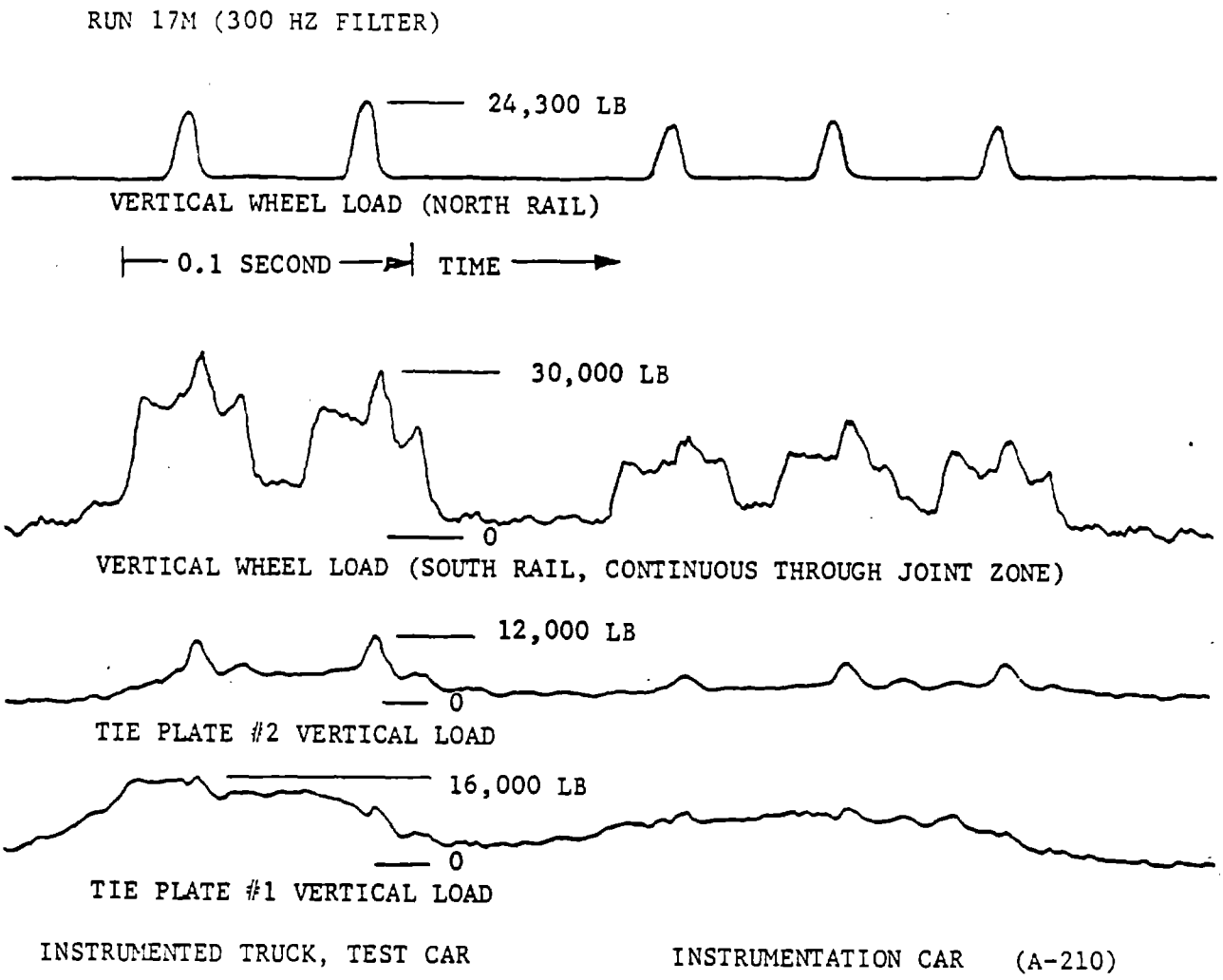

FIGURE 3-2. VERTICAL WHEEL/RAIL LOADS UNDER INSTRUMENTED TRUCK OF TEST CAR (HOPPER CAR, 70-TON LOAD), EASTBOUND AT 65 MPH

In addition to vertical load measurements, rail joint bolt hole strains were recorded at this instrumented joint. Standard 1/16-inch foil strain gages were applied to the first running-on bolt hole (for westbound trains) of the joint oriented as sketched below:

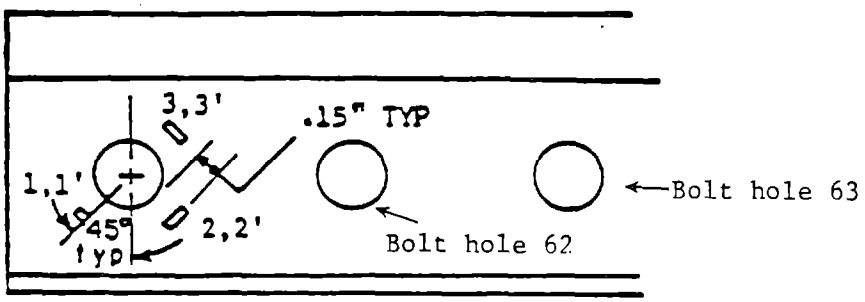

Prime Gage Numbers on Field Side

Gages were applied both to the field and gage sides of the rail and were recorded separately on the FM tape recorder. Calibrated, strain-gaged bolts were used upon reassembly of the joint. Prior to recording several typical freight trains, the bolts were tightened by a member of the section crew with a standard track wrench. Bolt tensions were measured after several trains had passed, using a strain indicator:

In Order, East to West						
Bolt	59	64	61	60	62	63
Tension (kips)	12.8	17.7	9.2	14.0	11.6	21.0

A typical example of recorded bolt hole strains under the lead truck of an 8-axle DDA-40X diesel unit at 68 mph is shown in Figure 3-3. The bolt hole strains show an almost instantaneous change in strain level with transfer of the wheel vertical load across the joint gap, then a saw-tooth decrease in level (compression of Gages 1 and 3, tension at Gage 2) as the wheel approaches the bolt hole. Some minor high-frequency, load impact dynamics are superimposed on this fundamental shape. The lower-frequency P_2 force peaks impose rather minor changes in bolt hole strain levels at this particular joint. Bolt hole strains under locomotive axles were found to run typically 600 microstrain maximum for westbound

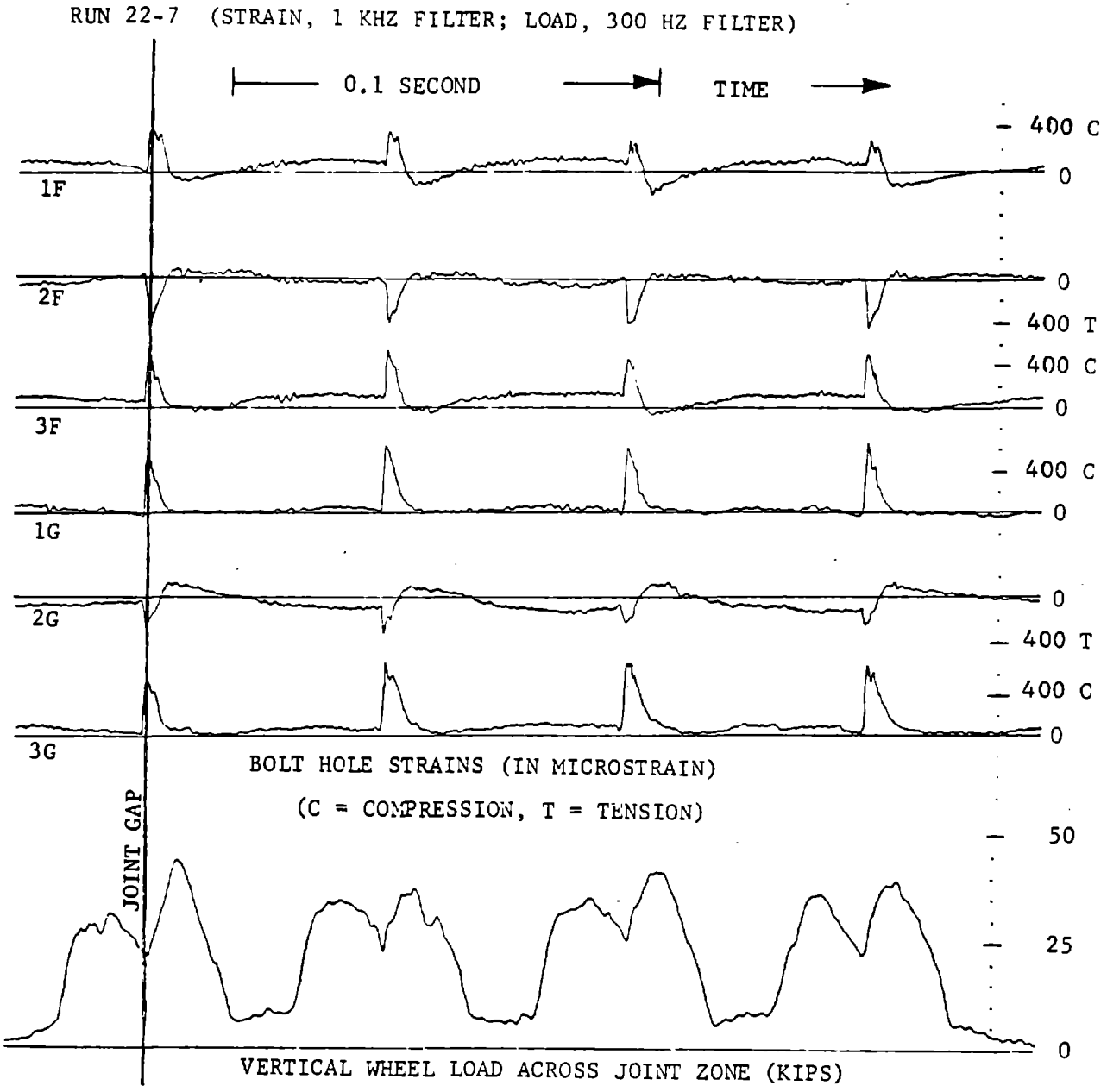

FIGURE 3-3. EXAMPLE OF BOLT HOLE STRAINS AND WHEEL LOAD AT INSTRUMENTED JOINT, TEST SECTION 1 (BJR TRACK), LEAD TRUCK OF TRAILING 8-AXLE (DDA-40X) LOCOMOTIVE UNIT, WESTBOUND AT 68 MPH

runs. Gages in locations 1F and 2G showed strain reversal (compression to tension, or vice versa) most strongly. For eastbound (running-off) traffic, the strain signature of Figure 3-3 was reversed, with somewhat lower strain peak levels recorded.

For another westbound freight at 69 mph consisting of four 6-axle locomotive units (SD-40-2, U33C, SD-45, SD-40), the following strain values were noted under the locomotive axles:

Gage Location	Bolt Hole Strain, microinch/inch*					
	1F	2F	3F	1G	2G	3G
Maximum Strain	-500	490	-580	-670	320	-780
Mean of Peaks	-306	406	-463	-579	262	-587
Standard Deviation of Peaks	95	39	46	54	33	101

*minus denotes compression

Instrumented joint data were scanned for flat wheel impact loads to see what effects these impacts might have on bolt hole strains. No high impact loads were noted on the "running-on" rail (over the strain-gaged bolt hole). However, a 409 kN (92,000 lb) impact load occurred on the "running-off" rail within the extended vertical load zone. It was interesting to note that there was no distinct response at the bolt hole strain gages to this impact, indicating that the joint bars effectively attenuate (or shunt) any stress waves at these frequencies.

Because the wayside-instrumented joint produced little "P_1" impact force, a more severe joint was chosen from within the test section to analyze wheelset loads. Two examples of instrumented wheel load signal are shown in Figure 3-4. In these figures, the appropriate strain gage bridge signal has been sampled at 4000 per second and modified by an inverse transfer function to eliminate positional error. The drop in vertical wheel load just prior to the rail joint is evident in this figure, followed by the P_1 impact load. Following this impact there is strong excitation of the wheel vibrational modes, from about 500 Hz on up. The wheel tends to "ring" for a number of cycles after impact, which results in strain signals not directly related to the wheel/rail load. The P_2 load peak is consequently masked by these wheel oscillations. The continuous (or digitally reconstructed) vertical load signal from an instrumented wheelset must therefore

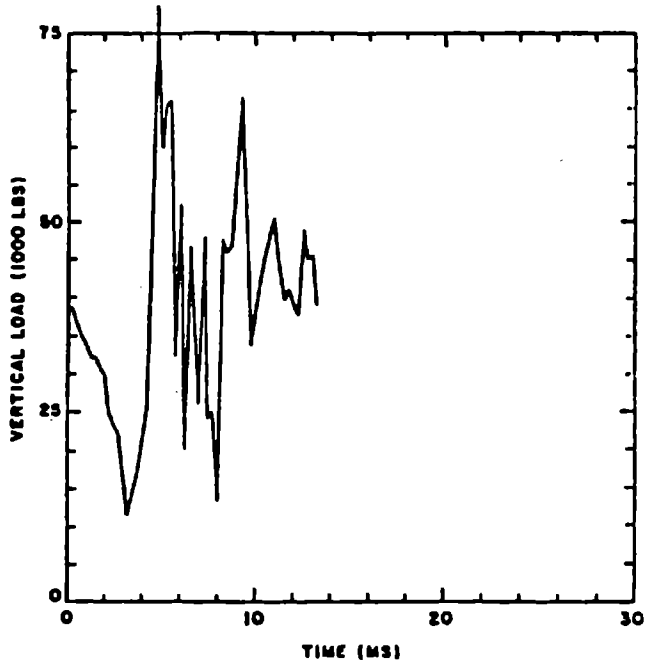

SPEED = 55 mph

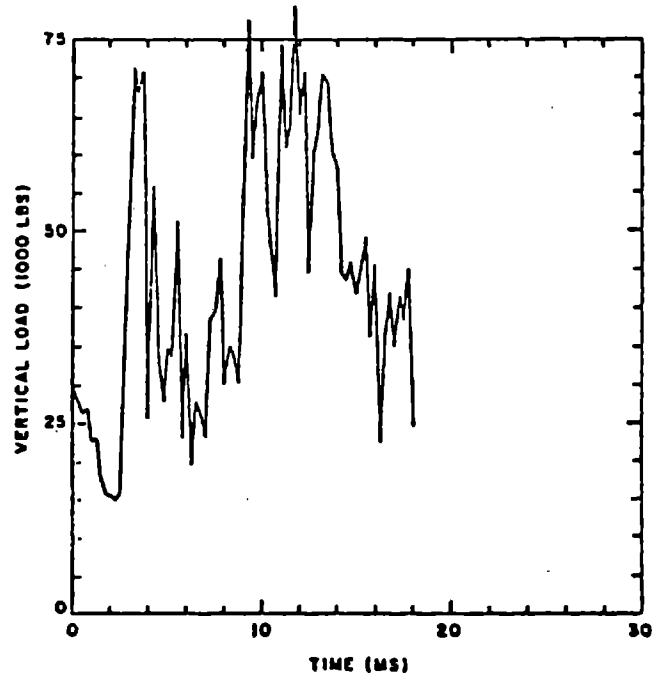

SPEED = 65 mph

FIGURE 3-4. EXAMPLES OF RAIL JOINT IMPACT LOADS MEASURED BY INSTRUMENTED WHEEL ON LOADED HOPPER CAR (JOINT #50, 4000 SAMPLES/SECOND, 25,800 LB WHEEL LOAD)

be filtered at a frequency below 200 Hz, which will sacrifice high-frequency (P_1) load information, but result in accurate low-frequency (P_2) impact load measurements.

3.3 FLAT WHEEL IMPACT LOADS

Flat wheel impact loads were measured occasionally by the short (in-crib) chevron gage circuits: for example, impact loads at several of the CWR track sites are illustrated in Figure 3-5 for one particularly bad set of wheels on a 100-ton freight car. The difference in load signal characteristics between the normal and flatted wheels is particularly graphic at Site 1, Axle 2 versus Axle 4. The flat wheel impact resembles a half-sine pulse approximately 6 milliseconds in duration.

To assure a greater probability of sampling the flat wheel population, the extended vertical load circuit was used at one CWR track site to provide a zone with an effective length of 0.9 m (35 in.), approximately one-third an average wheel circumference. Four evenly spaced ties of good quality were chosen for this zone, and the four instrumented tie plates were installed. In spite of care in selection, one of the ties proved to be of a softer wood (hemlock or cypress), while the other three were hardwood ties.

A typical flat wheel response within the extended vertical load zone is shown in Figure 3-6. In this example, the peak wheel flat impact load was 431 kN (97 kips), with a peak vertical tie plate load of 254 kN (57 kips) directly under the point of impact. A 300-Hz filtering frequency has been used with the oscillograph in reproducing this event (a 4-pole programmable Bessel filter), but negligible higher-frequency content was found in flat wheel impacts. For example, a 409-kN (92-kips) impact load near the instrumented rail joint was examined through different filter settings:

Run 22-10, Car 14

Filter Frequency (Hz)	Peak Impact Load (kips)	Peak Load, Tie Plate 1 (kips)	Peak Load, Tie Plate 2 (kips)
30	41	13.2	12.5
100	77	20.5	25
300	90	23	30
1000	92	24	31

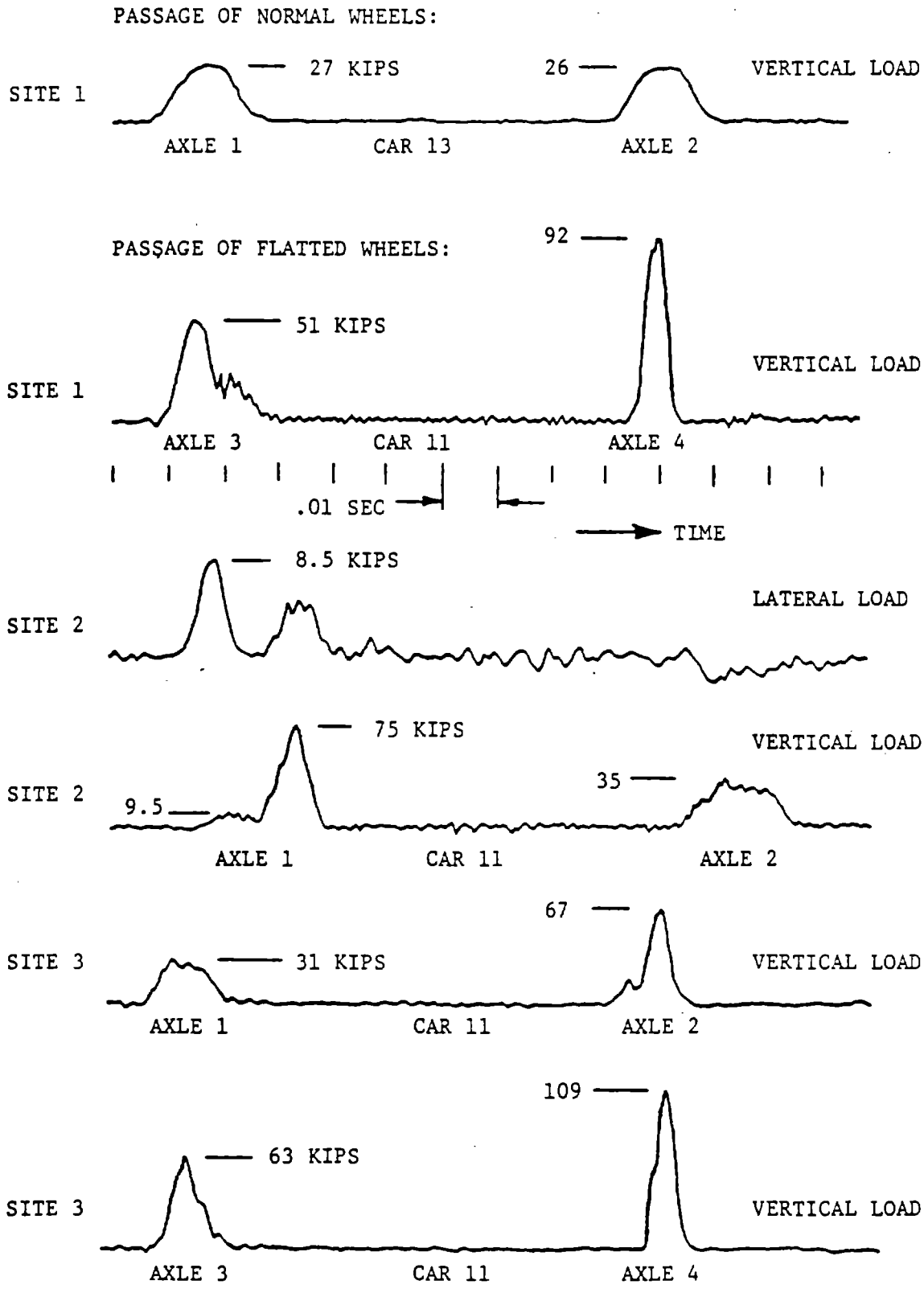

FIGURE 3-5. EXAMPLES OF WHEEL/RAIL LOADS UNDER NORMAL AND FLATTED WHEELS AT SHORT MEASUREMENT SITES, SMOOTH TANGENT TRACK, WESTBOUND FREIGHT TRAIN AT 46 MPH

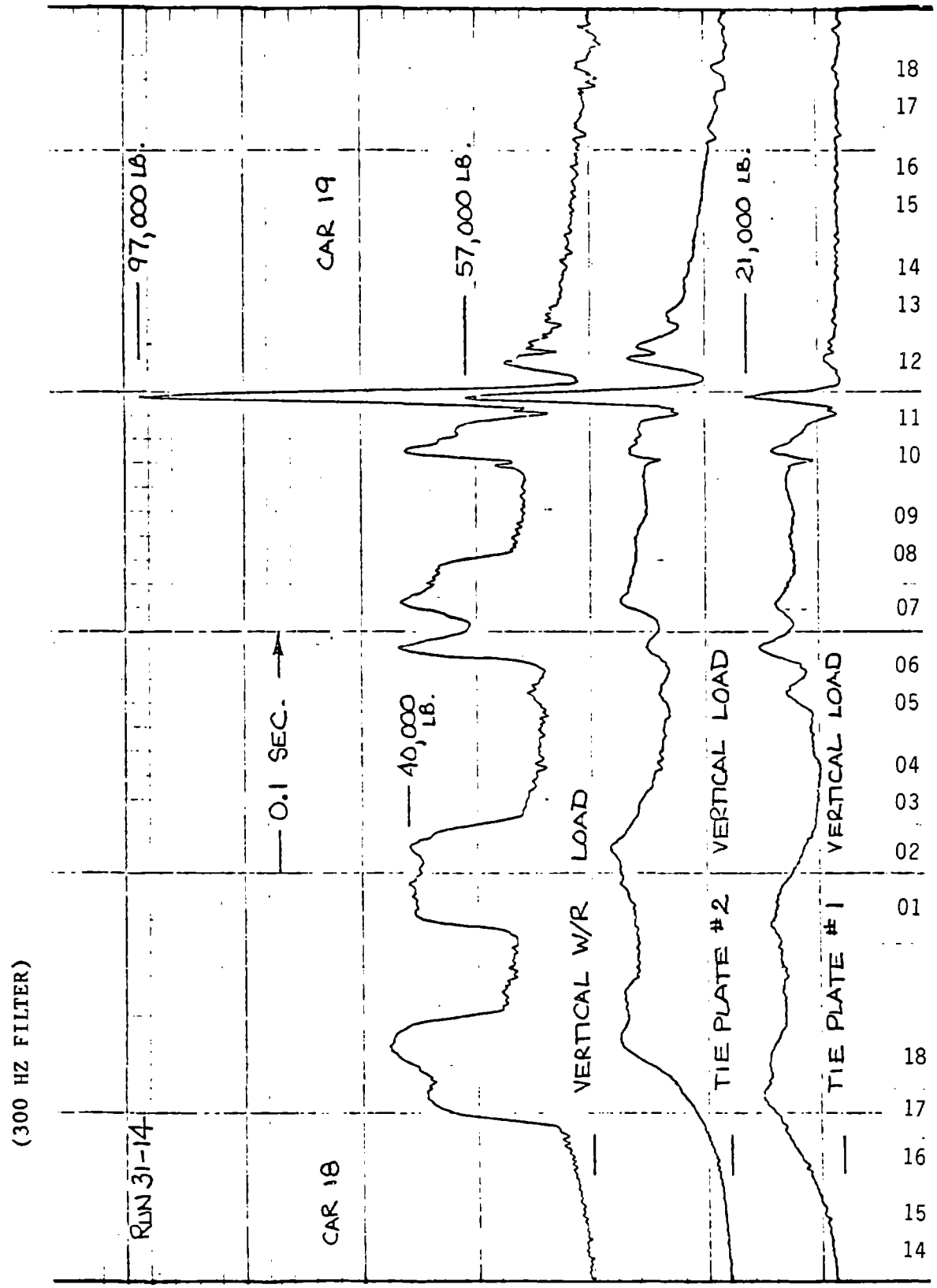

FIGURE 3-6. FLAT WHEEL IMPACT WITHIN VERTICAL CONTINUOUS MEASUREMENT ZONE -- TEST SECTION 2 (CWR TRACK), ADJACENT TRUCKS OF 100-TON COVERED HOPPER CARS IN WHEAT UNIT TRAIN AT 46 MPH

Another example of flat wheel impact loading is shown in Figure 3-7, with a filter frequency setting of 1000 Hz. This impact results in a strong 71 Hz response in the track structure, but there is little indication of higher frequency components in the load signal.

A substantial data base was developed during these field experiments for roughly 22,000 axles on the BJR and 24,000 axles on the CWR test sections. These data were classified by five categories of vehicles (locomotives, and freight cars in four gross weight bands) and four 10-mph speed bands for each of the BJR and CWR test sections. An examination of the load statistics for these individual categories showed that the vertical wheel loads form a normal (Gaussian) distribution over frequency-of-exceedance levels of approximately 98 to 10 percent, as shown in Figure 3-8. Beyond the 10 percent level of exceedance, a substantial deviation occurs, primarily due to loads from flatted wheels, so that it is necessary to handle the extreme-value statistics separately.

Data from the extended (35-in.) measurement zone were processed in two ways: first by statistical analysis of the peak vertical load occurring within the 35 inches, and second by analysis of the "dynamic load increment". The dynamic load increment was obtained experimentally by passing the signal through 1000-Hz and 30-Hz filters in parallel, and subtracting the two signals to obtain the higher-frequency dynamic load difference. There is strong evidence from the analysis of this signal that the population of "flat wheels" (or at least wheels generating dynamic load increments greater than approximately 22 kN (5 kips)) fall into an obviously-distinct population. The distribution function that best describes this population is the exponential function, which is a special case of the Weibull distribution. It is commonly used to describe the failure rate of assemblies of components (hydraulic pumps, washing machines, etc.)[15], and takes the form:

$$E_X(F_{dyn}) = e^{-(F_{dyn}/\overline{F}_{dyn})}, \text{ the exponential frequency-of-exceedance function,} \qquad [11]$$

where

$\overline{F}_{dyn}$ = the mean value of flat wheel impact (analogous to the "characteristic time" in failure rate).

With this clue to the nature of the extreme-value distribution, the experimental data from the 7 short (7-inch) measurement sites were used to

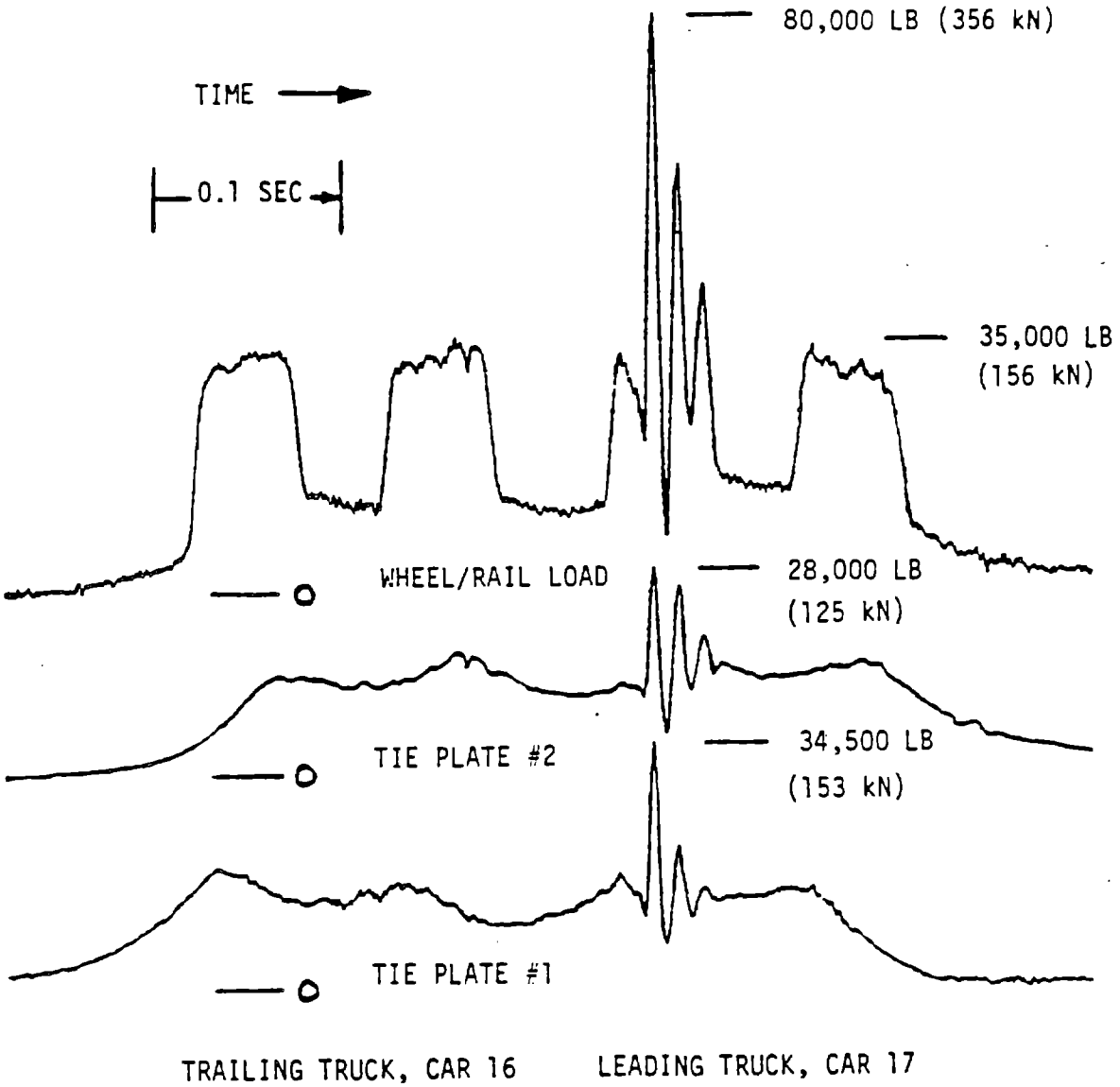

FIGURE 3-7. FLAT WHEEL IMPACT WITHIN EXTENDED VERTICAL MEASUREMENT ZONE IN CWR TRACK, ADJACENT TRUCKS OF 100-TON HOPPER CARS, 65 KM/H (40 MPH) TRAIN SPEED

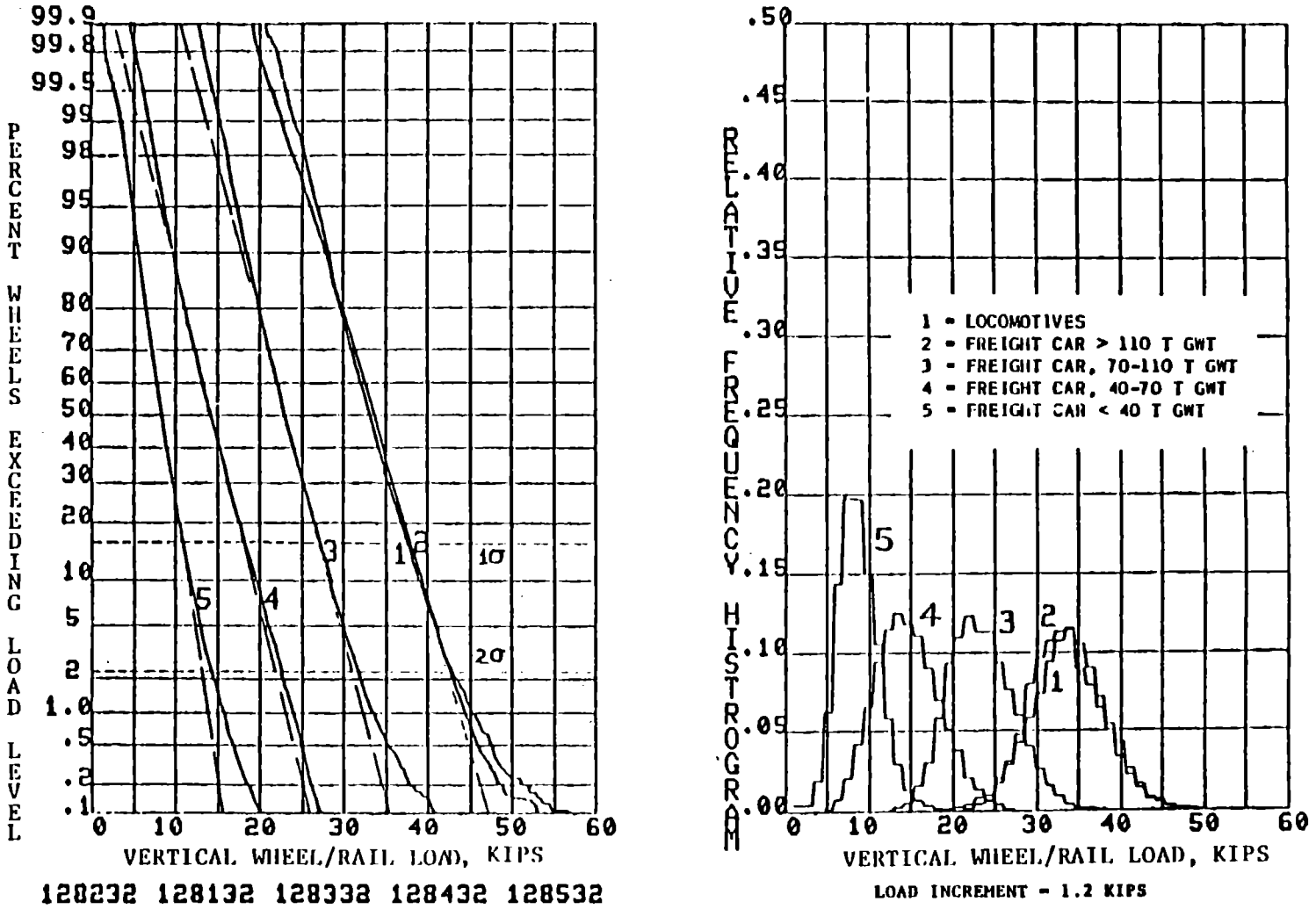

FIGURE 3-8. STATISTICAL PLOTS OF VERTICAL WHEEL/RAIL LOAD PEAKS, SUMMARY OF SEVEN MEASUREMENT SITES ON CWR TRACK, ALL SPEEDS

establish a least-squares best fit (at 5-kip intervals) to exceedance levels above the nominal three-standard-deviation load. The resulting function takes the form:

$$E_x(F_v) = R\, e^{-(F_v-\bar{F}_v)/\bar{F}_{dyn}} \qquad [12]$$

where

F_v = vertical wheel/rail load

$\bar{F}_v$ = mean vertical W/R load for vehicle class (normal distribution)

R = portion of wheel population in the extreme-value distribution.

Parameters describing the extreme-value distribution by vehicle class are listed in Table 3-1.

TABLE 3-1. PARAMETERS DESCRIBING VERTICAL EXTREME-VALUE (FLAT WHEEL) LOADS WITHIN CWR TEST SECTION

Vehicle Type	% Axles in Population	Mean Load, $\bar{F}_v$ (kips)	Exponential Function	
			$\bar{F}_{dyn}$(kips)	R
1. Locomotives	8.8	33.5	5.5	0.045
2. Cars > 110T GWT	17.7	32.9	7.4	0.045
3. Cars 70T - 110T	14.3	22.3	5.9	0.058
4. Cars 40T - 70T	29.6	14.1	4.0	0.019
5. Cars < 40T	29.6	8.4	4.0	0.110

A comparison of the resulting cumulative histogram of incremental vertical dynamic load peaks (all traffic) with the theoretical exponential distribution is shown in Figure 3-9. Further evidence of how well this theory fits the measured data is given in Figure 3-10, where the approximate distributions (normal plus

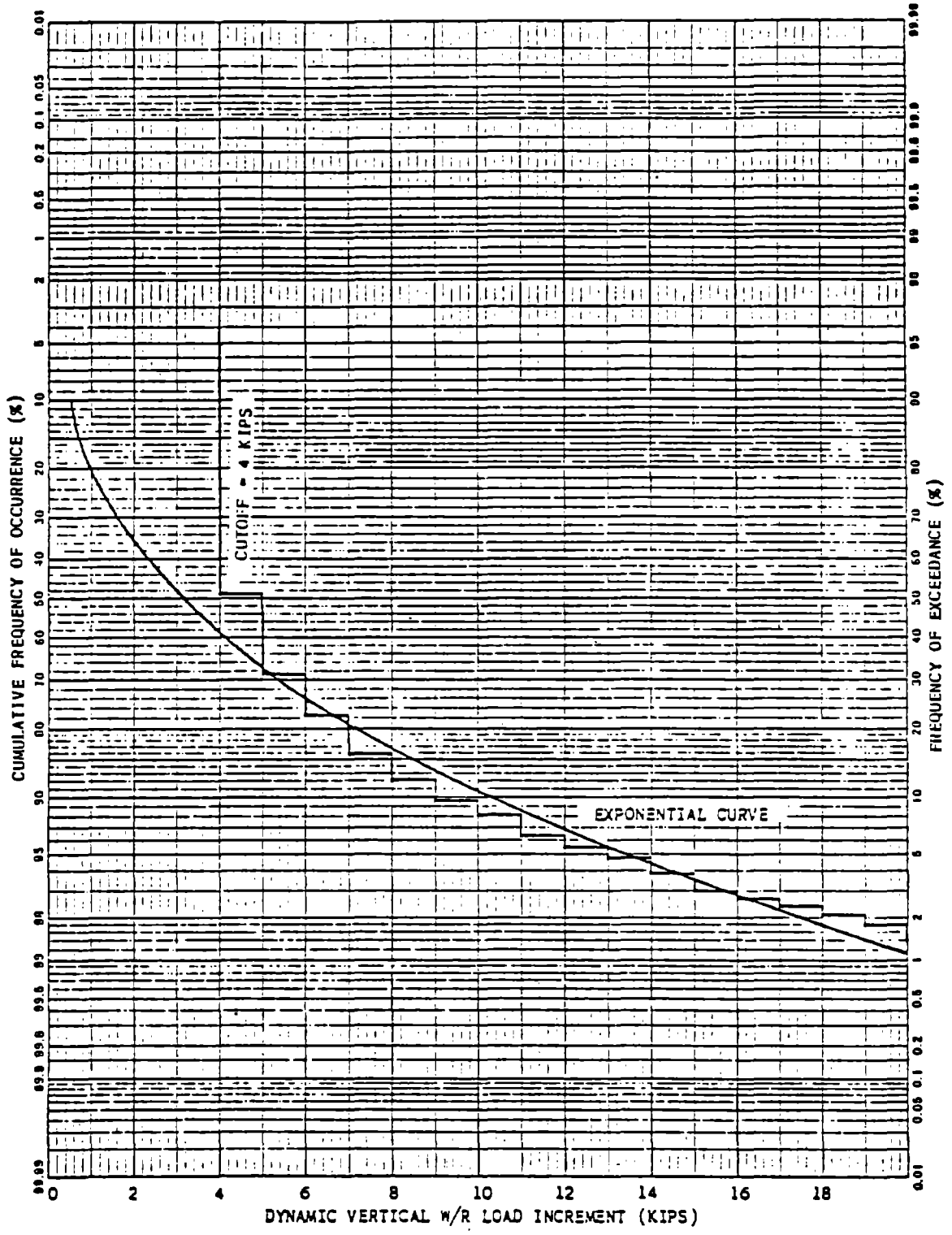

FIGURE 3-9. COMPARISON OF EXPONENTIAL DISTRIBUTION CURVE WITH CUMULATIVE HISTOGRAM OF DYNAMIC LOAD INCREMENT OCCURENCE GREATER THAN 4 KIPS

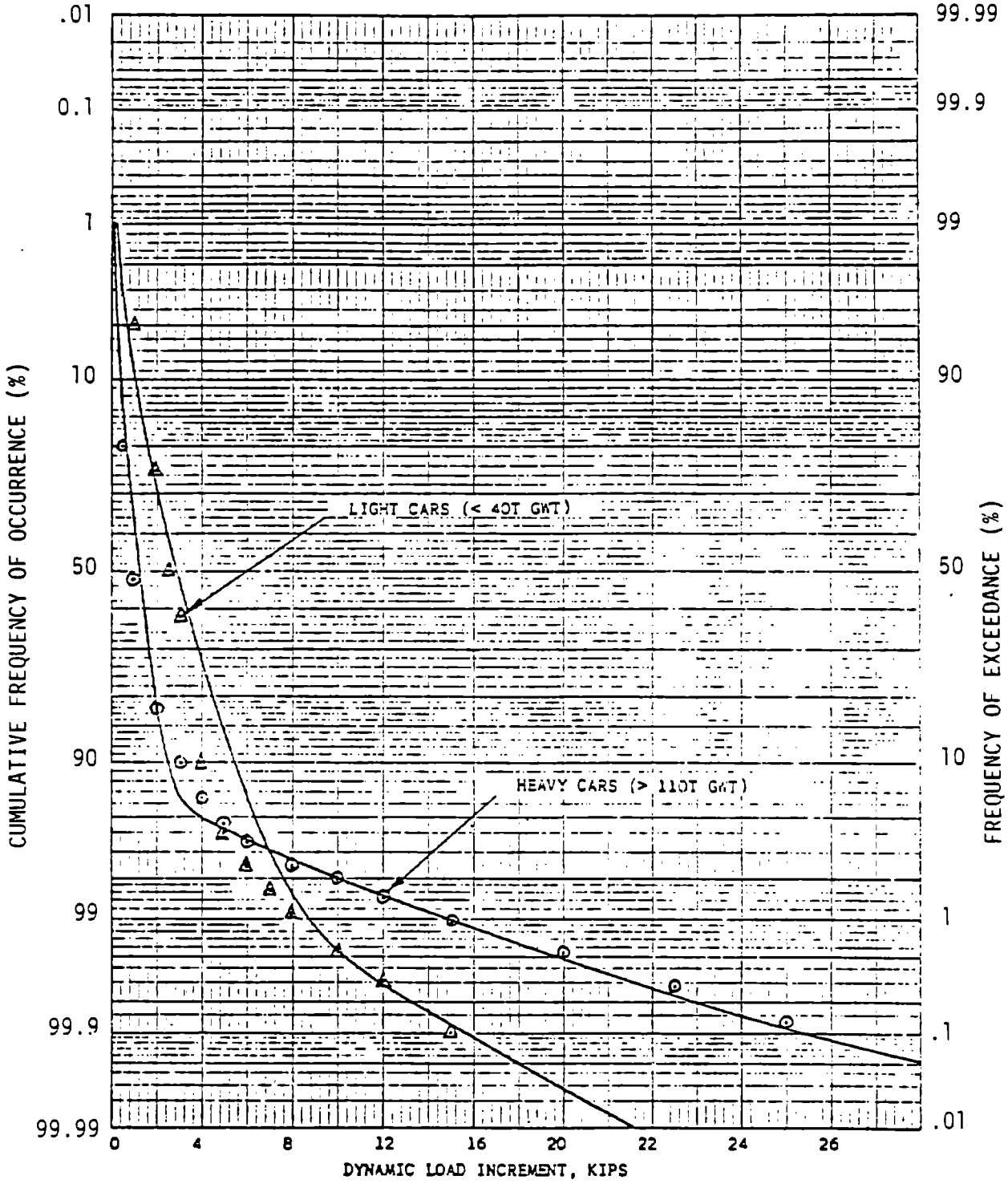

FIGURE 3-10. COMPARISON OF THEORETICAL EXCEEDANCE CURVES WITH MEASURED DYNAMIC LOAD INCREMENT DATA FOR LIGHT AND HEAVY CARS, ALL SPEEDS

TABLE 3-2. COMPARISON OF PREDICTED EXTREME-VALUE VERTICAL W/R LOADS WITH LOADS MEASURED WITHIN BOTH THE 7" AND EXTENDED (35") ZONES

Vertical W/R Load Level (Kips)	Predicted W/R Load Exceedance Level (All Traffic)		Measured Wheel/Rail Load Exceedance Levels (All Traffic)				35" Zone Scaled to 7" CWR
			(Av. of 7 Sites)		(Range of 7 Sites)		
	60 mph	30 mph	BJR*	CWR	BJR	CWR	
45	4.2×10^{-3}	2.0×10^{-3}	1.8×10^{-3}	3.1×10^{-3}	3.6E-4 to 5.5E-3	6.6E-4 to 1.1E-2	
50	8.7×10^{-4}	7.4×10^{-4}	4.2×10^{-4}	7.1×10^{-4}	8.9E-5 to 1.3E-3	3.1E-4 to 1.6E-3	7.2×10^{-4}
55	3.5×10^{-4}	3.5×10^{-4}	1.7×10^{-4}	3.8×10^{-4}	0 to 6.2E-4	1.3E-4 to 9.0E-4	
60	1.7×10^{-4}	1.7×10^{-4}	9.1×10^{-5}	2.0×10^{-4}	0 to 3.1E-4	8.8E-5 to 4.5E-4	1.7×10^{-4}
65	8.2×10^{-5}	8.2×10^{-5}	4.9×10^{-5}	8.9×10^{-5}	9 to 1.8E-4	0 to 1.8E-4	
70	4.0×10^{-5}	4.0×10^{-5}	2.1×10^{-5}	5.1×10^{-5}	0 to 5.1E-5	0 to 9.0E-5	6.0×10^{-5}
75	2.0×10^{-5}	2.0×10^{-5}	2.1×10^{-5}	1.3×10^{-5}	0 to 5.1E-5	0 to 4.4E-5	
80	9.7×10^{-6}	9.7×10^{-6}	1.4×10^{-5}	1.3×10^{-5}	0 to 5.1E-5	0 to 4.4E-5	1.2×10^{-5}
85	4.7×10^{-6}	4.7×10^{-6}	7.0×10^{-6}	1.3×10^{-5}	0 to 5.1E-5	0 to 4.4E-5	
90	2.3×10^{-6}	2.3×10^{-6}	7.0×10^{-6}	1.3×10^{-5}	0 to 5.1E-5	0 to 4.4E-5	1.2×10^{-5}

*Less than 1/2 the 100-ton freight car axles passed through the BJR test section than through the CWR test section: roughly 1710 vs. 3980.

exponential) for the dynamic load increment are compared with data for empty and loaded 100-ton freight cars.

A comparison of predicted and measured levels from the standard (7-inch) measurement sites is listed in Table 3-2. The predicted load exceedance levels show an excellent correlation with the average of the seven sites out to about 80 kips, above which level only a very few load events were actually measured. Note that roughly half as many 100-ton loaded freight cars were recorded through the BJR test section than were recorded through the CWR test section, which is reflected in the 2:1 difference in exceedance levels.

A predictive methodology for characterizing both the vertical and lateral wheel/rail load environment has been developed.[16,17] Extreme-value lateral loads also fall into an exponential distribution above roughly 27 kN (6 kips), but are statistically uncorrelated with the extreme-value vertical loads. Using the predictive methodology, percent level of exceedance for both vertical and lateral loads has been calculated for a typical example in Table 3-3 as related to tonnage of traffic (MGT = million gross tons per year). Note that extreme-value impact loads occur far more frequently than would be predicted by simply extrapolating the normal distributions.

TABLE 3-3. FREQUENCY OF EXCEEDANCE OF WHEEL/RAIL LOADS FROM PREDICTIVE FORMULAE, MIXED FREIGHT TRAFFIC, 60 MPH

% Level Exceeded	No. Axles Between Exceedances	Predicted Vertical Wheel/Rail Load, Kips	Predicted Lateral Wheel/Rail Load, Kips	Estimated Time Between Exceedances (Days)* 25 MGT Annual Traffic	50 MGT Annual Traffic	75 MGT Annual Traffic
50	2	15.6	-0.2			
10	10	34.8	1.2			
1	100	42.5	5.0			
0.1	1000	49.4	11.4	0.27	0.13	0.09
0.01	10^4	63.7	19.7	2.7	1.3	0.9
10^{-3}	10^5	80	29.2	27	13	9
10^{-4}	10^6	96	39.6	270	130	90
10^{-5}	10^7	112	50.5	2700	1300	900

*Time estimates based on 3708 axles/day for 25 MGT annual traffic (54,130 axles/MGT).

3.4 RAIL LONGITUDINAL STRAIN

One of the more interesting results from experiments reported by British Rail[11] concerns the propagation of bending and shear waves along the rail. Results indicated that flat wheel impact-induced strains in longitudinal (bending) and shear orientation will travel substantial distances along the rail with little attenuation, so that certain defects will be influenced by a wheel flat regardless of the impact location. To investigate this phenomenon, longitudinal strain data from the Union Pacific tests were examined in greater detail.

Although the longitudinal strain data were not recorded during the whole test period, approximately three days of revenue traffic data were obtained from each location. The vertical wheel/rail load and longitudinal strains were examined at slow chart speed (1 in./sec) for a number of trains to locate flat wheel impact events. These events were than recorded at higher chart speeds (10 to 40 ips) to expand the time scale. A representative time history is shown in Figure 3-11 of the passage of two axles of one truck (approximately a 20-ton axle load) through the measurement site. As each wheel approaches, the rail bends as a beam on elastic foundation, with the rail head in compression, the base in tension. Directly under the wheel/rail contact patch, the rail head acts as a separate beam with the web as its foundation, which results in a sudden reversal in strain, often reversing sign to tension. The "influence zone" is seen to be on the order of 4 inches. In this example, the two wheels are seen (from the balanced head strain reversal) to be tracking close to the centerline of the rail running surface.

A second example in Figure 3-12 shows how the longitudinal strains can be used to indicate the transverse position on the rail running surface of the wheel rail contact patch. The first wheel of two adjacent trucks shows a strong head strain reversal on the gage side, while the second wheel shows just the opposite effect, with a strong strain reversal on the field side. Balanced rail base strain signals indicate negligible lateral bending due to lateral load, and that the wheels of this truck are simply "crabbing" along on different wheel/rail contact paths.

The effects of both lateral and vertical loading on the longitudinal rail strains are shown in Figure 3-13. In this example, the trailing wheel of a traiing truck develops an 89 kN (20,000 lb) lateral load (an L/V ratio of roughly 0.8) that is clearly evident in the 700 microstrain tensile strain in the rail

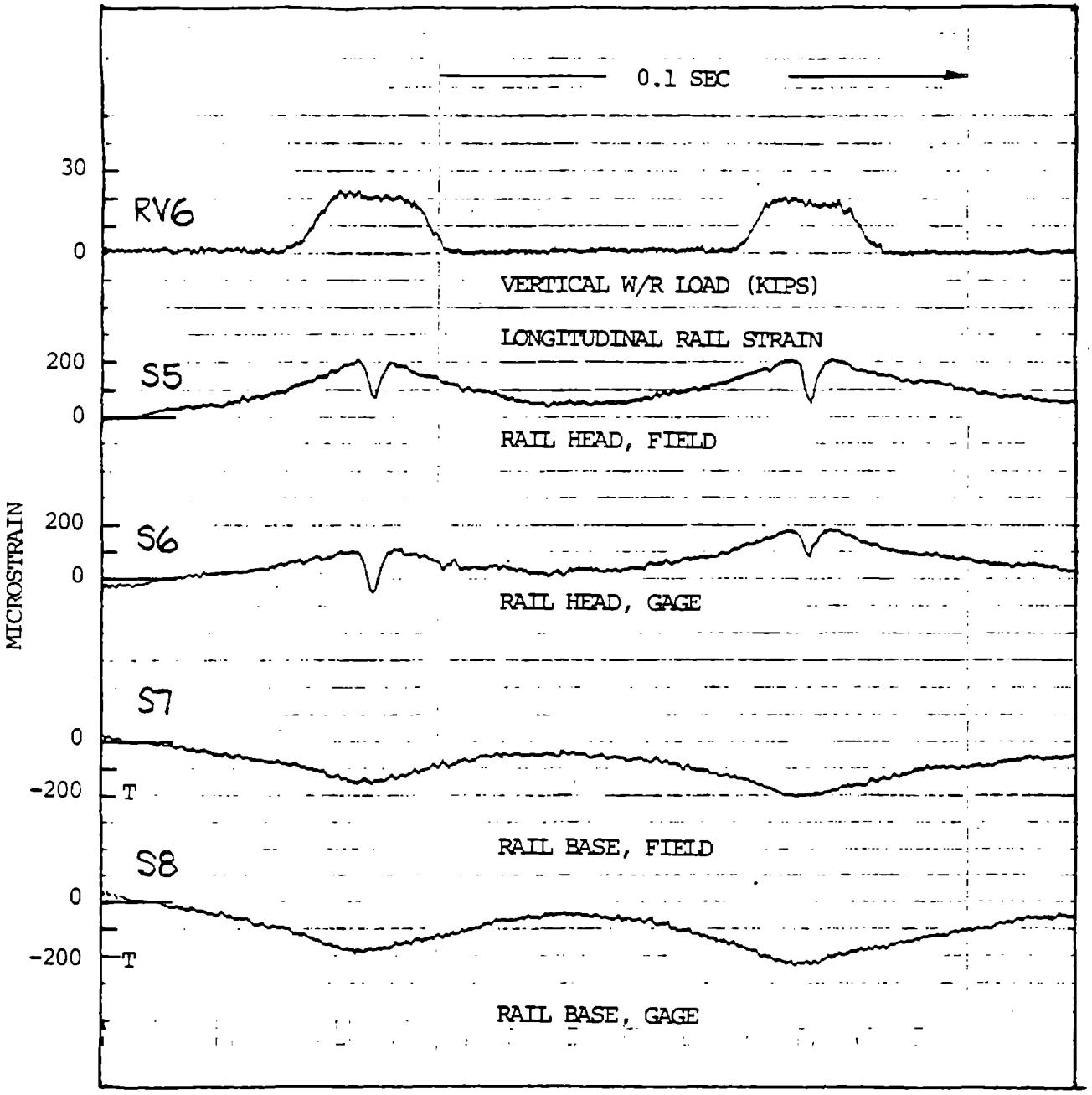

FIGURE 3-11. VERTICAL W/R LOAD AND RAIL LONGITUDINAL STRAINS UNDER WHEELS OF ONE TRUCK, CENTER OF CRIB AREA -- RUN 18-14, 47 MPH, BJR TANGENT TRACK SECTION

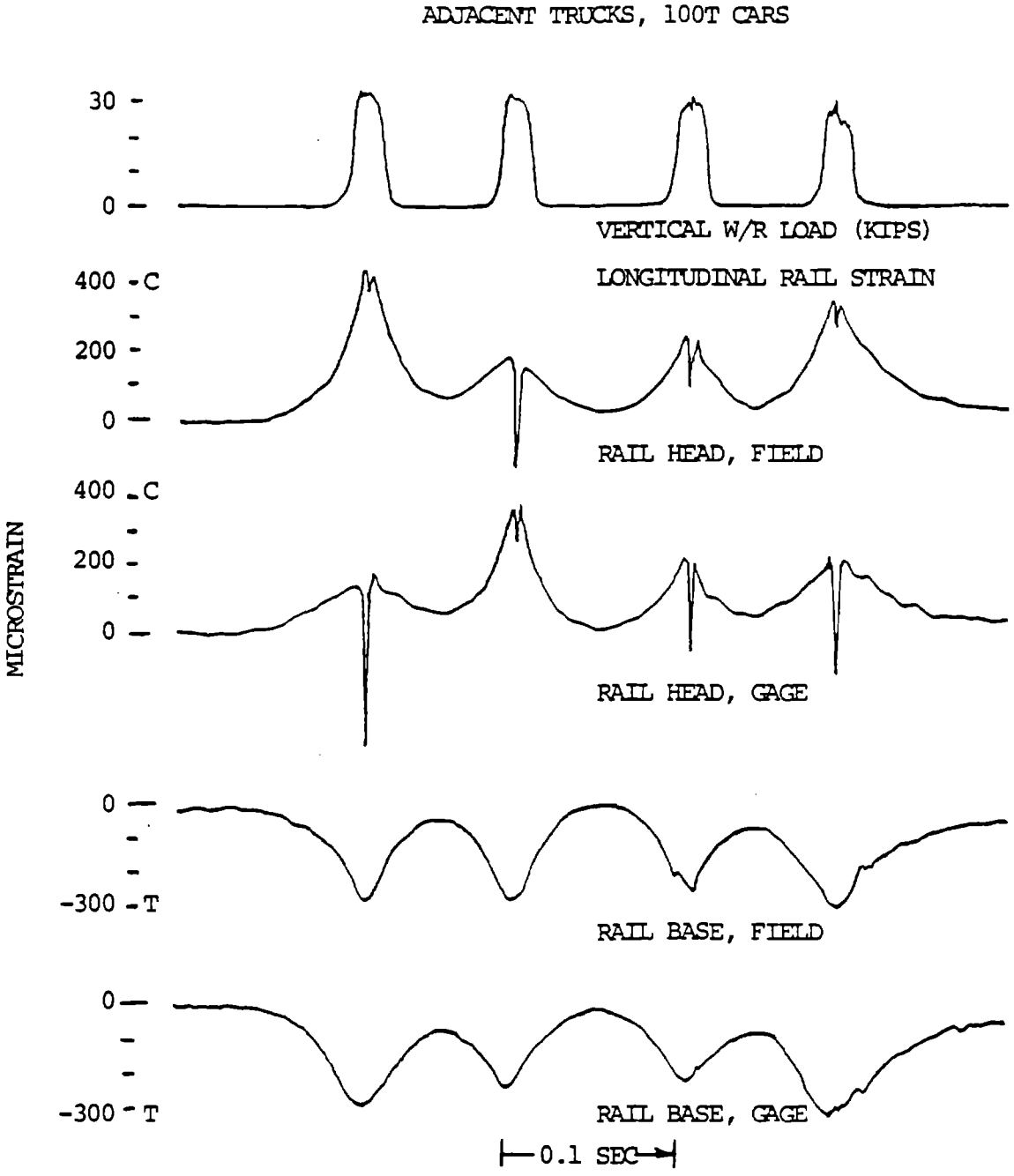

FIGURE 3-12. EXAMPLE OF RAIL HEAD STRAINS UNDER CHANGING TRANSVERSE POSITION OF THE W/R CONTACT PATCH -- RUN 18-14, 47 MPH, BJR TANGENT TRACK SECTION

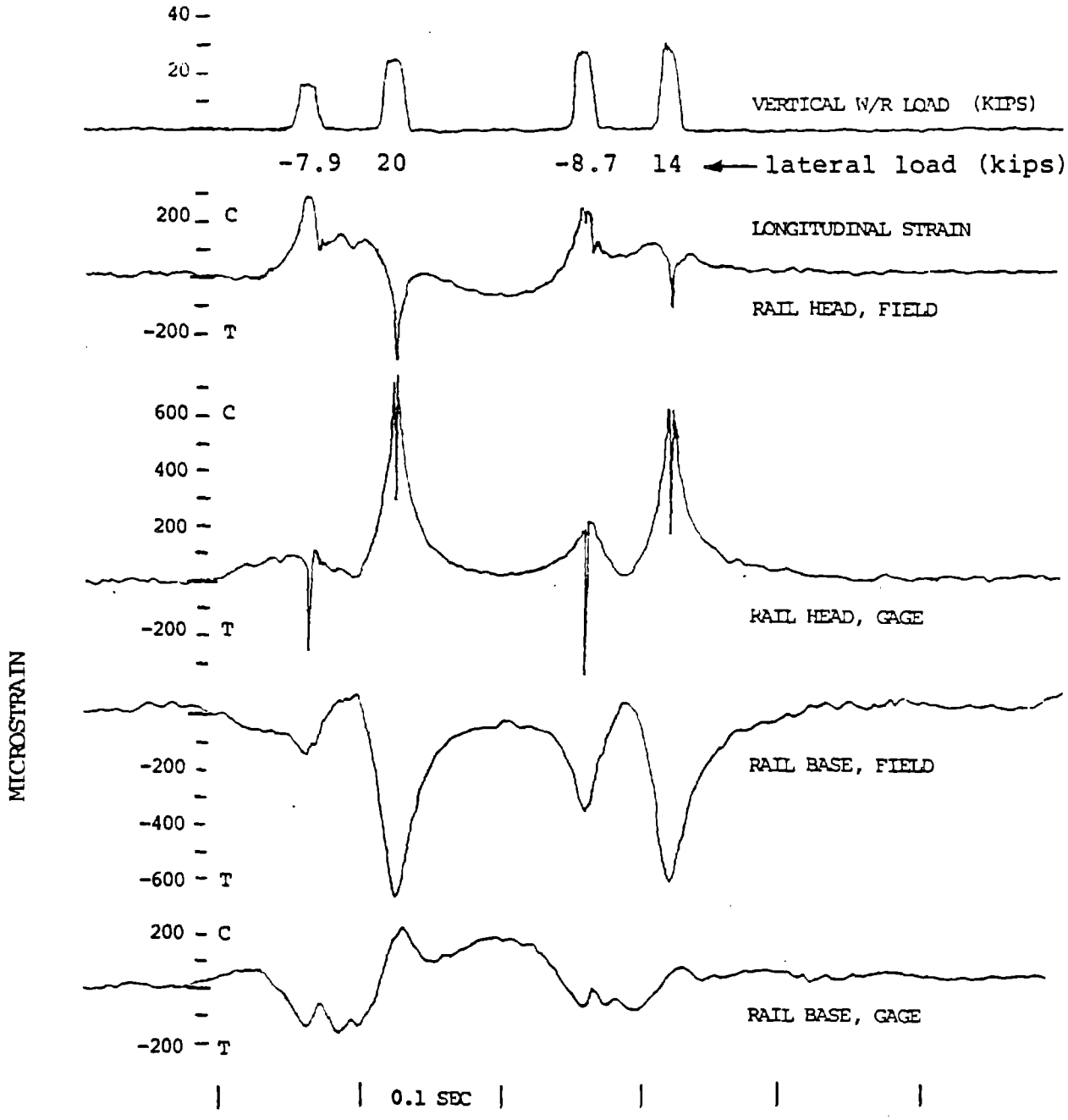

FIGURE 3-13. EXAMPLE OF LONGITUDINAL RAIL STRAINS DURING LATERAL LOADING AND HARD FLANGE CONTACT -- RUN 18-4, 64 MPH, BJR TRACK SECTION

base on the field side. The wheels of both trucks are obviously contacting the rail running surface well to the gage side, based on the strong strain reversal effect, in spite of inwardly-directed creep forces of 35 kN (8000 lb) and 38 kN (9000 lb) on the leading wheels.

Flat wheel impact loads up to 463 kN (104,000 lb) were recorded during these load measurement tests. An examination of a number of trains on both the BJR and CWR test sections, however, indicated no vertical loads greater than 254 kN (57,000 lb) at Site 6, the location of the longitudinal gages. Axles that were known to have caused impact loads of 356 kN (80,000 lb) to 431 kN (97,000 lb) at other sites[14] did not strike Site 6. These same wheelsets produced longitudinal strain oscillations less than 200 microstrain peak-to-peak when impacting no further than 1.4 m (4.7 ft) from the site. The peak load of 254 kN (57,000 lb) impacting at Site 6 on BJR track produced a 430 microstrain compression peak on the gage side, and bending wave oscillations of 200 microstrain peak-to-peak when impacting about 2.7 m (9 ft) away from the site.

An example of a wheel flat on an empty car is shown in Figure 3-14. The wheel flat is seen to impact roughly 2.7 m (9 ft) ahead of the site in the bending strain response of the longitudinal gages. Note also the response of the rail web shear strain gages of the wheel/rail vertical load circuit as the impact shear wave passes. (This is one reason why wheel detector transducers have been used for automated data processing, rather than the vertical wheel load itself, to avoid "false wheels" due to flat wheel impact loads under empty cars.) The impact at the site produces a 133 kN (30,000 lb) peak load on a 45 kN (10,000 lb) static wheel load approximately 1.9 milliseconds in duration, and a 200-Hz oscillation in longitudinal strains. Higher frequency components (300-350 Hz, 450-500 Hz, and a 900-1100 Hz "background noise") were also noted under a variety of wheel flats.

The Site 6 strain gage location in the BJR track section was located 4.3 m (14 ft) from the nearest joint in that rail. From the track geometry survey of rail surface, this joint was judged to be "average", on the order of 6 mm (1/4 in.) low. No evidence of higher-frequency (P_1) joint impact-induced strains was observed in any of the oscillographic recordings. An example of a flat wheel on a loaded 100-ton car is shown in Figure 3-15. This wheel evidently has two flat spots, the first about 67 cm (1.7 ft, or 65°) ahead of the flat impacting at Site 6. The next impact of this flat, about 2.7 m (9 ft) further down the rail, is

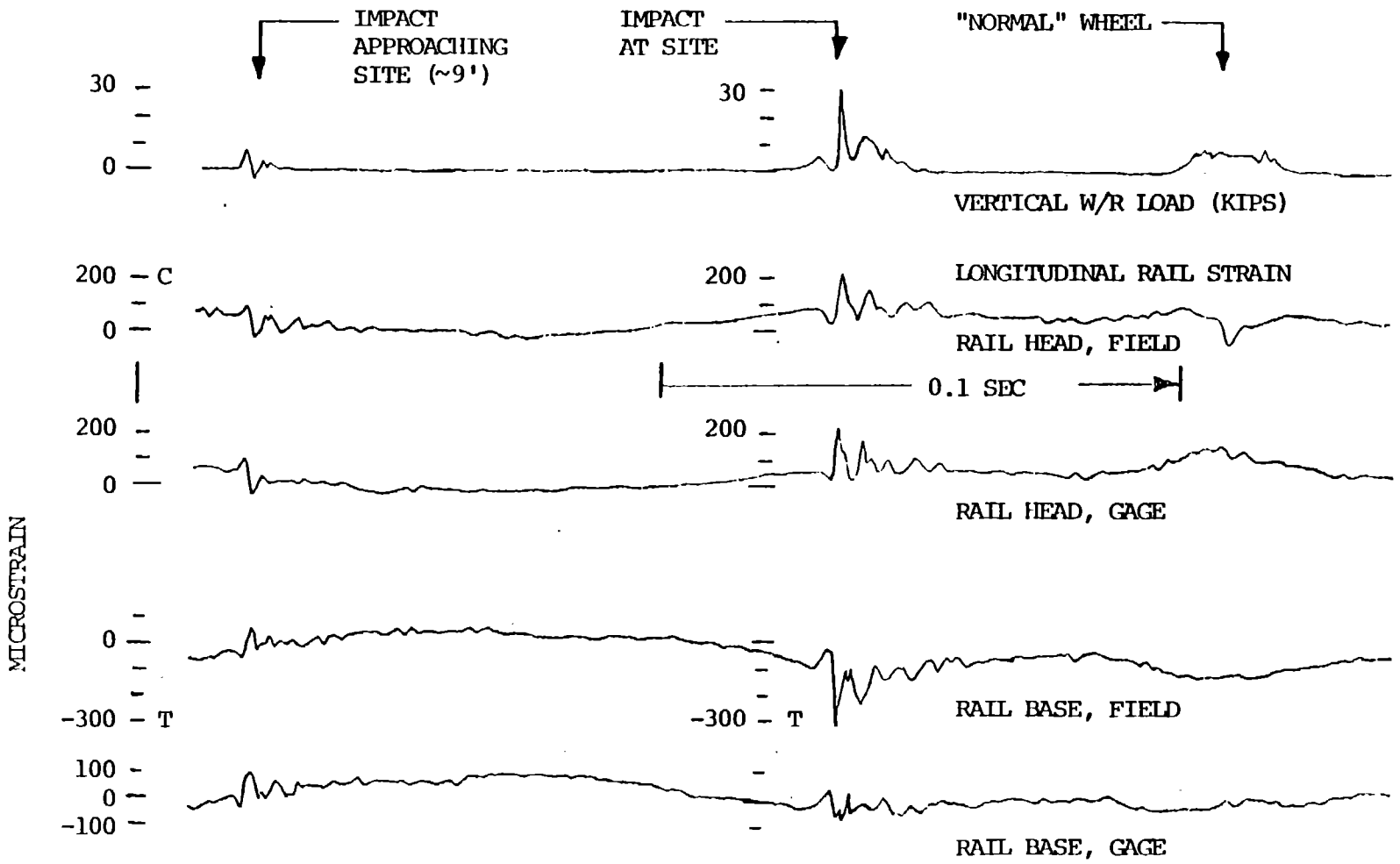

FIGURE 3-14. EXAMPLE OF LONGITUDINAL STRAINS UNDER FLAT WHEEL ON EMPTY CAR -- RUN 18-15, 55 MPH, BJR TRACK SECTION

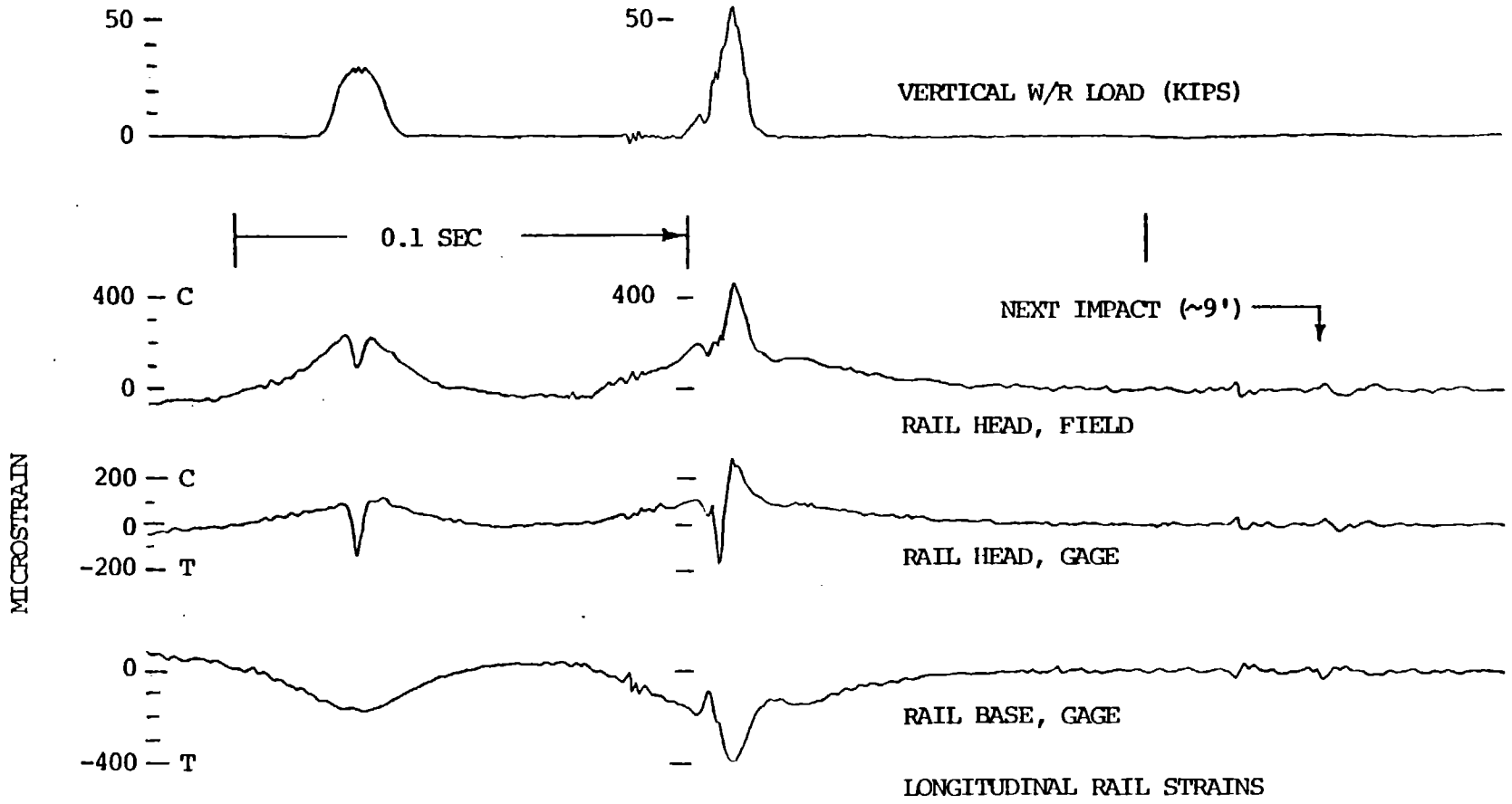

FIGURE 3-15. EXAMPLE OF LONGITUDINAL RAIL STRAINS UNDER FLAT WHEEL ON LOADED CAR -- RUN 31-14, 50 MPH, CWR TRACK SECTION

considerably attenuated on this CWR track, resulting in strains less than 100 microstrain peak-to-peak.

Based on the longitudinal strain data examined in this study, there is no evidence that high-level bending strains are propagated for any great distance along the rail.* Longitudinal strains measured on the rail head fillet or the rail base did not exceed 200 microstrain peak-to-peak from severe flat wheel impact loads beyond the nearest tie. The nearest wheels (between the measurement point and the impact point) were found to attenuate the longitudinal strains well below 50 microstrain, so that impacts were hardly discernible in the background vibration levels. There was no evidence of longitudinal strains due to joint impact loads at a relatively low joint (9 to 10 mm in depth) located 4.3 m (14 ft) from the measurement site. The most severe longitudinal strains noted on the underside of the rail head were due to the head bending as a continuous beam on the web as a foundation, which resulted in tensile-directed strains in an "influence zone" within a few inches of the contact patch. The normally compressive rail head strains (as the wheel approaches) will suddenly reverse directly under the wheel, as shown in Figure 3-12. Combined with lateral load effects, these rail head fillet strains were noted to range up to 350 microstrain (72.4 MN/m^2, 10,500 lb/in^2 in stress) tensile from the rail "zero" strain level. Tensile strains directly under a flat wheel impact from a loaded freight car may range as high as 700 microstrain. This dynamic strain, superimposed on the tensile stresses existing in cold rail, could strongly influence rail flaw initiation, growth, and ultimate fracture.

3.5 LABORATORY RAIL IMPACT EXPERIMENTS

To further investigate the phenomena of impact load-induced strains propagated along the rail from the point of loading, a relatively simple experiment was set up in Battelle's laboratory.

*The "hogging strains" noted by British Rail researchers is due most probably to the longitudinal component of the vertical impact load induced by using an "analogous wheel flat," an indentation in the rail.

A 13-ft length of 131 lb/yd worn rail was used for these experiments. The rail was ultrasonically examined to assure that the rail head contained no major flaws. Two 1/16-inch strain gages were placed 21 inches apart in a longitudinal orientation on the bottom of the rail head, 3/8 inch in from the gage surface. Experimental dimensions are shown in the sketch in Figure 3-16.

Each strain gage was powered from a constant-voltage supply as shown in the circuit of Figure 3-17. A Hewlett-Packard dual-channel digital signal analyzer (Model 5420A) with a maximum 75 kHz per channel sampling rate (25.6 kHz data bandwidth) was used to monitor the transient strain pulses. This allowed display of both time history and amplitude spectrum plots of both gage outputs, as well as digital plotting and storage of results on cassette tape for further analysis, if required. Signals were calibrated directly in microstrain. A 7-pound hammer was used to generate the force impulse, and the analyzer was triggered by an electrical circuit through the hammer and rail.

The experimental set-up was checked by striking the rail at one end (Point A, Figure 3-16) at the neutral axis, setting up the classical reflected stress wave patterns shown in Figure 3-18. By checking the time between positive-going strain peaks, a wave propagation rate of 201,000 in/sec is calculated, which closely matches the theoretical rate:

$$c = \sqrt{E/\rho} = 30(10)^6\ (386)/(0.281)]^{0.5} = 202{,}000 \text{ in/sec.} \qquad [13]$$

It can be seen that this type of stress wave has very little attenuation in the rail. A vertical hammer blow directly over Gage 1 (see Figure 3-16) is shown in Figure 3-19 to result in a half-sine tensile strain pulse from this gage, roughly 300 microseconds in duration and 540 microstrain in amplitude. This is due to the rail head bending as a beam on the web as a continuous foundation. Gage 2 responds with a strain peak of 74 microstrain (tensile) 350 microseconds later, at an apparent propagation rate of 60,000 in/sec. The propagation rate of a bending wave in a beam is dependent upon the frequency of forced oscillation[18], so that

$$c_b = [\omega^2 E h^2 / 12 \rho_m]^{1/4} \qquad [14]$$

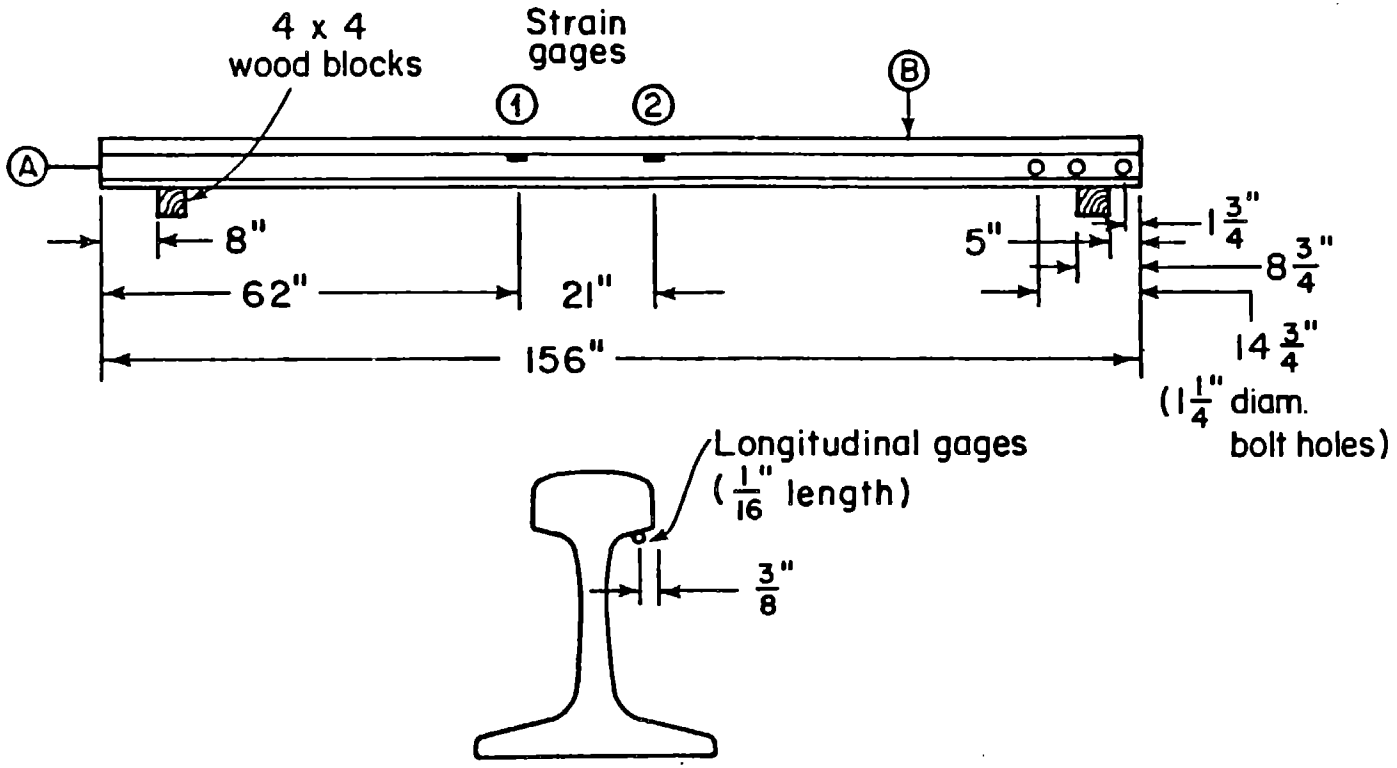

FIGURE 3-16. DIMENSIONS OF RAIL IMPACT EXPERIMENT

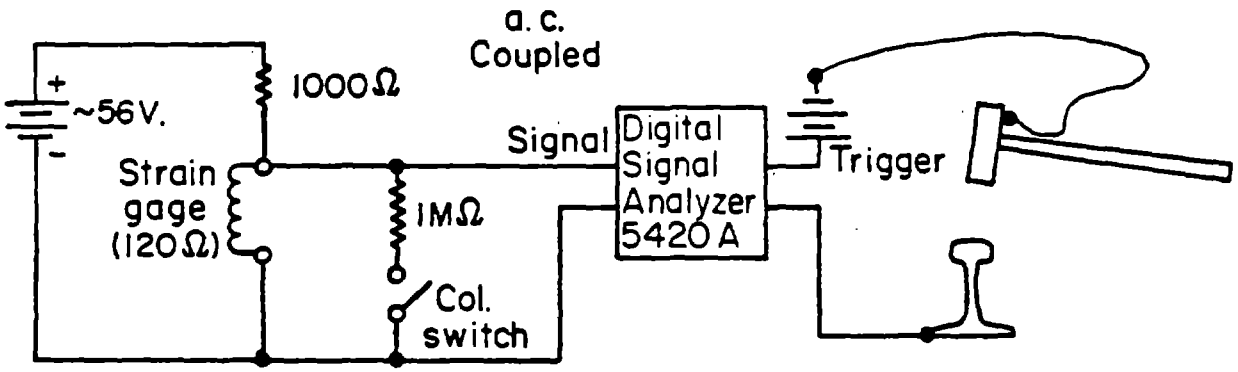

FIGURE 3-17. CIRCUIT DIAGRAM OF RAIL IMPACT EXPERIMENTS

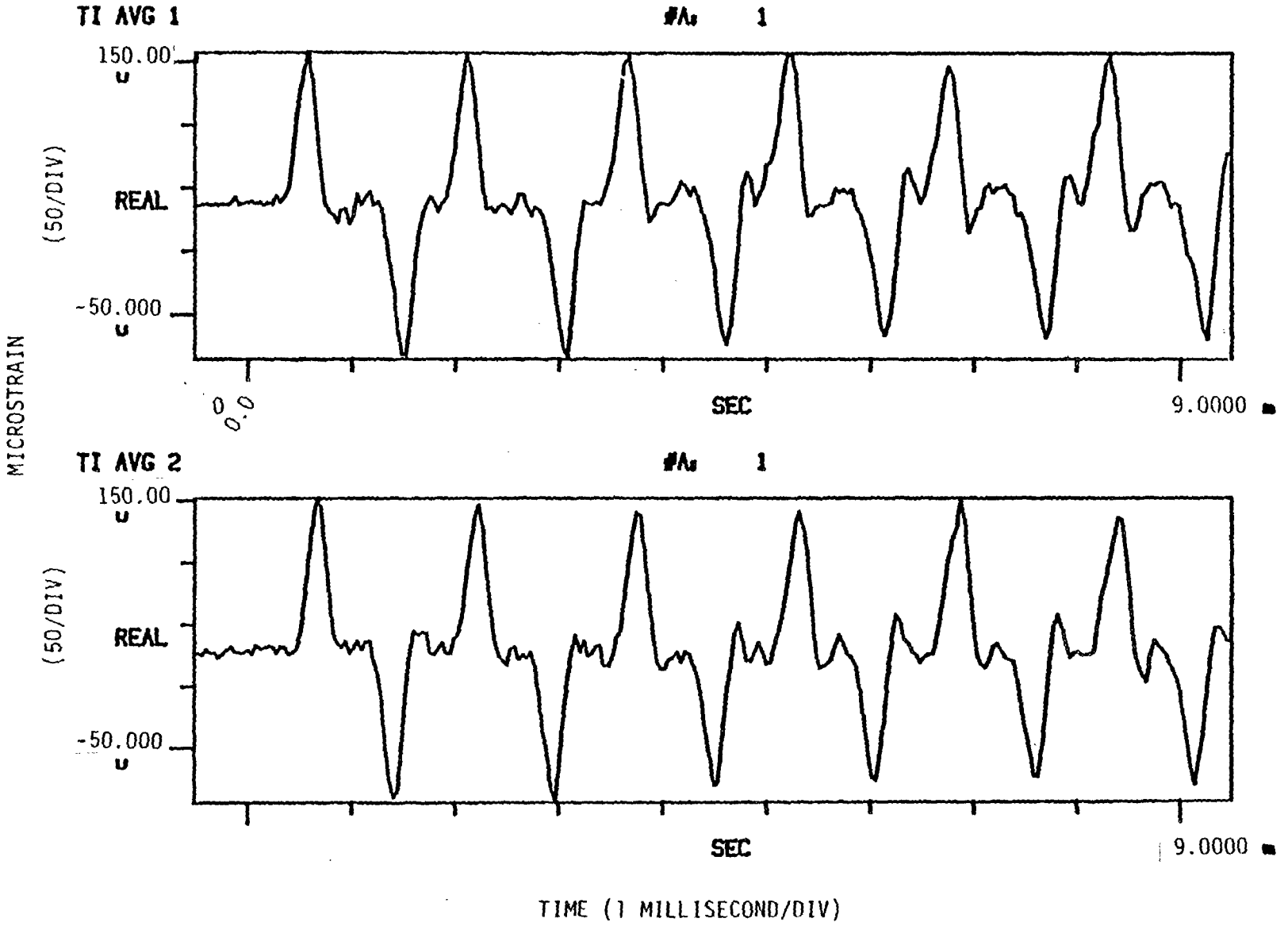

FIGURE 3-18. STRAIN GAGE RESPONSE TO LONGITUDINAL IMPACT AT RAIL END, NEUTRAL AXIS (LONGITUDINAL GAGES ON UNDERSIDE OF RAIL HEAD)

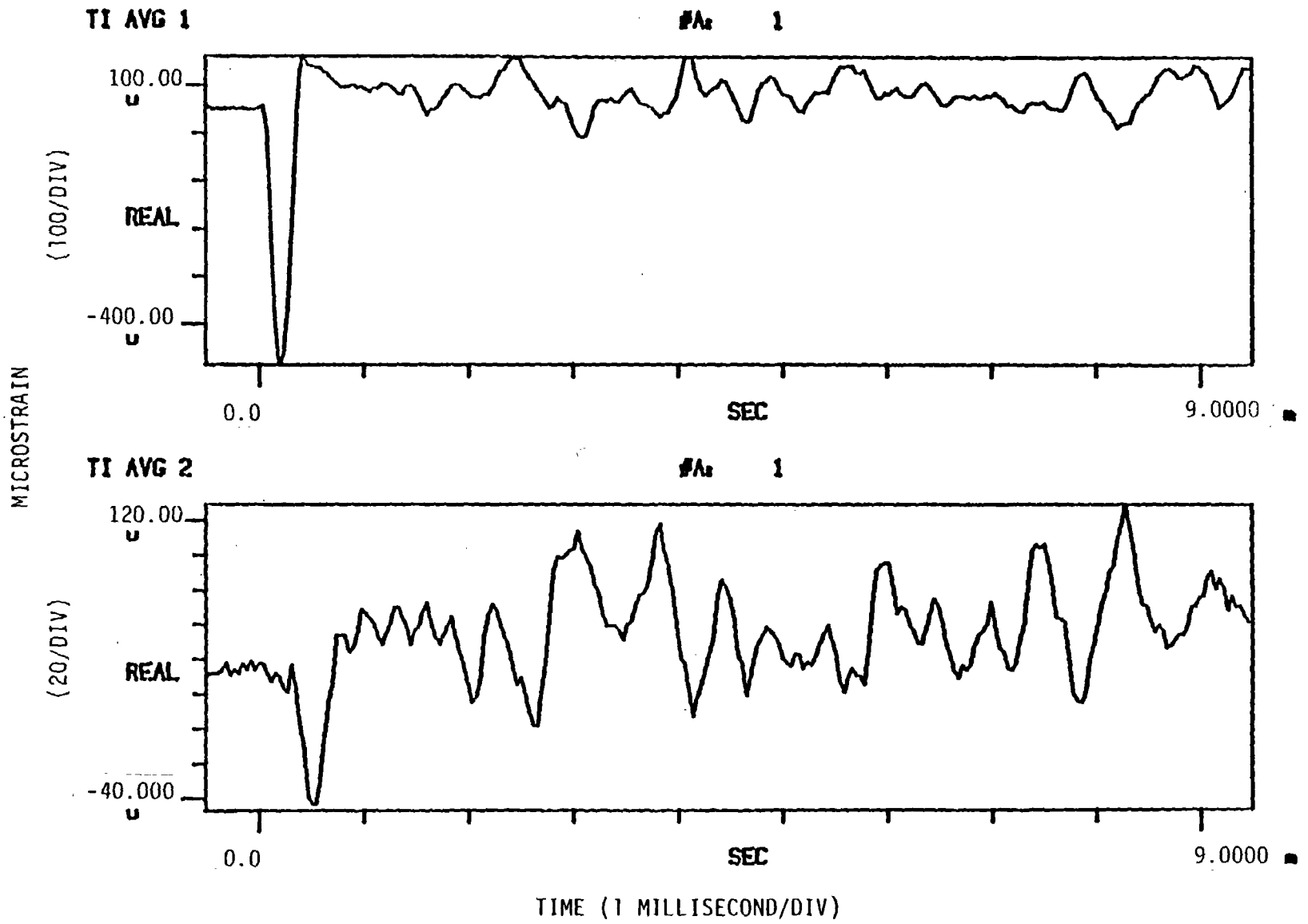

FIGURE 3-19. STRAIN GAGE RESPONSE TO VERTICAL IMPACT DIRECTLY OVER GAGE #1 (LONGITUDINAL GAGES ON UNDERSIDE OF RAIL HEAD)

where

ω = forcing frequency, rad/sec

E = modulus of elasticity

h = beam (rail head) thickness in direction of bending

ρ_m = density.

If we assume a fundamental period for the hammer blow of 600 microseconds (ω= 10,470 rad/sec), a propagation rate of 30,300 in/sec may be calculated. The effect of the web as a continuous foundation, therefore, doubles the free-beam wave propagation rate. Bending wave propagation rates for the rail as a whole may also be calculated:

$$c_b = [\omega^2 EI/\rho_m A]^{1/4} \qquad [15]$$

where

I = moment of inertia in bending

A = cross-sectional area.

Again, using the half-sine fundamental frequency of 10,470 rad/sec, the wave propagation rate is calculated at 72,700 in/sec. However, the strain pulse at Gage 2 in Figure 3-19 is tensile ("hogging"), so the phenomenon is not whole-rail bending, but is associated with the head itself. This is explored further in Figure 3-20, where the average transient responses to 10 hammer blows at Point B (see Figure 3-16), which is 60 inches from Gage 1, 39 inches from Gage 2, are plotted. Again, a pronounced tensile strain peak (100 to 110 microstrain) is seen, with a propagation rate of ~60,000 in/sec (1,525 m/sec). After this point, of course, the effects of whole-rail bending and longitudinal reflected stress waves tend to confuse the picture. Note that the initial "zero" strain value is due to "front-end" offsets or common mode errors, not to an actual strain level in the rail.

Amplitude spectra were generated for the two strain gages in response to a hammer blow directly over Gage 1, using an analysis bandwidth of 12.5 kHz. These spectra are plotted in Figures 3-21 and 3-22. Above 2 kHz the strain amplitude spectrum is attenuated by 24 dB (a ratio of 15.8) from peaks below 1 kHz for Gage 1, and by 20 dB (a ratio of 10) from peaks below 1 kHz for Gage 2. The strain

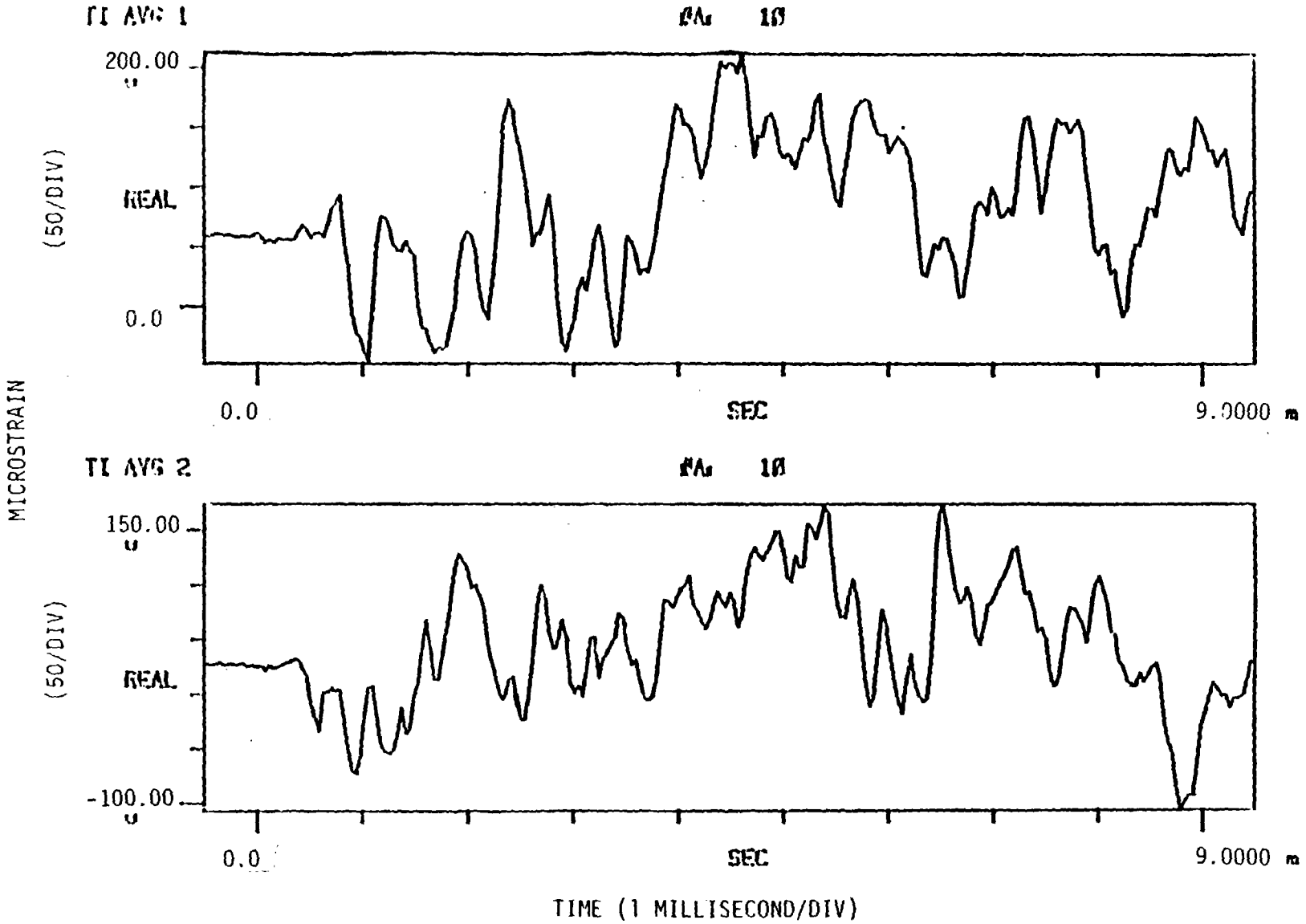

FIGURE 3-20. STRAIN GAGE RESPONSE TO VERTICAL IMPACT 1 METER BEYOND GAGE #2, AVERAGE OF 10 IMPACTS (LONGITUDINAL GAGES ON UNDERSIDE OF RAIL HEAD)

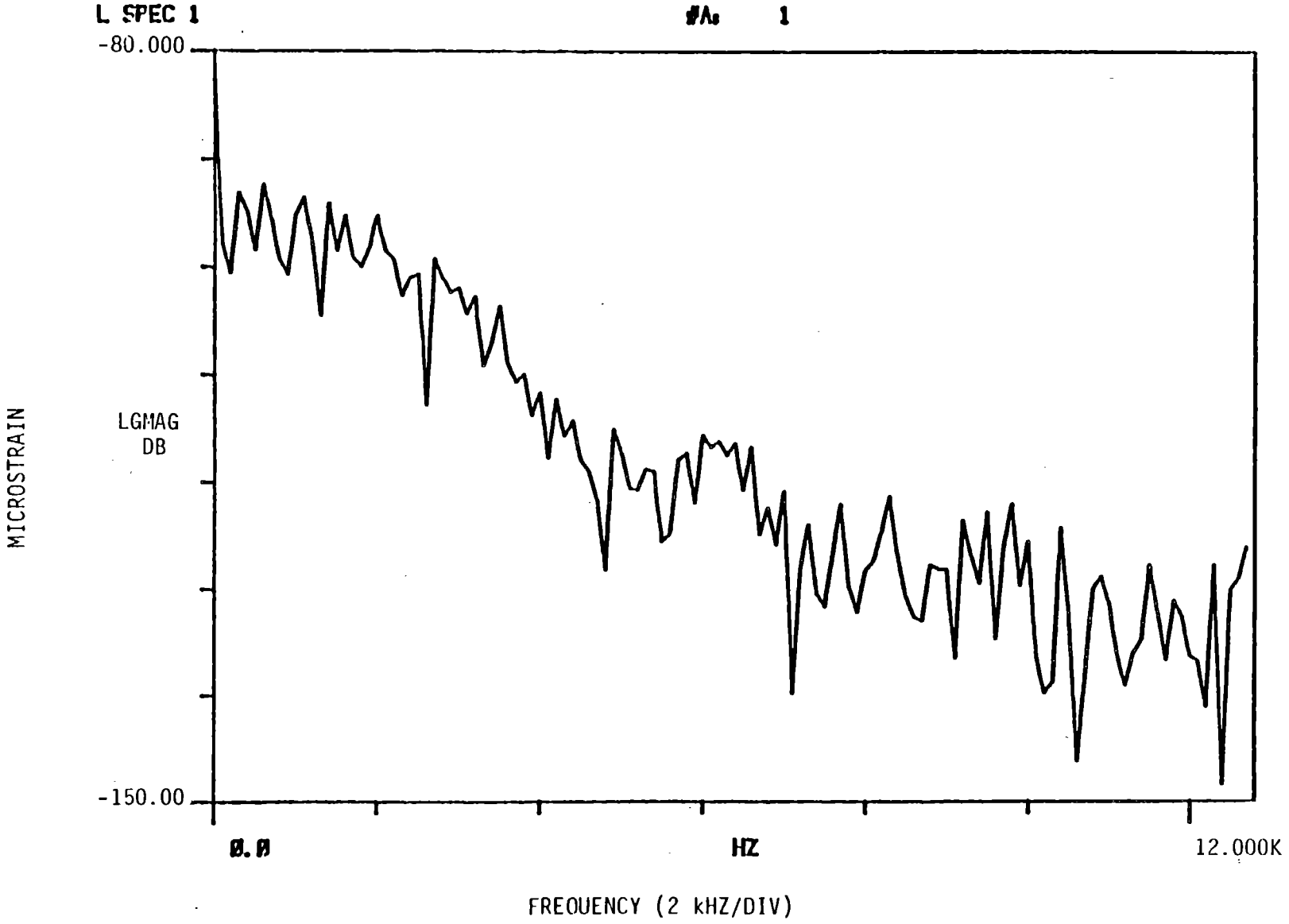

FIGURE 3-21. AMPLITUDE SPECTRUM OF STRAIN GAGE #1 RESPONSE TO VERTICAL IMPACT DIRECTLY OVER GAGE (SEE FIGURE 3-19)

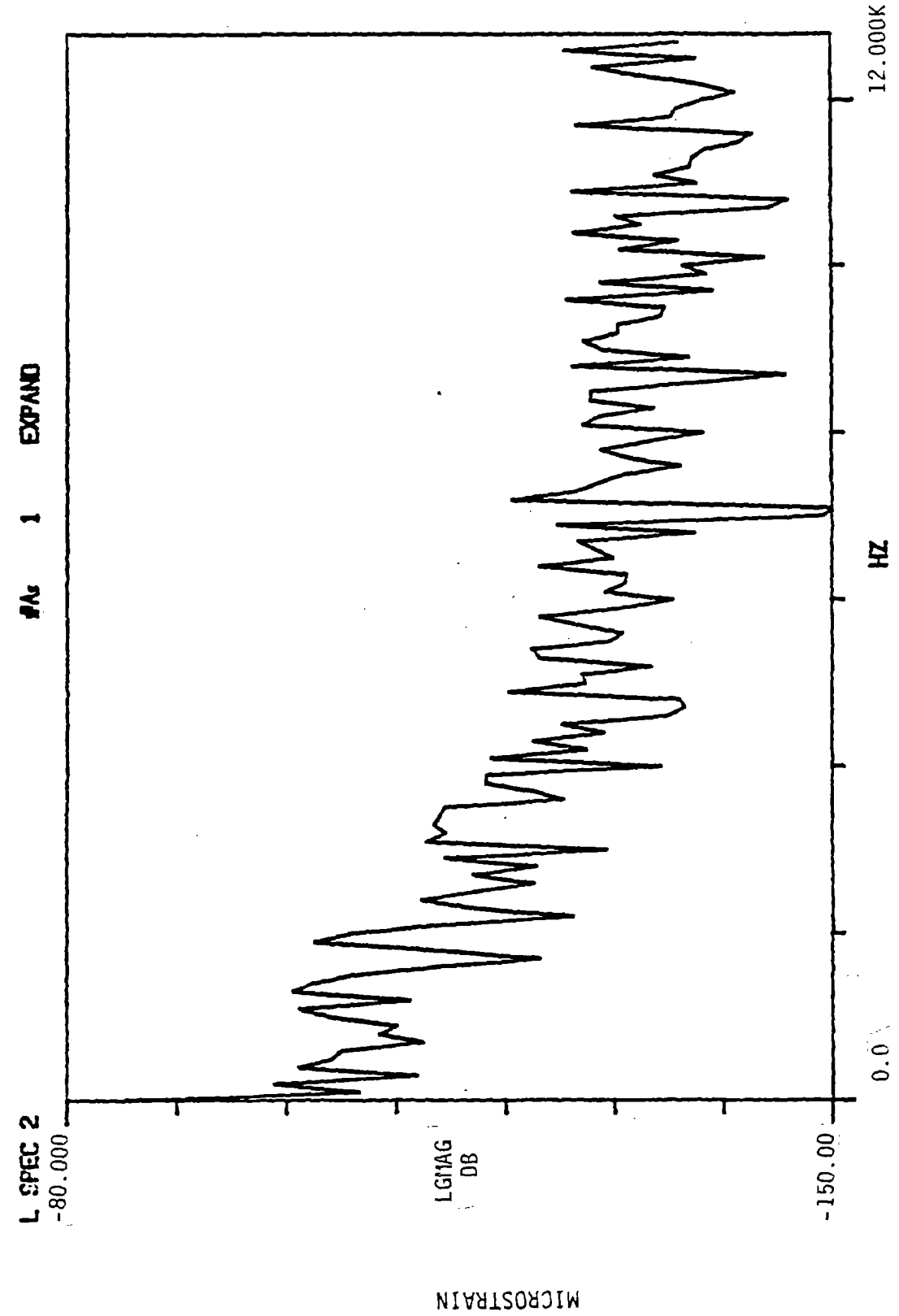

FIGURE 3-22. AMPLITUDE SPECTRUM OF STRAIN GAGE #2 RESPONSE TO VERTICAL IMPACT AT GAGE #1 (21" AWAY)

amplitude spectrum of Gage 2 is 7.5 dB lower (a ratio of 2.4) than the spectrum of Gage 1 for peaks below 1 kHz. This indicates that a bandwidth of 2.0 to 2.5 kHz is sufficient to characterize impact-induced strain phenomena in the rail. Amplitude spectra for the two gages in response to 10 hammer blows at Point B are shown in Figures 3-23 and 3-24 for a 12.4 kHz analysis bandwidth and the plots expanded to 4 kHz. Dissimilarities in the spectra are due to the relative positions of the gages with respect to reflected stress waves in the 13-foot rail length.

From these experiments we may deduce that the tensile strain pulse at the base of the rail head is primarily a bending wave propagated in the rail head as a beam on the web as a foundation. Since the wave velocity is dependent on the impulse wavelength (frequency), the rail will act as a dispersive medium and the pulse will change shape as it propagates[18,19], and will be attenuated by losses in the medium. It appears that the tensile strain at a remote gage is substantially less than the tensile strain directly under the impact load (by a factor of 7 in the example shown in Figure 3-19).

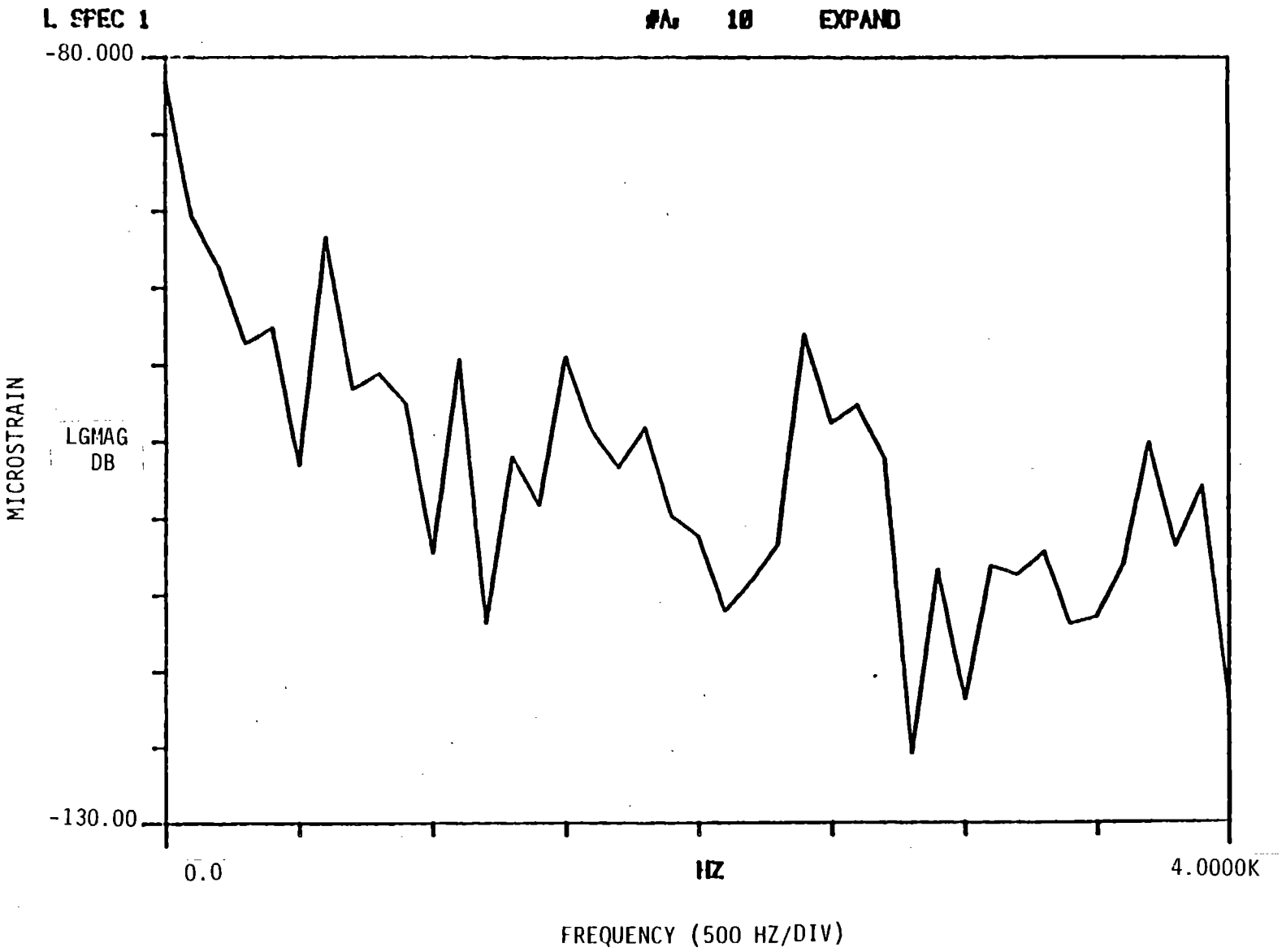

FIGURE 3-23. AMPLITUDE SPECTRUM OF STRAIN GAGE #1 RESPONSE TO VERTICAL IMPACT 1.5 METERS FROM GAGE (SEE FIGURE 3-20)

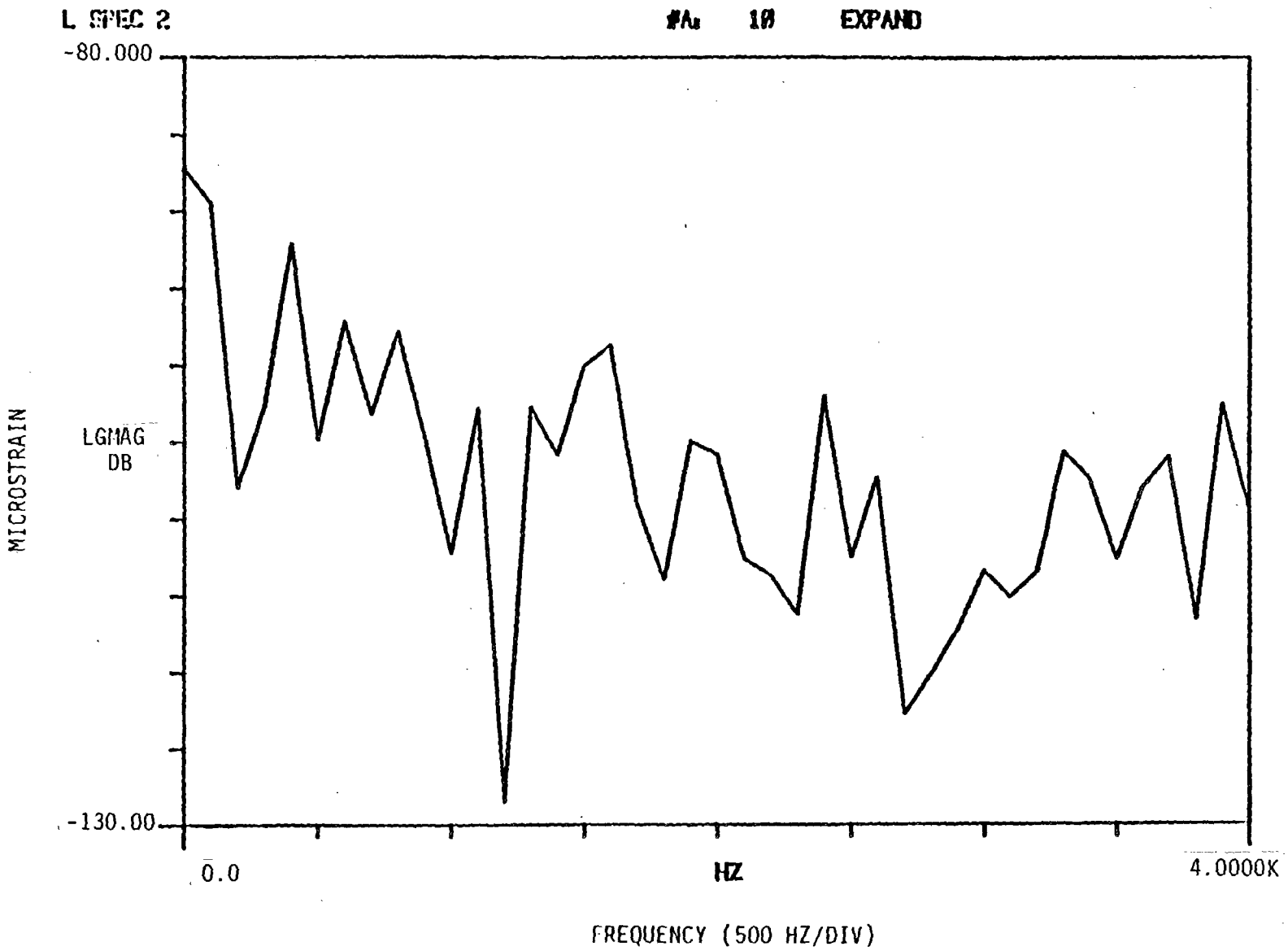

FIGURE 3-24. AMPLITUDE SPECTRUM OF STRAIN GAGE #2 RESPONSE TO VERTICAL IMPACT 0.5 METER FROM GAGE (SEE FIGURE 3-20)

4. COMPUTER SIMULATION OF IMPACT LOADS

4.1 THE MATHEMATICAL MODEL

The widespread interest in wheel/rail impact loads has led to the development and use of a wide variety of analytical models. These range in complexity from simple two-mass models to complex finite-element models of the track. Sato and Kosuge[20] have recently employed a simple lumped-parameter model consisting of the wheelset (unsprung) and rail effective masses to study rail head surface roughness on the high-speed Shinkansen line of the Japanese National Railways. Newton and Clark of British Railways, on the other hand, have used a much more complex hybrid model[21], which consists of a Discrete Support Model with a simple Euler beam to calculate the wheel/rail contact force, and then a Timoshenko beam model on elastic (Winkler) foundation to calculate rail strains in response to this force. In this discrete support model, a modal analysis is used to calculate the forced motion of the track, using the normal modes associated with the undamped track natural frequencies. A similar approach was employed by Mair[22,23] in his study of rail corrugation.

Battelle's vertical wheel/rail impact load model was originally developed to explore the effects of rail joint and flat wheel geometries on wood-tie track structures.[24] This simplified, 4 degree-of-freedom (DOF) lumped-parameter model consisted of two track masses (the effective rail and tie/ballast masses) and two vehicle masses (an unsprung wheelset and a sprung half-car body). The nonlinear Hertzian contact stiffness between wheel and rail suggested by Jenkins [4] was programmed, as well as zero negative force (wheel lift). A nonlinear stiffness K_R between the rail and track structural mass (tie and ballast) was used to simulate the observed stiffening behavior[13] under increasing load:

$$K_R = k(F_{wz}/F_o)^{0.5} \qquad [16]$$

where

F_{wz} = vertical wheel/rail force

F_o = static wheel load

k = a constant.

Track mass, stiffness and damping parameters were calculated from the traditional beam-on-elastic-foundation (BOEF) relationships. Model-predicted loads compared well with wheel loads measured with an instrumented wheelset on a 100-ton hopper car.[13] In this same study, impact loads were measured by rail strain-gage circuits under passing revenue trains. Although the actual wheel profile geometries were not known, the load magnitudes and time durations compared well with predictions from the model using assumed wheel flat shapes on wood tie track. Equations and parameters for this model are given in Tables 4-1 and 4-2, respectively.

Efforts to use this simple model to predict impact loads on stiffer concrete-tie track, however, were not successful. As predicted by Newton and Clark,[21] the simple BOEF model tended to overestimate the peak impact loads. Additional degrees of freedom were added to the model, including the side frame/equalizer beam mass and mass-moment of inertia. Tie and ballast masses were separated and a nonlinear rail/tie (pad) stiffness was added, based on laboratory test results. This seven degree-of-freedom (DOF) model shown in Figure 4-1 predicted impact loads that compared well with measured loads under a known wheel profile.[25]

A specialized version of the computer program, called IMPWHL, was created to use the measured circumferential wheel profile data. The measurements of effective wheel rolling radius are introduced in tabular form, up to 120 points, on given length increments. The program currently uses a simple linear interpolation between points to generate the wheel/rail vertical error position and velocity. Other mathematical methods for providing a smoother input function, such as the cubic spline, have been considered; but the results to date do not justify the use of these more complex algorithms.

Initial computer runs with the measured profiles were compared with time-history traces of impact loads "captured" within the influence zones of the impact detector circuits. This provided a short time-history "snapshot" of the passing wheel load -- roughly 8 milliseconds at full amplitude at 60 mph (97 km/h), only 4 milliseconds at 120 mph (193 km/h). If the initial impact occurred at the leading "skirt" of the circuit, the secondary load peaks could be observed. By repeated runs, a fairly complete picture of load response could be reconstructed.

TABLE 4-1. EQUATIONS OF MOTION FOR SIMPLIFIED (4 DOF) WHEEL/RAIL IMPACT LOAD MODEL

$\ddot{Z}_c$	$= 4F_{kz}/M_c$	(1)
$\ddot{Z}_a$	$= (F_{wz} - F_{st} - R_c F_{kz})/M_a$	(2)
$\ddot{Z}_r$	$= (F_{tr} - F_{wz})/M_r$	(3)
$\ddot{Z}_t$	$= (F_{tt} - F_{tr})/M_t$	(4)
F_{kz}	$= [F_{snub}\,\mathrm{sign}(\frac{d}{dt}) + K_z][R_c Z_a - \rho Z_c]$	(5)
	where $\rho = 2$ for rail joint, 1 for wheel flats	
R_c	$= (1 + L_{ba}/g)/4$ for joint, $= 1/2$ for wheel flats	(6)
F_{wz}	$= (2K_H\,\Delta Z_w/3)^{1.5} + C_H\,\Delta\dot{Z}_2 \geq 0$	(7)
ΔZ_w	$= Z_r - Z_a + e_z + \Delta Z_H$	(8)
$\Delta\dot{Z}_w$	$= \dot{Z}_r - \dot{Z}_a + \dot{e}_z$	(9)
ΔZ_H	$= 1.5(F_{st})^{.6667}/K_H$	(10)
F_{tr}	$= (0.5K_J\,\Delta Z_{tr})^2 + C_r\,\Delta\dot{Z}_{tr}$	(11)
ΔZ_{tr}	$= Z_t - Z_r + \Delta Z_r$	(12)
$\Delta\dot{Z}_{tr}$	$= \dot{Z}_t - \dot{Z}_r$	(13)
ΔZ_r	$= 2(F_{st})^{0.5}/K_r$	(14)
K_J	$= K_r\, f(e_z)$ for rail joint, $= K_r$ for wheel flats	(15)
F_{tt}	$= K_t\,\Delta Z_{tt} - C_t\dot{Z}_t$	(16)
ΔZ_t	$= F_{st}/K_t$	(17)

TABLE 4-2. PARAMETERS FOR 4 DOF WHEEL/RAIL IMPACT LOAD MODEL

	Parameter	Rail Joint	Flat Wheel	Units
WCAR	Weight of car body and cargo	.1840E+6	.2416E+6	lb
WTRF	Weight of truck frame (bolster)	.1700E+4	.1700E+4	lb
WSF	Weight of side frame	.1500E+4	.1500E+4	lb
WAXLE	Weight of axle	.1710E+4	.1710E+4	lb
WHL	Weight of wheel	.7700E+3	.7700E+3	lb
WRT	Effective weight of rail	.1270E+3	.1230E+3	lb
WTB	Effective weight of tie/ballast	.6390E+3	.5270E+3	lb
KZ	Spring group vertical stiffness	.2500E+5	.2500E+5	lb/in
KEH	Wheel/rail contact stiffness*	.8930E+7	.9690E+7	lb/in
KRR	Rail/tie stiffness*	.1650E+7	.1800E+7	lb/in
KTT	Tie/ballast stiffness*	.3260E+6	.5890E+6	lb/in
FSNUB	Spring group vertical snubbing	.2310E+4	.2310E+6	lb
CH	Wheel/rail damping	.3430E+3	.3520E+3	lb-sec/in
CR	Rail/tie damping	.8850E+3**	.9110E+3**	lb-sec/in
CT	Tie/ballast damping	.4560E+3	.5980E+3	lb-sec/in
LBA	Side frame lateral separation	.7900E+2	.7900E+2	in
G	Effective gage	.5950E+2	.5950E+2	in
RWHL	Wheel tread radius	.1800E+2	.1800E+2	in
EIRAIL	EI of rail (133 lb/yd)	.2490E+10	.2490E+10	lb/in^2
DT	Integration step size	.500E-3	.0100E-3	sec
DELSM	Long wavelength joint dip	.400E+0		in
DELCSP	Short wavelength joint dip	.1000E+0		in
RJ	Ratio, joint to nominal stiffness	.7500E+0		
BETAT	5/("track span")	.0208E+0		in^{-1}
BETAR	5/("rail span")	.1080E+0		in^{-1}
DELZR	Rail deflection*	.3127E-1	.3667E-1	in
DELZT	Tie/ballast deflection*	.7914E-1	.5603E-1	in
DELZH	Wheel/rail contact approach*	.4335E-2	.5108E-2	in
MA	Wheelset effective mass	.4767E+1	.5055E+1	$lb\text{-}sec^2/in$
KTR	Track structure overall stiffness	.2722E+6	.4438E+6	lb/in
FST	Static wheel vertical load	.2580E+5	.3300E+5	lb

*Under static wheel load.
**In compression (1/5 in extension stroke).

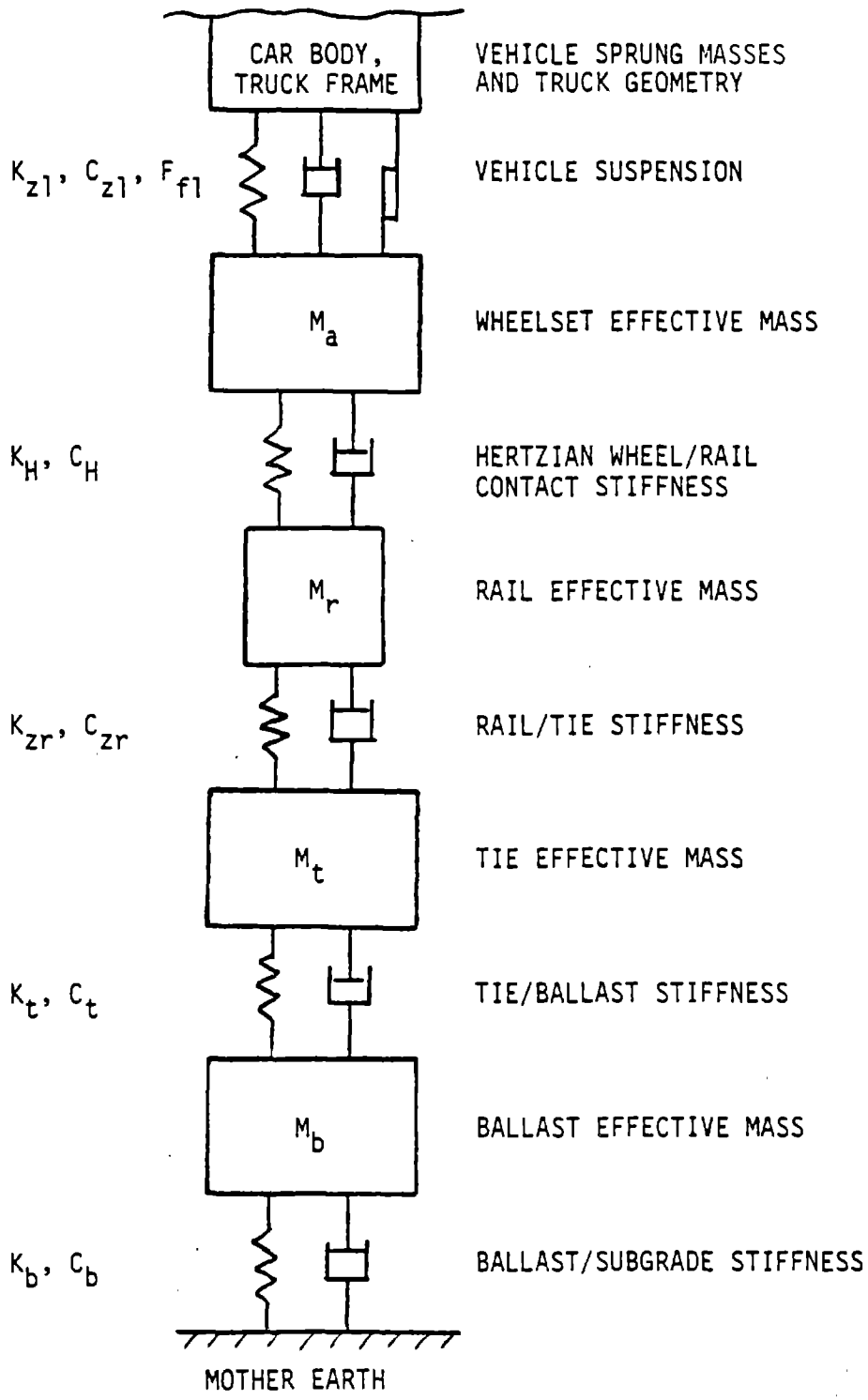

FIGURE 4-1. SKETCH OF 7 DOF WHEEL/RAIL DISCRETE-MASS IMPACT LOAD MODEL

These first computer runs showed a strong oscillatory load response at 330 Hz which was not observed in the measured loads. This frequency is prominent in the track response to a drop-hammer impact load with no preload, as shown in Figure 4-2; it is associated with the second (asymmetrical) transverse bending mode of the concrete tie. Tests[26] showed that this response peak is suppressed as the preloading wheelset is moved closer to the point of impact. It appeared that this tie bending mode could be acting as a tuned absorber, consequently, it was decided to include the first four tie transverse bending modes in the model.

Concrete tie bending modes were defined in laboratory tests on a similar CC-244 C tie, supported by pads under the rail seats. A modal analysis was performed on this tie using a Hewlett-Packard Model 5423A dual-channel analyzer by attaching an accelerometer to one corner and striking locations along the tie with an instrumented hammer. Results for the first three transverse bending modes are shown in Figure 4-3. (Two torsional bending modes at 365 and 406 Hz were also observed.) Based on an average bending rigidity from the first three measured modes, the fourth (asymmetrical) bending mode frequency was calculated to be 1033 Hz. Only the first bending mode of the tie appears to shift significantly in the track from the laboratory-measured value, increasing from 108 Hz to 154 Hz, as seen in Figure 4-2. Measured damping of these modes was small, roughly 0.5 percent of critical: as expected, the concrete tie literally "rings like a bell."

The approach used in modeling the tie bending modes is the mode-acceleration method described by Thomson[27] and Springfield[28], and employed by Sewell, Parish and Durling[29] to model rail vehicle body bending modes. Using this method, it is assumed that tie support is primarily in the rail seat area, so that the mode shape of a free-free beam and the transfer impedance at the rail seat may be used. Linear superposition of the deflections of the different mode shapes is then assumed. Starting with the Lagrange equation:

$$\frac{d}{dt}\frac{\partial T}{\partial \dot{q}_i} - \frac{\partial T}{\partial q_i} + \frac{\partial D}{\partial \dot{q}_i} + \frac{\partial V}{\partial q_i} = Q_i \qquad [17]$$

T = total kinetic energy,

D = total dissipated energy,

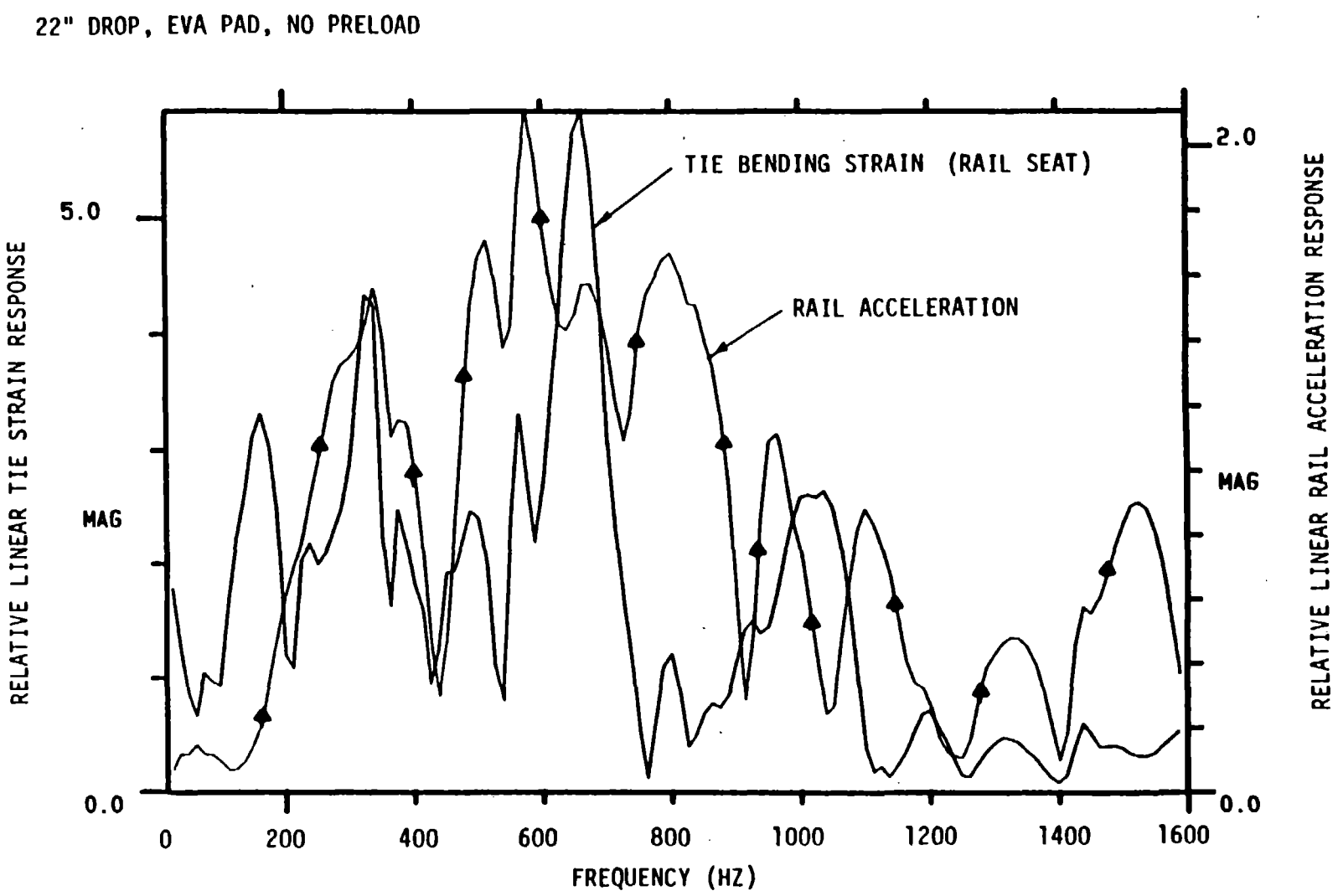

FIGURE 4-2. CONCRETE TIE TRACK RESPONSE TO DROP-HAMMER IMPACT LOAD

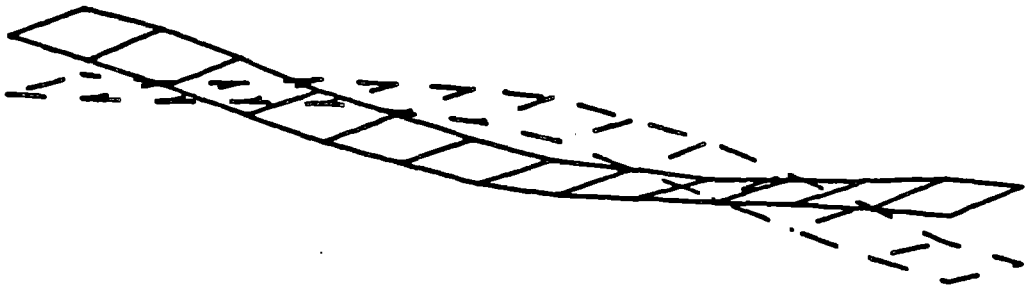

FIRST MODE: 108 HZ

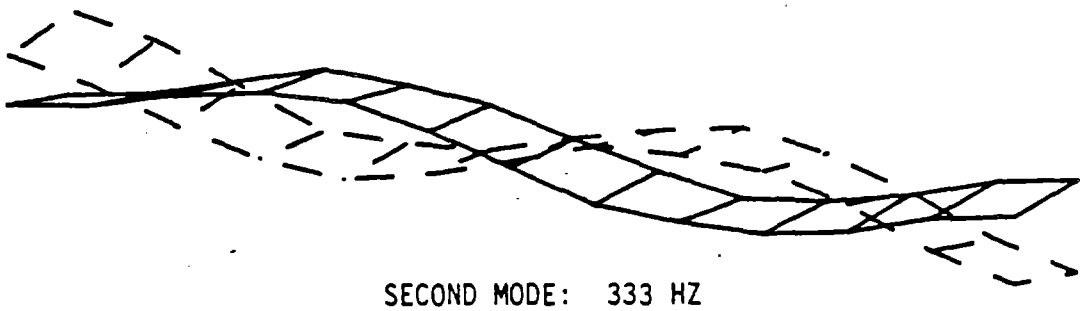

SECOND MODE: 333 HZ

THIRD MODE: 633 HZ

FIGURE 4-3. SHAPES OF CONCRETE TIE TRANSVERSE BENDING MODES

V = total potential energy,

q_i = generalized displacement,

$\dot{q}_i$ = generalized velocity,

Q_i = generalized force associated with i^{th} coordinate.

For the tie dynamic system sketched below:

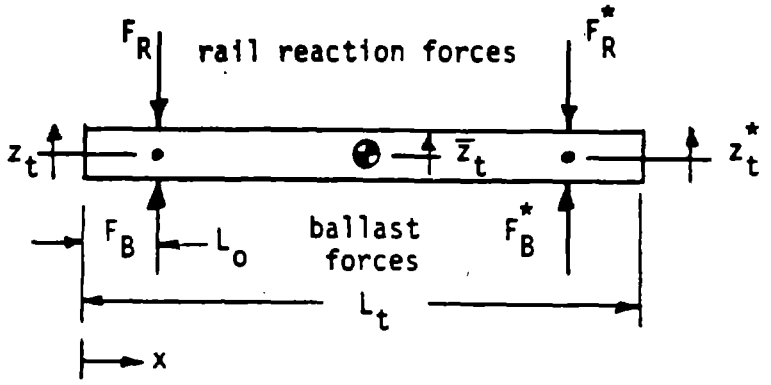

$$T = \frac{m}{2} \int_0^{L_t} [\, \dot{w}(x,t) + \dot{\bar{z}}(t) \,]^2 \, dx \qquad [18]$$

$w(x,t) = q(t)\ \phi(x)$, where $q(t)$ = generalized coordinate of the beam, $\phi(x)$ = the assumed mode shape.

$$V = \frac{EI_t}{2} \int_0^{L_t} [\, \frac{\partial^2 w(x,t)}{\partial x^2} \,]^2 dx \qquad [19]$$

$$D = \frac{C_t}{2} \int_0^{L_t} [\, \frac{\partial^2 \dot{w}(x,t)}{\partial x^2} \,]^2 dx \qquad [20]$$

$$Q = (F_B - F_R)\ \phi(L_o) + (F^*_B - F^*_R)\ \phi(L_t - L_o) \qquad [21]$$

For the assumed free-free beam bending mode shape, the n^{th} mode becomes:

$$\phi_n(x) = \cosh\beta_n x + \cos\beta_n x - \alpha_n(\sinh\beta_n x + \sin\beta_n x) \qquad [22]$$

where

$$(\cosh\beta_n L_t)(\cos\beta_n L_t) = 1 \qquad [23]$$

The integrals of the n^{th} mode shape descriptor then become:

$$\int_0^{L_t} \phi_n^2(x)\, dx = L_t \qquad [24a]$$

$$\int_0^{L_t} \phi_n(x)\, dx = 0 \qquad [24b]$$

$$\int_0^{L_t} \frac{d^2 \phi_n(x)}{dx^2}\, dx = \beta_n^4 L_t \qquad [24c]$$

The problem at this point becomes one of calculating numerical values for (in order) $\beta_n L_t$, α_n, $\Phi_n(L_o)$, $\phi_n(L_t - L_o)$, and $\beta_n^4 L_t$. Substituting the above integrals back into the Lagrange equation, we obtain:

$$\begin{aligned} &M_t \ddot{q}_n(t) + [2\xi_n \omega_n M_t + (C_r+C_t)\phi_n^2(L_o) + (C_r+C_t)\phi_n^2(L_t - L_o)]\dot{q}_n \\ &+[\omega_n^2 M_t+(K_r+K_t)\phi_n^2(L_o) + (K_r+K_t)\phi_n^2(L_t - L_o)]q_n \\ &+[\phi_n(L_o)]\,[C_r(\dot{\bar{z}}_t - \dot{z}_r) + C_t(\dot{\bar{z}}_t - \dot{z}_b) + K_r(\bar{z}_t - z_r) + K_t(\bar{z}_t - z_b)] \\ &+[\phi_n(L_t - L_o)]\,[C_r(\dot{\bar{z}}_t - \dot{z}_r^*) + C_t(\dot{\bar{z}}_t - \dot{z}^*) + K_r(\bar{z}_t - z_r^*) \\ &+K_t(\bar{z}_t - z_b^*)] = 0 \end{aligned} \qquad [25]$$

$$\begin{aligned} &M_t \ddot{\bar{z}}_t+(C_r+C_t)\dot{\bar{z}}_t + (K_r+K_t)\bar{z}_t - C_r(\dot{z}_r+\dot{z}_r^*) \\ &-K_r(z_r+z_r^*) - C_t(\dot{z}_b+\dot{z}_b^*) - K_t(z_b+z_b^*) \\ &+ \sum_1^n [\phi n(L_o) + \phi_n(L_t - L_o)]\,[(C_r+C_t)\dot{q}_n + (K_r+K_t)q_n] = 0 \end{aligned} \qquad [26]$$

where

$$\omega_n^2 = EI_t \beta_n^4 L/M_t \qquad [27]$$

$$2\xi_n \omega_n = C_t \beta_n^4 L/M_t \qquad [28]$$

An additional degree of freedom, the tie rigid-body roll mode (about the track longitudinal axis) can be added; however, it simplifies matters to consider just the dynamics of one rail (half the track) by letting $\bar{z}_t = z_t$, the vertical motion at the one rail seat, and dropping the $\Phi_n(l_t - L_o)$ terms.

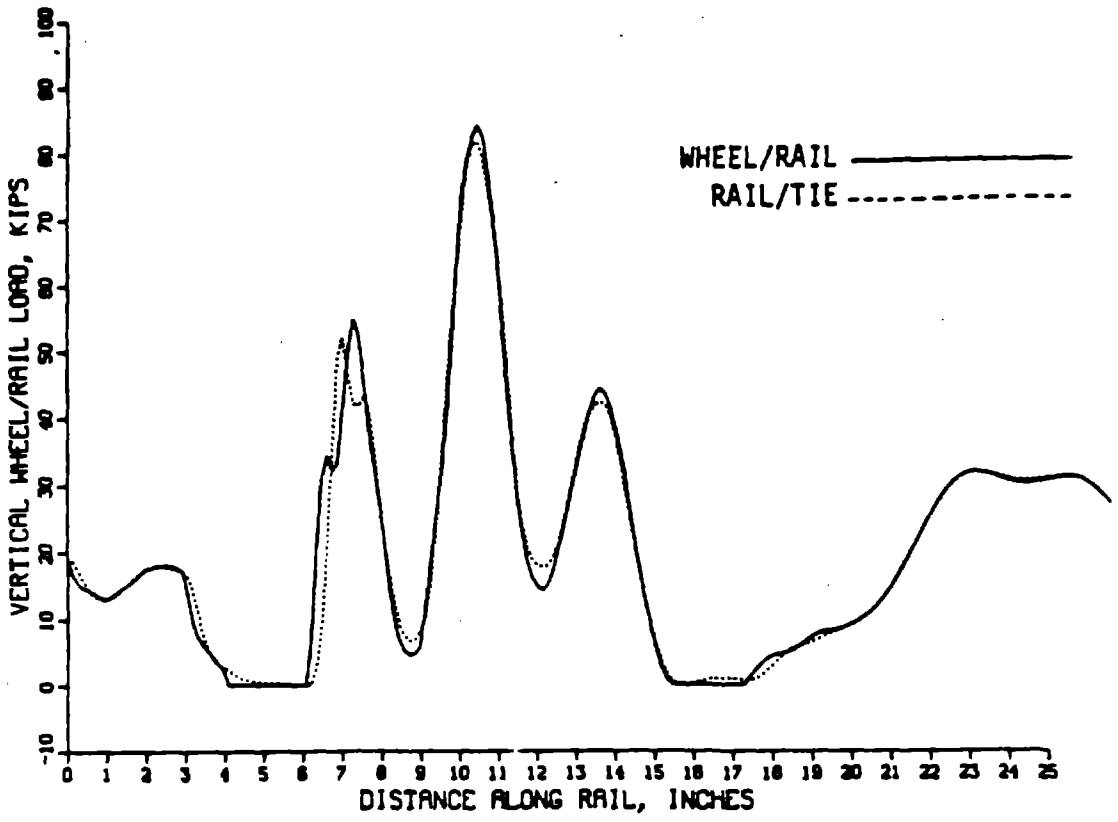

a. 7 DEGREE-OF-FREEDOM MODEL (WITHOUT TIE BENDING MODES)

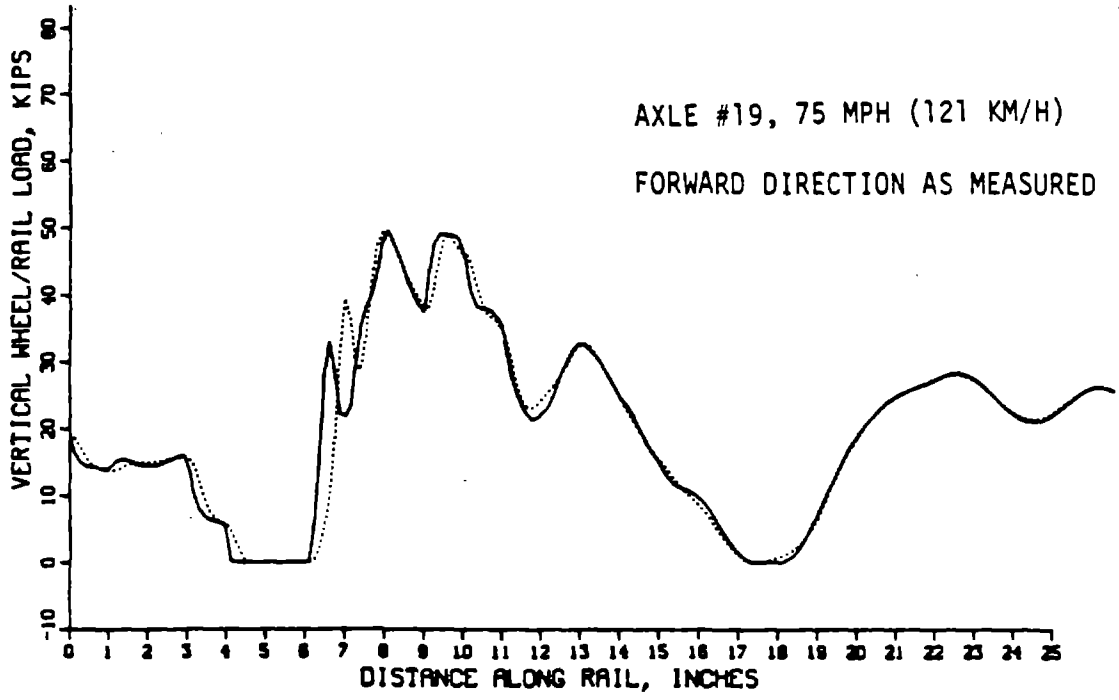

b. 11 DEGREE-OF-FREEDOM MODEL (WITH TIE BENDING MODES)

FIGURE 4-4. COMPARISON OF 7 AND 11 DEGREE-OF-FREEDOM IMPACT MODELS

A specific example comparing measured load from a "direct hit" on a rail circuit with predicted loads for the same wheel profile is shown in Figure 4-5. The predicted response in this example shows a somewhat more oscillatory behavior than the measured response in the 800-1000 Hz frequency range. This may be due to the piecewise-linear representation of the profile input. However, the rail itself exhibits a transverse bending mode near 800 Hz (see Figure 4-2) that is not specifically considered in the model (this mode is influenced both by wheel static load and adjacent wheel loads). This mode could also act as a tuned absorber at these frequencies.

Track system parameters, particularly the damping values, were varied over a wide range to determine their effect on predicted load response. Rail seat pad damping was varied over a range of elastomeric loss factor from 0.5 to 2.5 with relatively little change in load response. Tie bending-mode damping was varied from the laboratory-measured 0.5 percent, when supported at the rail seat areas, to 5.0 percent of critical damping. This change had the most noticeable effect on the minor higher-frequency oscillations in the predicted load response. The response curves of Figure 4-5 use the 5.0 percent value in all four bending modes. Vehicle and track parameters used in the model are listed in Table 4-3.

4.2 RAIL JOINT IMPACT LOADS

Results from the simplified wheel/rail impact model (Tables 4-1 and 4-2) were found to be reasonably accurate when using the parameter values of the softer wood-tie track. Wood ties exhibit much greater inherent damping and have not produced the prominent beam-bending modes seen in concrete ties in load or acceleration measurements.

Despite the best laid plans, the installation of the load cell tie plates[13] resulted in an instrumented joint that was essentially "flat" in geometry. Measurements at this joint, as shown in Figure 3-2 for the 105 km/h (65 mph) test run, showed some "P_2" response -- about 20 percent over the static load -- due to change in track stiffness at the joint. No "P_1" impact force is evident, however. A relatively severe joint was chosen from the test section (see Section 3.2) for analysis of wheel force measurements and computer prediction. An approximate representation of "Joint No. 50" in the BJR test section was used for this exercise. This joint was identified by matching the space curves from a track geometry survey with the continuous vertical load from the instrumented wheel.

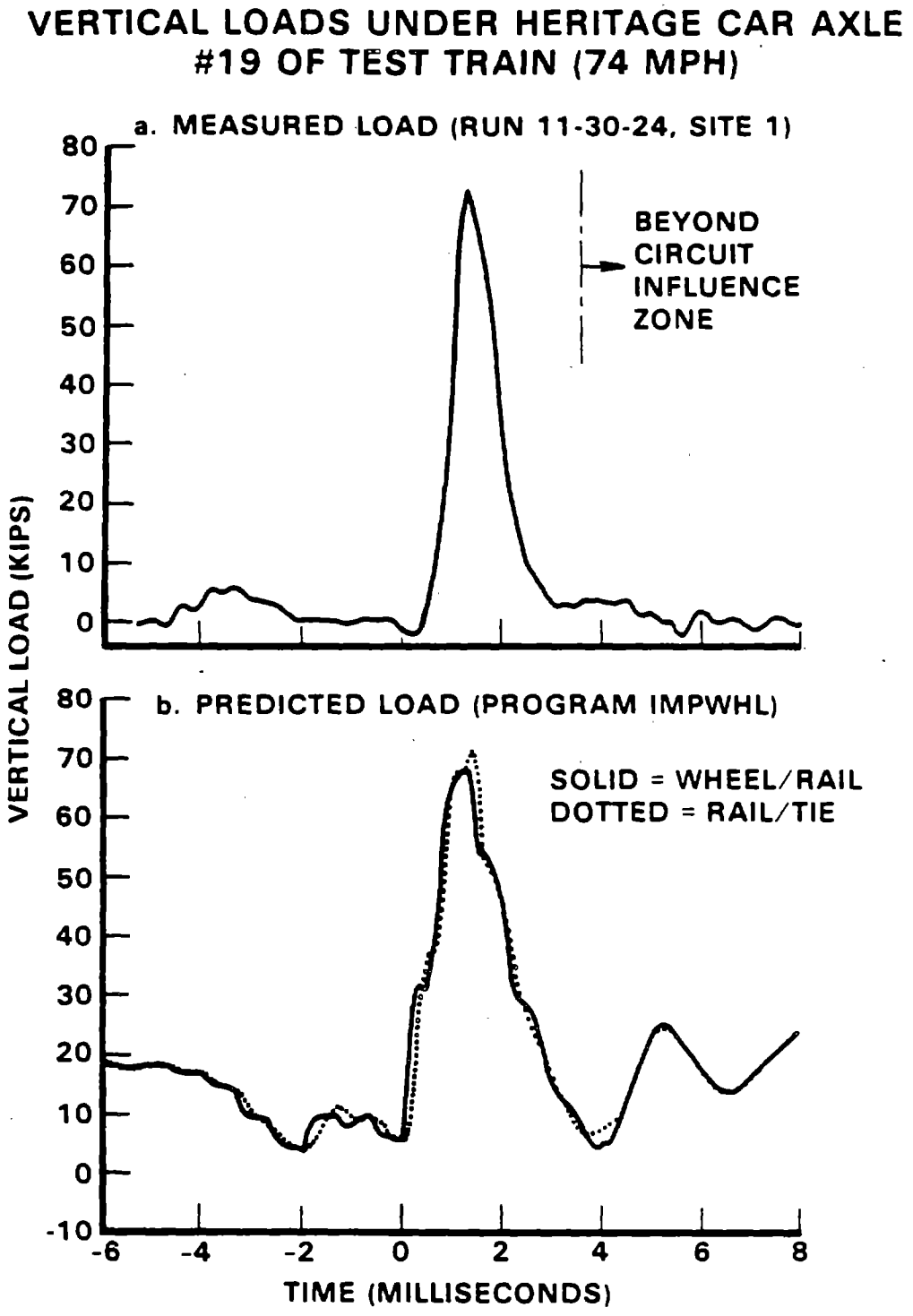

FIGURE 4-5. COMPARISON OF PREDICTED AND MEASURED LOAD TIME-HISTORIES FOR HERITAGE CAR WHEEL TREAD ANOMALY

TABLE 4-3. PARAMETERS REPRESENTING AMCOACH PASSENGER CAR ON NORTHEAST CORRIDOR CONCRETE TIE TRACK

VEHICLE AND TRACK PARAMETERS -		
WCAR(CAR BODY WEIGHT)	= .1009E+06	LB
WTRF(TRUCK FRAME/BOLSTER WEIGHT)	= .3050E+04	LB
WSF(SIDE FRAME WEIGHT, EACH SIDE)	= .1890E+04	LB
WAXLE(AXLE, BRAKE DISC, ETC., WEIGHT)	= .2050E+04	LB
WHL(WHEEL, BRG., ETC., WEIGHT, EACH SIDE)	= .7100E+03	LB
WR(EFFECTIVE WEIGHT OF RAIL)	= .7950E+02	LB
WT(EFFECTIVE WEIGHT OF TIE)	= .5510E+03	LB
WB(EFFECTIVE WEIGHT OF BALLAST)	= .1913E+04	LB
MA(CALCULATED EFFECTIVE MASS OF HALF-WHEELSET)	= .3731E+01	LB-SEC2/IN
PJSF(SIDE FRAME MASS MOMENT IN PITCH)	= .4245E+04	LB-IN-SEC2
RJA(WHEELSET MASS MOMENT IN ROLL)	= .5254E+04	LB-IN-SEC2
KZ1(VERTICAL PRIMARY SUSPENSION STIFFNESS, PER TRUCK)	= .2000E+06	LB/IN
KZ2(VERTICAL SECONDARY SUSPENSION STIFFNESS, PER TRUCK)	= .3700E+04	LB/IN
KBRG(BEARING VERTICAL STIFFNESS, PER WHEEL)	= .1613E+06	LB/IN
KTHE(SIDE FRAME STIFFNESS IN PITCH ON SUSPENSION)	= .5000E+07	LB-IN/RAD
KH(1.5/HERTZIAN FLEXIBILITY CONSTANT)	= .3022E+06	#WHATEVER$#
KRR(CALCULATED RAIL/TIE TANGENT STIFFNESS)	= .7853E+07	LB/IN
KTT(TIE/BALLAST EFFECTIVE VERTICAL STIFFNESS)	= .2040E+07	LB/IN
KB(BALLAST EFFECTIVE VERTICAL STIFFNESS)	= .1087E+07	LB/IN
CZ1(VERTICAL PRIMARY SUSPENSION DAMPING, PER TRUCK)	= .1500E+03	LB-SEC/IN
CZ2(VERTICAL SECONDARY SUSPENSION DAMPING, PER TRUCK)	= .2400E+03	LB-SEC/IN
CBRG(BEARING VERTICAL DAMPING, PER WHEEL)	= .1250E+03	LB-SEC/IN
CTHE(SIDE FRAME DAMPING IN PITCH ON SUSPENSION)	= .1000E+06	LB-IN-SEC/RAD
CH(EFFECTIVE WHEEL/RAIL CONTACT DAMPING)	= .2510E+03	LB-SEC/IN
CRR(RAIL/TIE EFFECTIVE VERTICAL DAMPING)	= .5050E+03	LB-SEC/IN
CTT(TIE/BALLAST EFFECTIVE VERTICAL DAMPING)	= .6830E+03	LB-SEC/IN
CB(BALLAST EFFECTIVE VERTICAL DAMPING)	= .1393E+04	LB-SEC/IN
LA(TRUCK AXLE SPACING)	= 102.00	IN
LBA(LATERAL DISTANCE BETWEEN BEARING ADAPTERS)	= 46.00	IN
G(LATERAL DISTANCE BETWEEN WHEEL/RAIL CONTACT POINTS)	= 59.50	IN
RWHL(NOMINAL WHEEL RUNNING RADIUS)	= 18.00	IN
EIRAIL(RAIL BENDING RIGIDITY, EI)	= .2490E+10	LB-IN2
FTRUP(MAXIMUM UPLIFT FORCE ON RAIL)	= .4000E+04	LB-IN2
OMEGA1(1ST TIE BENDING MODE NATURAL FREQUENCY)	= 679.00	RAD/SEC
ZETA1(1ST TIE BENDING MODE DAMPING RATIO)	= .02000	
PHILO1(1ST TIE BENDING MODE INFLUENCE COEFFICIENT)	= .14700	
OMEGA2(2ND TIE BENDING MODE NATURAL FREQUENCY)	= 2098.00	RAD/SEC
ZETA2(2ND TIE BENDING MODE DAMPING RATIO)	= .02000	
PHILO2(2ND TIE BENDING MODE INFLUENCE COEFFICIENT)	= -.84910	
OMEGA3(3RD TIE BENDING MODE NATURAL FREQUENCY)	= 3979.00	RAD/SEC
ZETA3(3RD TIE BENDING MODE DAMPING RATIO)	= .02000	
PHILO3(3RD TIE BENDING MODE INFLUENCE COEFFICIENT)	= -1.30400	
OMEGA4(4TH TIE BENDING MODE NATURAL FREQUENCY)	= 6488.00	RAD/SEC
ZETA4(4TH TIE BENDING MODE DAMPING RATIO)	= .02000	
PHILO4(4TH TIE BENDING MODE INFLUENCE COEFFICIENT)	= -1.14800	

representation of "Joint No. 50" in the BJR test section was used for this exercise. This joint was identified by matching the space curves from a track geometry survey with the continuous vertical load from the instrumented wheel. From the geometry space curves, the profile of Joint No. 50 appeared to be a combination of two distinct dipped functions: the first with a span of about 6 m (20 ft) and a dip of 10 mm (0.4 in.); and the second with a span of about 1.2 m. (3.9 ft) and a dip of 2.5 mm (0.1 in.). This latter feature apparently represents rail end batter. A combined geometry function was therefore used:

$$B_x = |\beta_T V t - 2.5| \quad [29]$$

$$B_y = |\beta_R V t - (\beta_R/\beta_B)\, 2.5| \quad [30]$$

$$e_{z1}(t) = -\Delta_T[1 - \mathrm{Sin}(\pi B_x/5)] \text{ for } B_x < 2.5 \quad [31]$$

$$= 0 \text{ for } B_x \geq 2.5,$$

$$e_z2(t) = -\Delta_R\,[1 - \mathrm{Sin}(\pi B_y/5)] \text{ for } B_y < 2.5 \quad [32]$$

$$= 0 \text{ for } B_y \geq 2.5$$

$$e_z(t) = e_{z1} + e_{z2} \quad [33]$$

The appropriate derivatives of these functions were used to generate the geometry input velocities to the wheel, e_z (t). In addition, the rail/tie stiffness at the joint was decreased by the following function:

$$f_{jnt} = [1 - \mathrm{Sin}(\pi B_y/5)]^2 \text{ for } B_y < 2.5 \quad [34]$$

$$= 0 \text{ for } B_y \geq 2.5$$

$$K_{jnt} = K_R[1 - (1 - R_j)F_{jnt}] \quad [35]$$

where

t = time, sec

K_R = rail/tie vertical stiffness

K_{jnt} = vertical stiffness near joint (substitute for K_R)

R_j = ratio of stiffness at joint gap to nominal rail/tie stiffness.

The predicted response of the test car to Joint No. 50 is shown in Figure 4-6 for a speed of 105 km/h (65 mph). Impact load peaks of 312 kN (70,000 lb) for P_1 and 215 kN (48,000 lb) for P_2 were calculated. The calculated value for the P_1 peak as if measured at the tie plates (beneath the rail effective mass) was

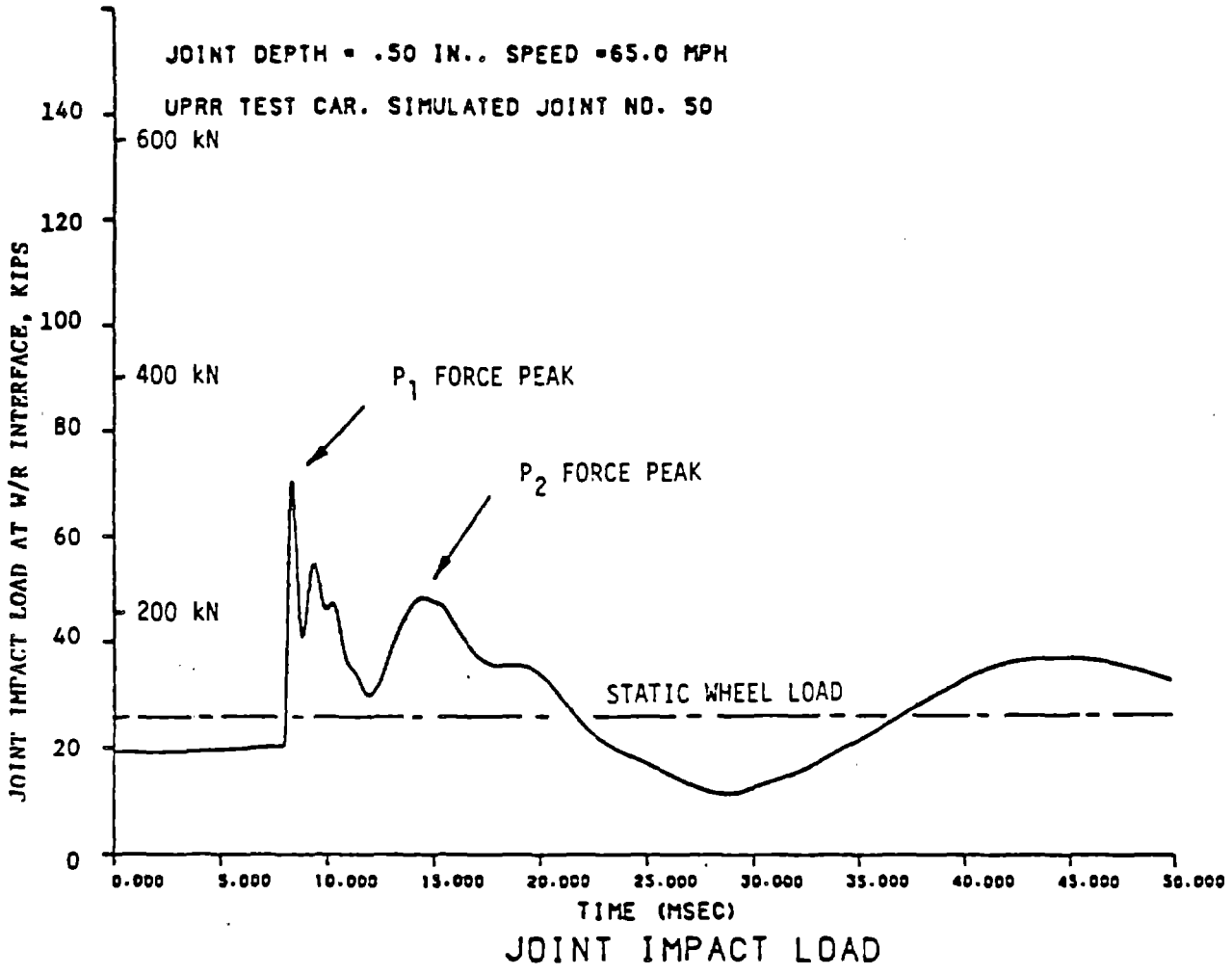

FIGURE 4-6. VERTICAL IMPACT LOADS DEVELOPED AT DIPPED JOINT, SIMULATED UNION PACIFIC HOPPER CAR (70-TON LOAD)

reduced to 250 kN (56,000 lb), showing that some attenuation can be expected at the load cell tie plates of this high-frequency component. Impact load measured by the instrumented wheelset at Joint No. 50 has been shown in Figure 3-4. The oscillations due to wheel plate modal response to impact tends to obscure the true value of the P_2 peak. If the load signal is filtered, the resulting P_2 peak value compares quite well with the computer-predicted peak load in Figure 4-6.

For the "nominal" dipped joint, the approximate relationships in Equations [1] and [5] would predict maximum values of P_1 = 258 kN (58,000 lb) and P_2 = 170 kN (38,000 lb). The higher measured and computer-predicted values result from the short wavelength "cusp" at this particular rail joint. Predicted impact load peaks versus train speed are plotted in Figure 4-7 and show a monotonic increase in both P_1 and P_2 load with increased speed. Maximum values from wheel measurements at a sampling rate of 1000 per second are also shown. It can be seen that at this lower rate the P_1 impact peak can be missed.

4.3 FLAT WHEEL IMPACT LOADS ON WOOD-TIE TRACK

The simplified, 4 DOF wheel/rail impact load model was used for initial studies of the effects of wheel flats on wood-tie track loads. On the less-stiff, more highly-damped wood tie structure, results from the model appeared to correlate well with measured load data, although the actual wheel tread profiles were unknown.

Smaller wheel flats, on the order of 25 mm (1 in.) in length, generate impact response well within the short (in-crib) strain gage patterns. An example of this is shown in Figure 4-8, where the impact load of a small flat on the trailing wheel of an empty freight car is "captured." Predicted response from the computer model is shown in Figure 4-9 in comparison with the load trace of Figure 4-8. Note that for a fraction of a millisecond the wheel/rail load drops to zero as the wheel becomes "airborne", and a shorter-duration impact load (about 1 millisecond long) results in a 133 kN (30,000 lb) peak on a 36 kN (8000 lb) static wheel load. A short tensile spike in longitudinal rail head strain (200 microstrain) can be seen in Figure 4-8 on the field-side gage. In this case, the impact load occured directly over the gage, where in the other example the load occurred two to three

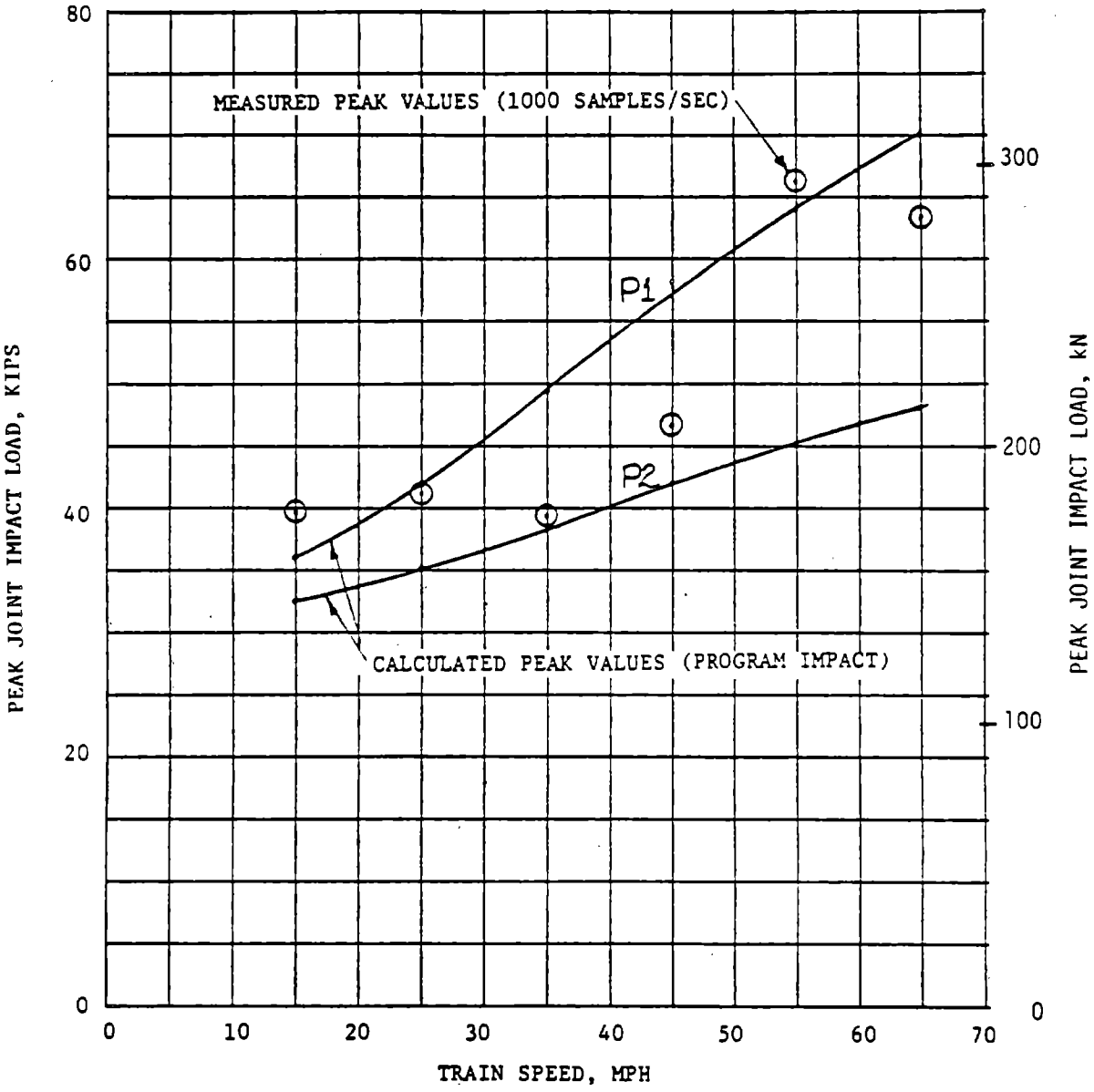

FIGURE 4-7. PREDICTED JOINT IMPACT LOADS VERSUS TRAIN SPEED -- JOINT #50, UPRR TEST HOPPER CAR (70-TON LOAD)

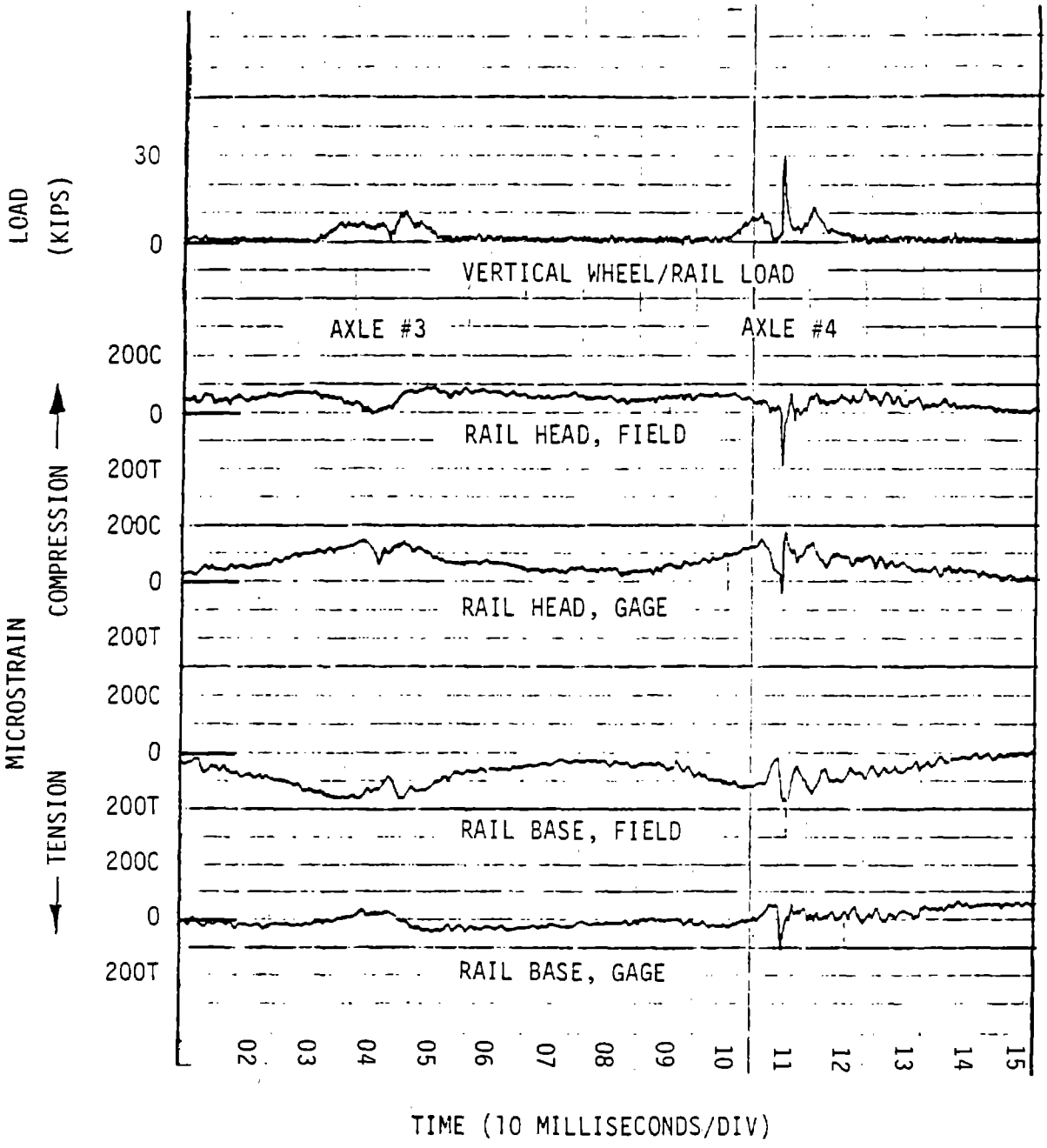

FIGURE 4-8. LONGITUDINAL RAIL STRAINS UNDER FLAT WHEEL ON EMPTY FREIGHT CAR -- RUN 18-15, 55 MPH, BJR TRACK SECTION

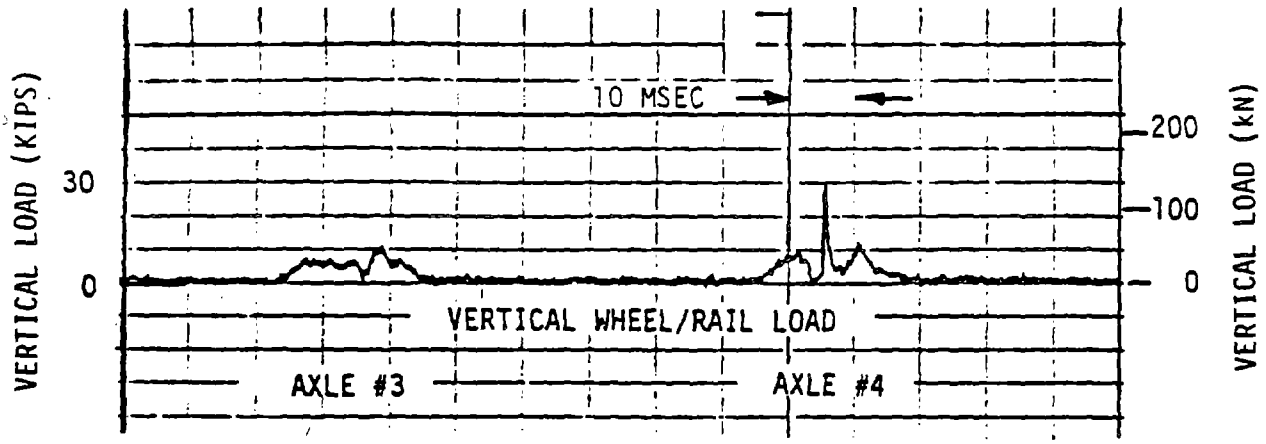

a. VERTICAL IMPACT LOAD UNDER FLAT WHEEL ON EMPTY FREIGHT CAR, 55 MPH (MEASUREMENT SITE 6, CWR TRACK)

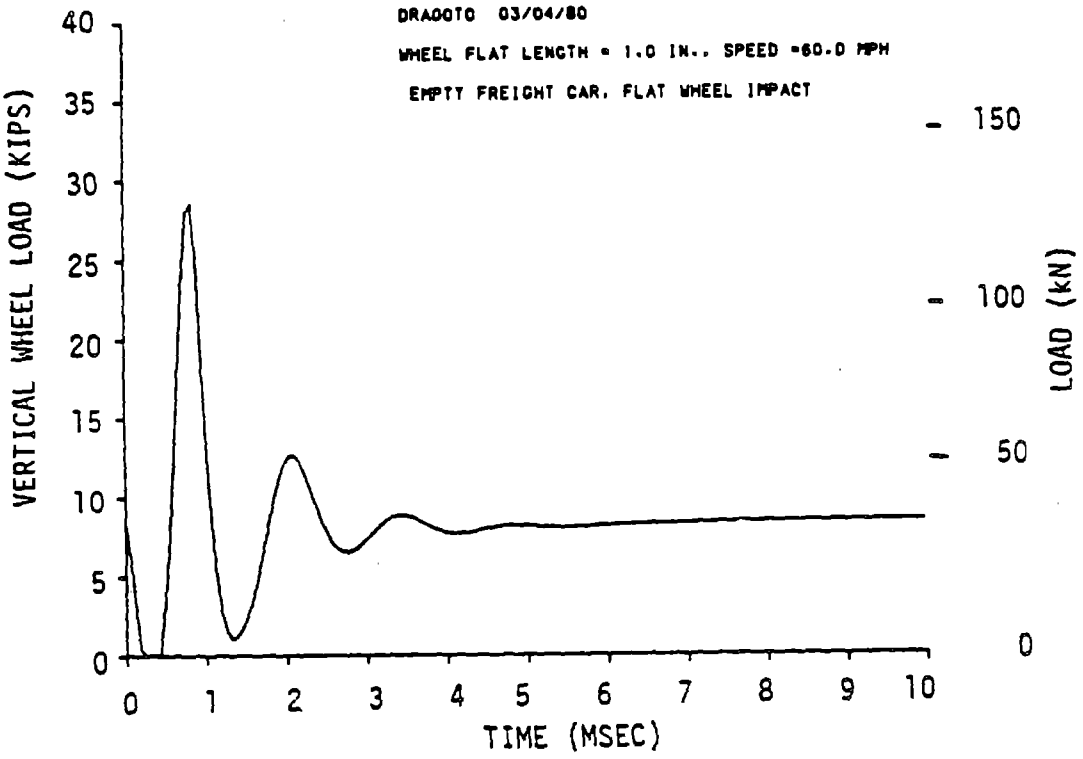

b. PREDICTED FLAT WHEEL IMPACT RESPONSE UNDER EMPTY FREIGHT CAR, Program IMPACT

FIGURE 4-9. COMPARISON OF MEASURED AND PREDICTED FLAT WHEEL IMPACT LOAD RESPONSE, EMPTY FREIGHT CAR

inches ahead of the gage. Examination of other impact loads -- not necessarily "flats", but just small rough spots -- shows impact durations less than 1 millisecond, but no sign of high tensile strains. Strain oscillations on the order of 200 microstrain peak-to-peak may be seen superimposed on the head compressive (bending) strain due to these impacts.

British Rail defines the depth of a wheel flat by the following relationship:

$$d = L^2/16R_w$$

where

L = flat length

R_w = wheel radius.

This depth, which they define as a "rounded" flat shape, is roughly one-half the depth of a freshly-slid flat, which is defined by:

$$d = R_w - \sqrt{R_w^2 - L^2/4}$$

The computer model was used with the British Rail "rounded" flat to explore the effects on peak impact load of flat length and train speed. These results are plotted in Figure 4-10 for an empty 100-ton freight car, and in Figure 4-11 for a loaded 100-ton freight car, using nominal wood-tie track parameters (see Table 4-2). Rather strong resonant effects are seen in the results, and it is interesting to note that with the loaded car at 97 km/h (60 mph) the peak load is independent of flat length. With shorter-length flats at higher speeds, impact loads are substantially attenuated by the rail effective mass, so that tie plate loads are relatively low. Larger flats at lower speeds result in impact loads that pass unattenuated to the ties and ballast, however; and tie plate loads of 254 kN (57,000 lb) have been recorded during the field experiments.

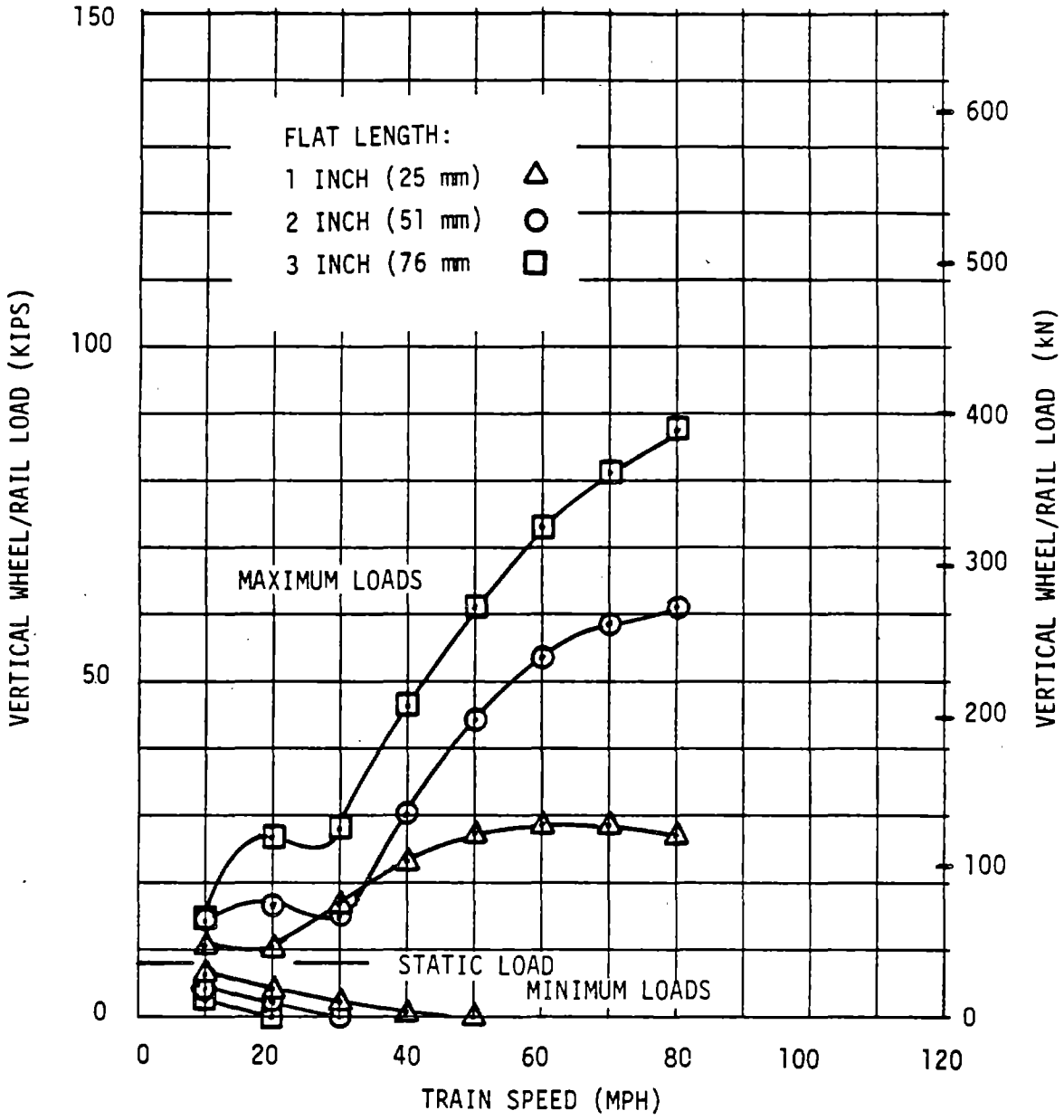

FIGURE 4-10. VERTICAL WHEEL/RAIL IMPACT LOADS UNDER SIMULATED EMPTY (100-TON) FREIGHT CAR, WOOD-TIE TRACK STRUCTURE -- Program IMPACT, BR "ROUNDED" FLAT SHAPE

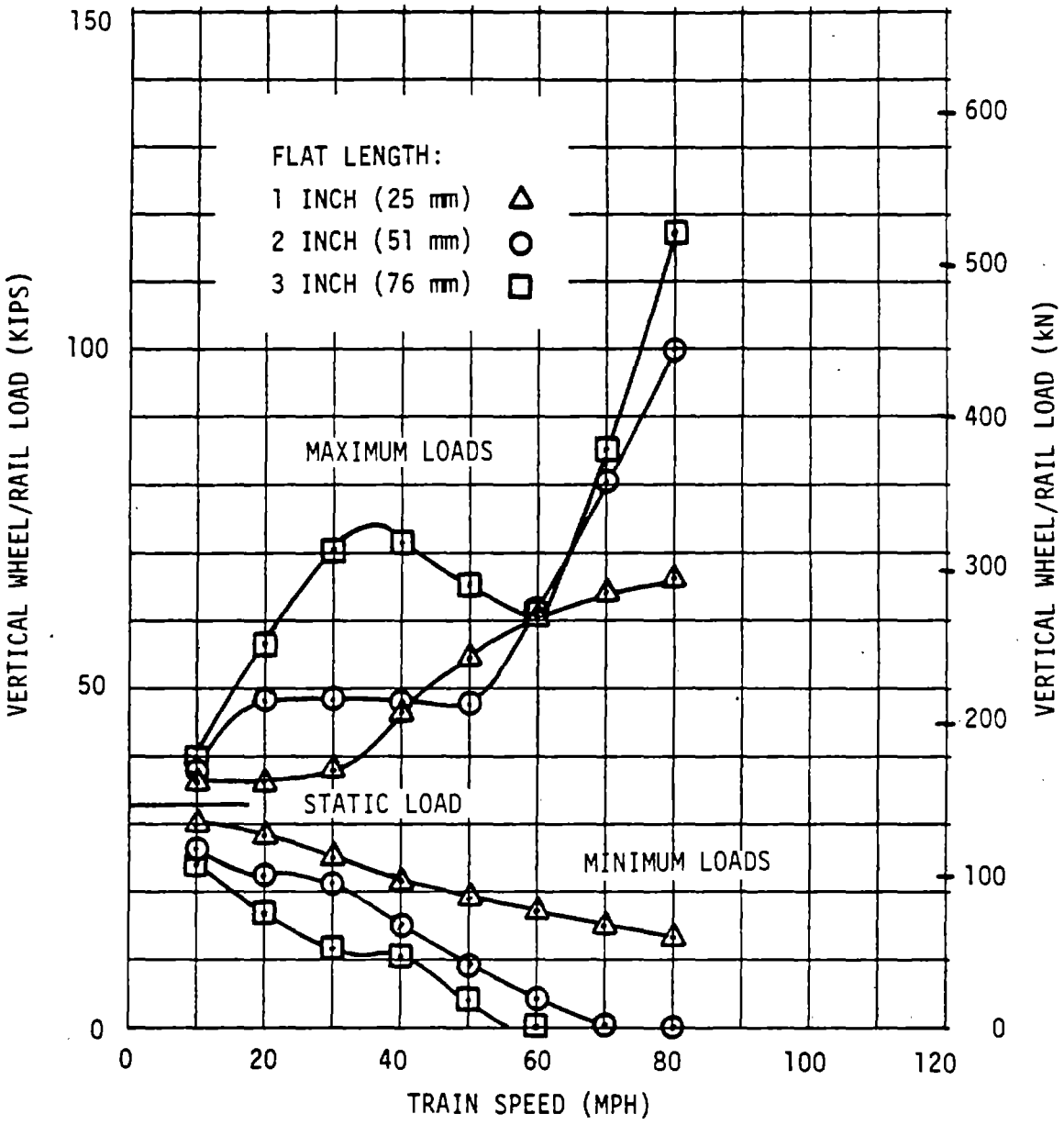

FIGURE 4-11. VERTICAL WHEEL/RAIL IMPACT LOADS UNDER SIMULATED 100-TON FREIGHT CAR, WOOD-TIE TRACK STRUCTURE -- Program IMPACT, BR "ROUNDED" FLAT SHAPE

Program results show the following zero-load ("airborne wheel") speeds:

Wheel Flat Length (in.)	Flat Depth (36" wheel), in.	Zero-Load Speed (mph) Empty Car	Loaded Car
1	.0017	45	--
2	.0069	29	70
3	.0156	18	55

Approximate formulae from Ver, et al.[30] using the same vehicle and track parameters show critical (loss of contact) speeds of 53 mph for the loaded car, 25 mph for the empty car, independent of wheel flat size, on a resilient rail.

More recent research has resulted in a better definition of actual wheel profiles. Instead of traditional "flat", profiles become battered into longer-wavelength geometry errors. For example, several measured profiles 0.9 mm (0.035 in.) in depth were typically 152 to 178 mm (6 to 7 inches) in wavelength. Other profiles ranged up to 3 mm (0.121 in.) in depth and 406 mm (16 in.) in length. These profiles in general will develop higher loads at higher speeds, with little evidence of a low-speed resonance.

4.4 FLAT WHEEL IMPACT LOADS ON CONCRETE-TIE TRACK

Concrete ties, in addition to being more massive than wood ties, have greater bearing area and result in a higher track modulus (stiffer track): typically 10,000 to 12,000 lb/in/in. per rail, compared with 3000 to 6000 lb/in/in. for good wood-tie track. Concrete tie bending modes are important to the dynamic response at the wheel/rail interface as described in Section 4.1.

To explore the effects of the longer wavelength profile errors on a freight car, the model was used with parameters for a typical 100-ton-capacity car. Peak loads for four possible profiles are plotted in Figure 4-12: a freshly-slid 1 in. (25 mm) flat spot, a battered 2 in. (51 mm) flat with a versine shape and about one-half the depth of a freshly-slid flat of that length, and the profile errors of test Axles #7 and #19 (see Section 5). High, speed-dependent loads are evident under the latter two long-wavelength profile errors.

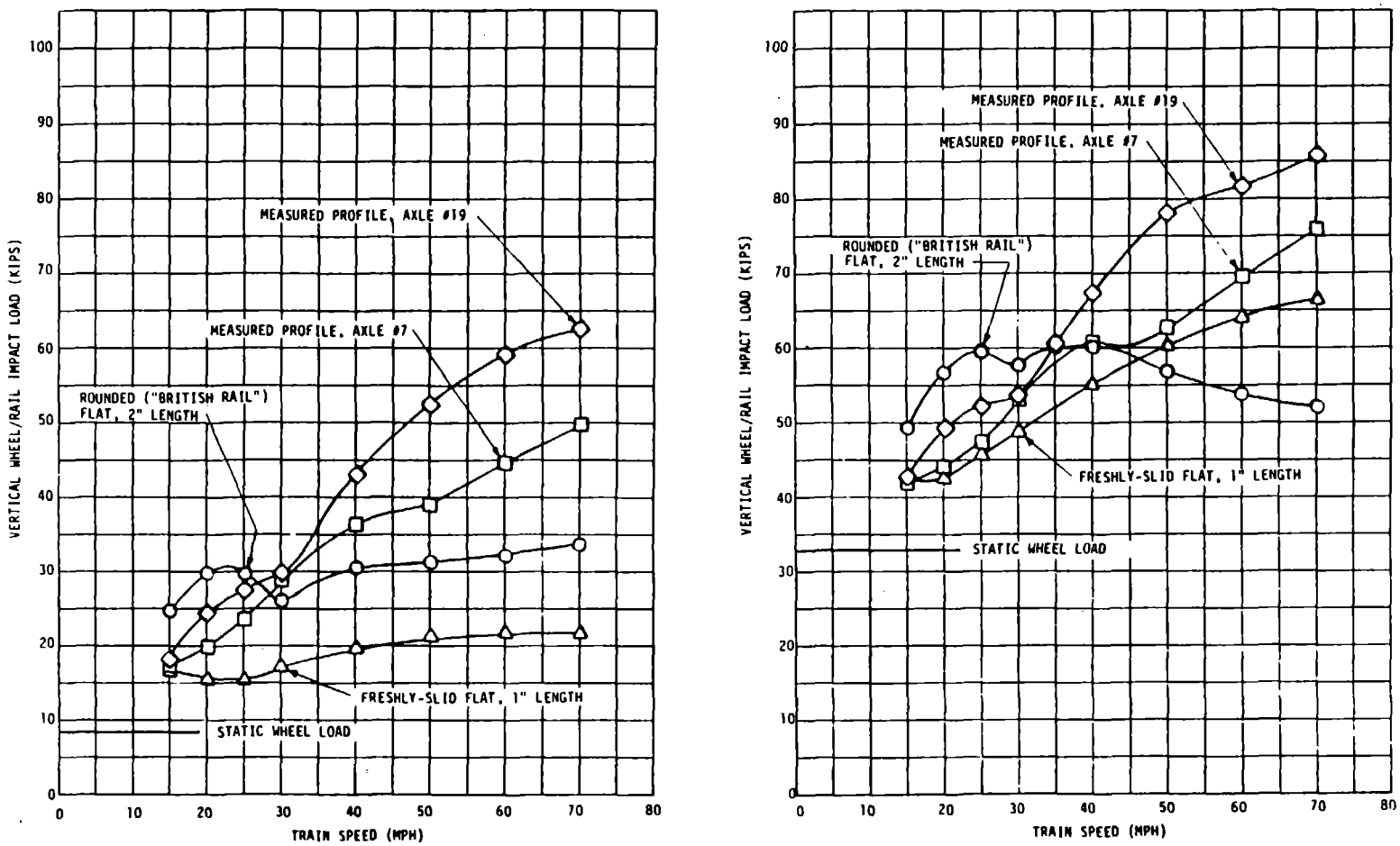

FIGURE 4-12. PREDICTION OF PEAK VERTICAL IMPACT LOAD UNDER 100-TON FREIGHT CAR WITH DIFFERENT WHEEL PROFILE ERRORS (BATELLE PROGRAM IMPWHL)

5. EXPERIMENTS ON THE NORTHEAST CORRIDOR

A series of tests was conducted on the Northeast Corridor in late November of 1983 using a special Amtrak test train. In these tests the train was run over a wide range of speeds through a wayside test zone, the Edgewood impact detector site. The objectives of these tests were twofold: (1) to determine the influence of speed on wheel/rail vertical loads produced by worn wheel profiles on passenger equipment, and (2) to correlate wheel tread conditions with the resulting impact loads. Other experiments were also conducted during this time period to characterize the track dynamic response to impact loads.[31]

The test train consisted of an AEM-7 electric locomotive, three Amcoach cars, and two "Heritage" cars (older passenger equipment from pre-Amtrak service). The cars were selected from revenue trains based on high impact loads developed by one or more wheelsets when passing the impact detector site. Several wheelsets newly-cut to the standard Association of American Railroads (AAR) 1:20 taper were also included in the consist. These cars represent fundamentally different truck designs: the Amcoach with the Budd Pioneer III truck with its elastomeric primary suspension, and the Heritage car with an equalizer beam, coil-spring primary suspension and swing-hanger supported secondary suspension.

The track structure through the impact detector test site was the current standard Northeast Corridor track: concrete ties on 24-in. (0.61 m) centers, 140 lb/yd (69.4 kg/m) continuous welded rail, and the stiff EVA rail seat pads with Pandrol clips. The track has a measured tangent stiffness under the nominal wheel load of 650,000 lb/in. (114 MN/m), or a track modulus of 10,400 lb/in/in. per rail (71.7 MN/m^2).

During the tests, wheel load measurements were recorded from the impact detector circuits in both analog and peak-load (tabulated) formats. Standard ORE rail-web chevron strain-gage circuits[32] are used as vertical load transducers in four successive crib (between-tie) areas. The gage spacing and circuit characteristics provide a trapezoidal load "influence zone", roughly eight inches (203 mm) in length at full amplitude, with 4-in. (101 mm) "skirts" of decreasing amplitude at each end. Therefore, the impact detector in this configuration provides four successive "snapshots" of passing wheel load, and a 25 to 30 percent

probability of detecting the highest impact load for each wheel pass. Repeated runs were therefore required in each speed band to increase the probability of measuring the highest impact loads under each wheel of the train.

An example of vertical wheel loads under a given wheel passing the impact detector site is shown in Figure 5-1. This wheel had a single distinct profile anomaly, as shown in Figure 5-2, that impacted directly over Site #1 in this particular run. Loads within the influence zones of the other two sites show relatively little dynamic variation about the nominal 16,000-lb (71 kN) vertical wheel load.

Immediately following the tests, some of the wheelsets were removed from the cars for measurement of profiles at the Ivy City (Washington, DC) wheel shop. Examples of four of these profiles are given in Figure 5-2. A special profilometer was designed to measure the changes in effective radius of wheel rotation around the circumference of the wheel. This profilometer consisted of a piece of rail head guided in the plane of wheel rotation, on the desired cant angle. The rail head was spring-loaded on a plunger to move in or out on the wheel radial line. The wheel was then rotated while cradled in its own bearings. Changes in position of the rail head as it followed the contact patch were measured at the plunger with a dial indicator. These measurements provided a direct input to the modified version of the earlier described computer model at the wheel/rail contact patch without the need of any geometry transformations.

5.1 RAIL SURFACE PROFILES

An additional opportunity to validate the model was gained when by chance an "engine burn" or rail surface anomaly occurred during October 1983, almost centered on one of the rail strain-gage circuits of the Edgewood impact detector. This defect was initially described as 1.75 in. (44 mm) in length, 0.017 in. (0.43 mm) in depth, from the rail centerline outward, and rusty on its bottom surface. Load time-histories were recorded during runs of the Amtrak test train, and comparative runs with the impact load model were made with "best-guess" profile shapes with some success. In April 1984, a newly-designed rail running-surface profilometer was used to measure surface anomalies (engine burns, welds) on the Northeast Corridor track. This profilometer consists of a one-radian segment of a 36-in. (0.914 m) diameter passenger car wheel. The precision-ground wheel segment

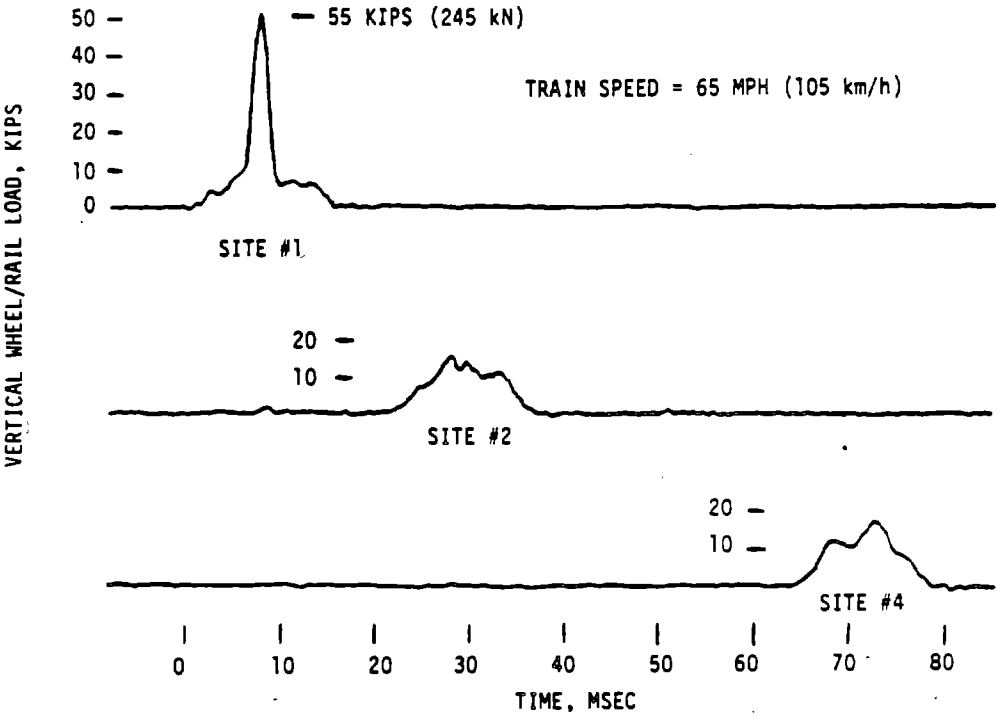

a. VERTICAL LOADS UNDER AMCOACH AXLE #7

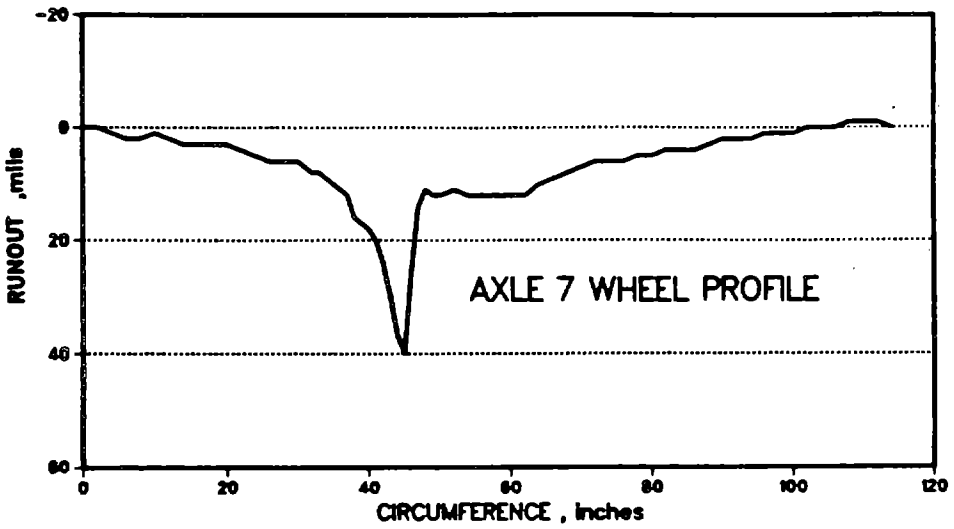

b. CIRCUMFERENTIAL PROFILE OF AMCOACH AXLE #7, RIGHT WHEEL

FIGURE 5-1. EXAMPLE OF WHEEL VERTICAL LOADS THROUGH IMPACT DETECTOR SITE UNDER AMTRAK TEST TRAIN

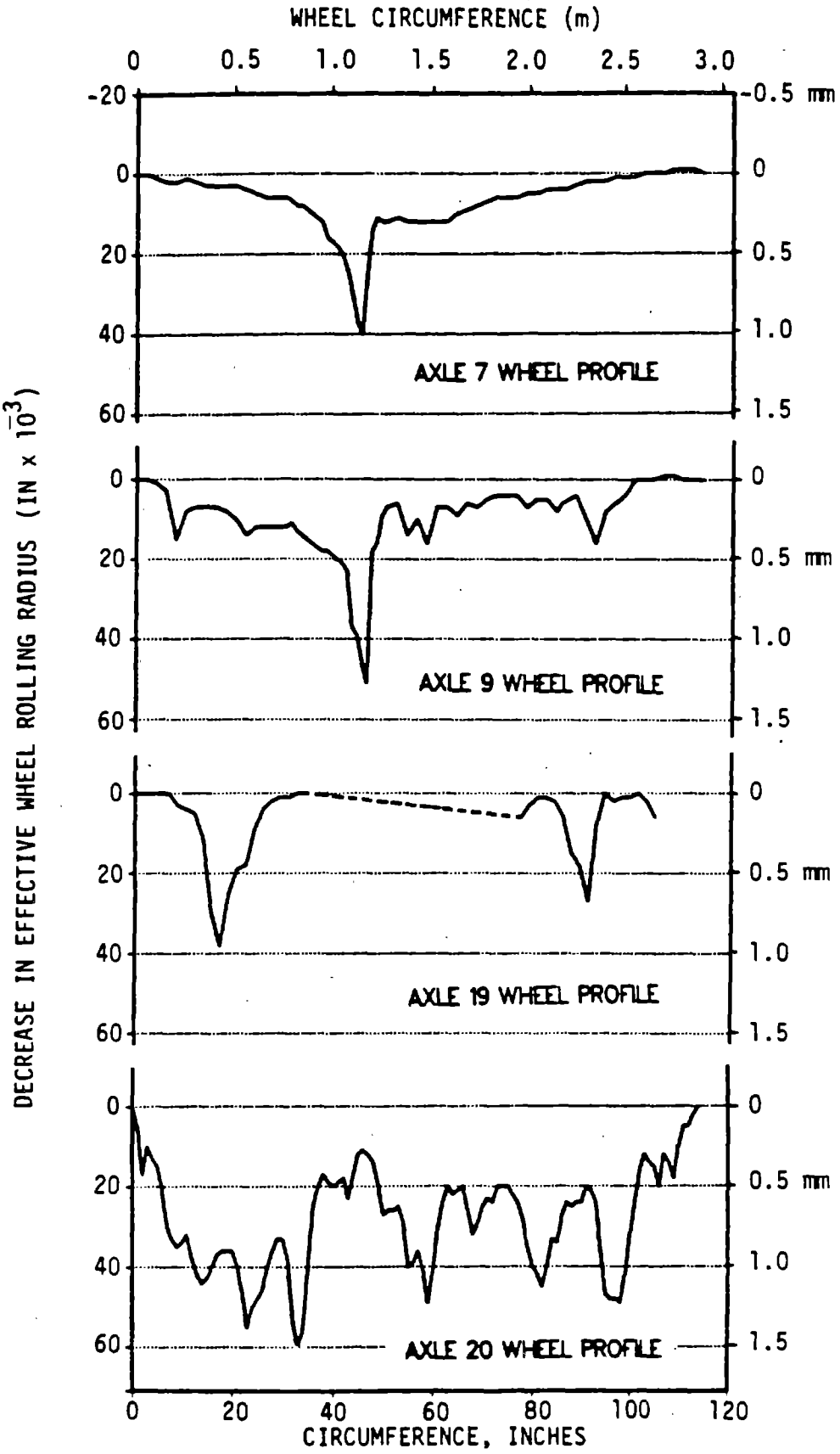

FIGURE 5-2. EXAMPLES OF WHEEL PROFILES USED ON TEST TRAIN

center of rotation is guided vertically on pairs of bearings in a A-frame and an intermediate link assembly, all of which in turn are guided longitudinally on linear bearings and two parallel, hardened and ground rods. This assembly is fastened to a horizontal frame that rests on two points on the rail being measured, and one point on the opposite rail, establishing the plane of the track. Pivoted shims on this third point allow the effective wheel taper of the precision wheel segment to be varied from plus 1:20 (the standard AAR taper) to a minus 1:20 (a hollow-worn wheel tread). Electrical signals from the integral, battery powered and signal conditioned rotary indexing potentiometer and vertical displacement transducer are plotted on the X and Y axes of an X-Y plotter, giving a continuous plot of the vertical position of wheel center of rotation versus distance along the rail. This also becomes a direct input to the computer model, without the need for geometry transformations. A sketch of the profilometer is given in Figure 5-3.

Measurements of the "engine burn" at the Edgewood impact detector are shown for different wheel tapers in Figure 5-4. The rail has started to exhibit a slight service-bent shape of long wavelength on either side of the surface defect. More severe (older) engine burns measured with the profilometer showed long-wavelength dips on the order of 60 in. (1.52 m) that resembled dipped rail joints. The "burn" itself in Figure 5-5 causes the wheel to drop 0.015 to 0.018 in. (0.38 to 0.46 mm) in a span of 6 to 7 in. (150 to 180 mm). A gradual increase in impact factor under Amcoach wheels -- from 1.71 to 1.83 -- has been noted from impact detector data over the past eight months, indicating that the defect is slowly increasing in depth and wavelength as it is battered under traffic.

Examples of wheel load time-histories under a newly-turned wheel on an Amcoach of the test train (Axle #11) at three different train speeds are shown in Figure 5-6. Predicted response for the measured 1:20 taper profile of Figure 5-4 at these three speeds is shown in Figure 5-7. It must be remembered that the measured load is captured only within the 8-inch influence zone of the rail circuit, while the predicted load is continuous with wheel motion. Therefore the oscillatory load response at about 200 Hz is seen only in the low-speed run through the measurement site. Since at higher speeds the problem becomes more and more "three-dimensional" as the wheel moves beyond the responding track structure, the predicted loads become less accurate with time past the initial excitation.

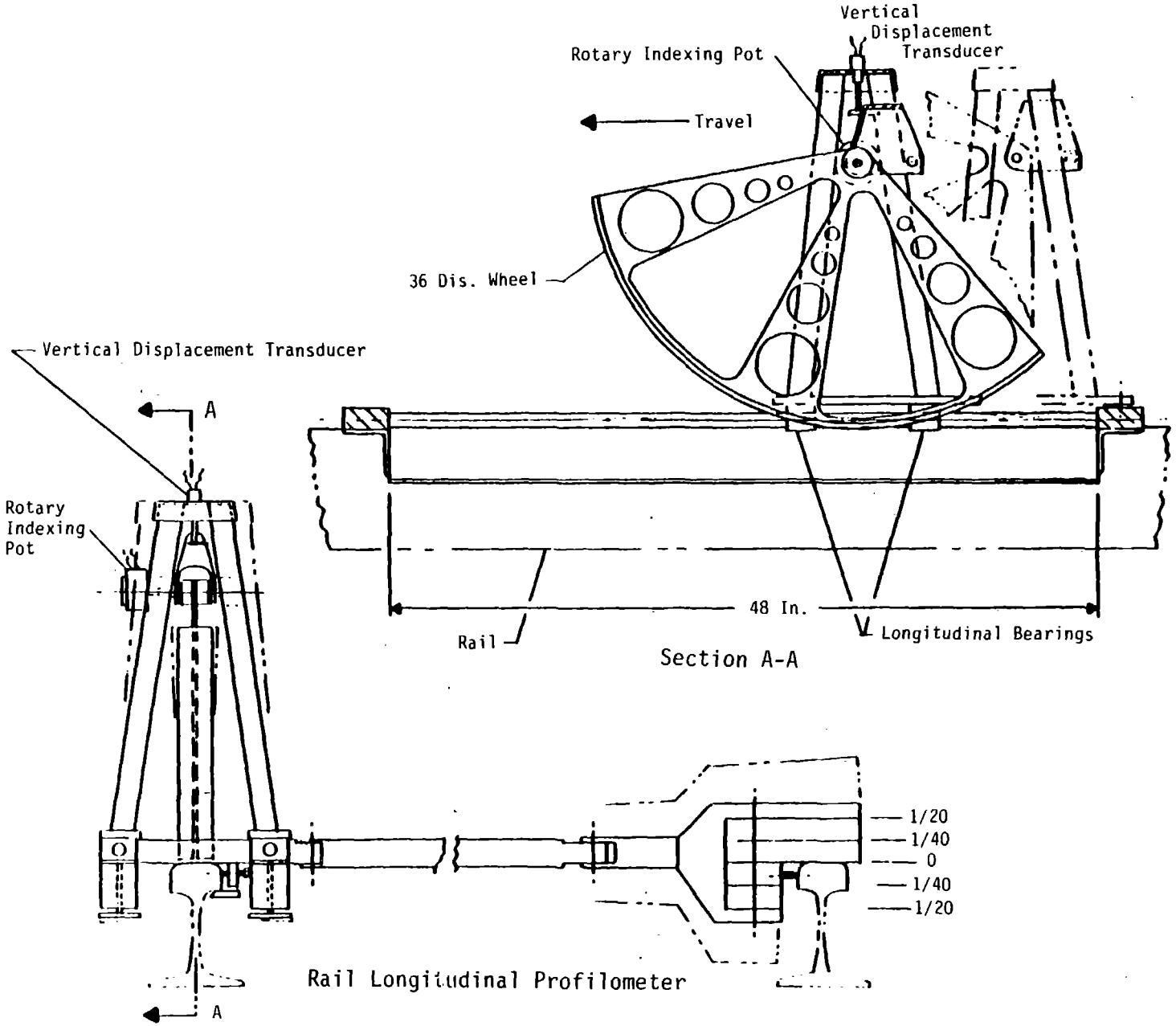

FIGURE 5-3. RAIL RUNNING-SURFACE PROFILOMETER

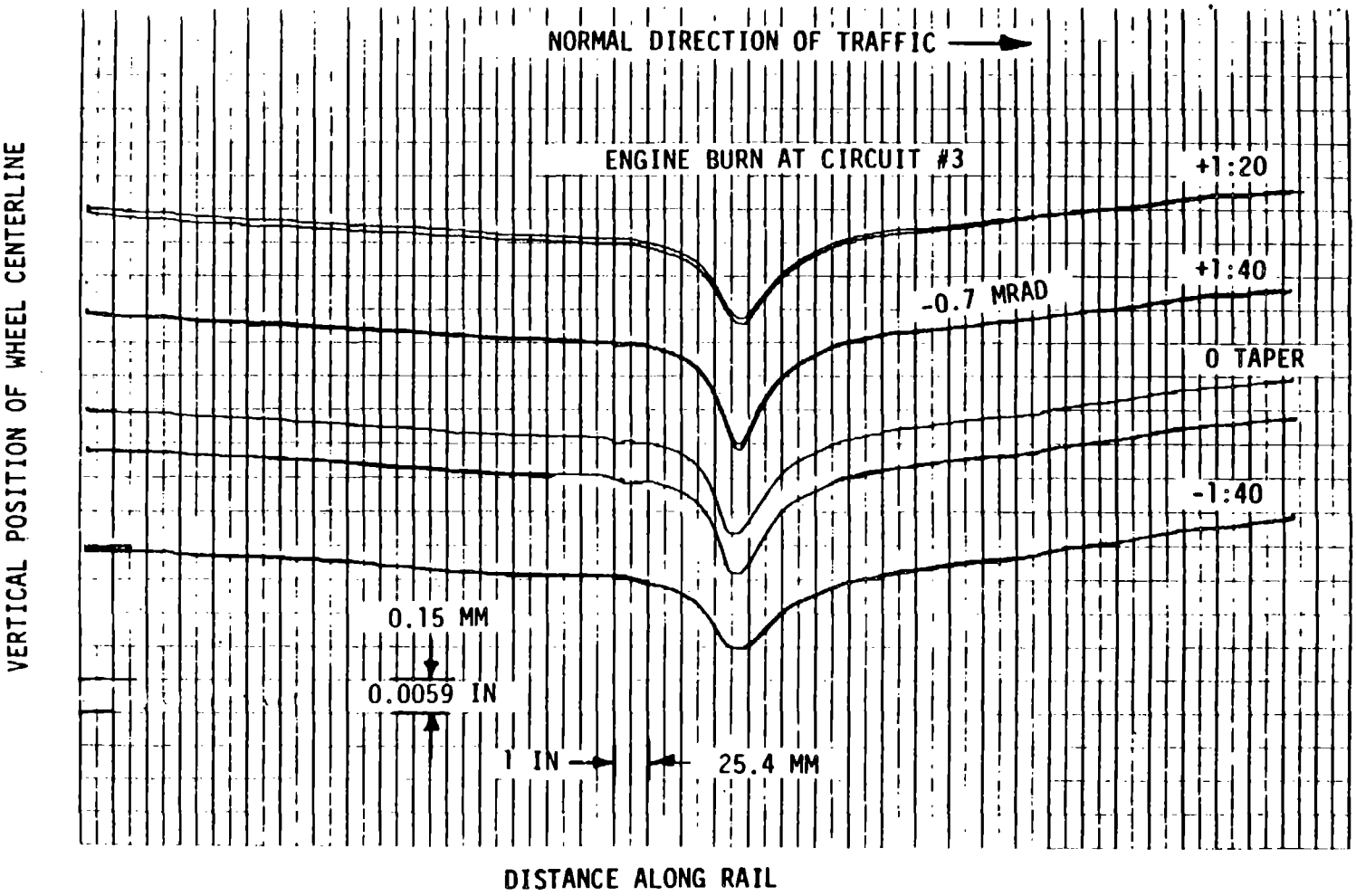

FIGURE 5-4. MEASURED RAIL RUNNING-SURFACE PROFILE AT ENGINE BURN, EDGEWOOD IMPACT DETECTOR CIRCUIT #3

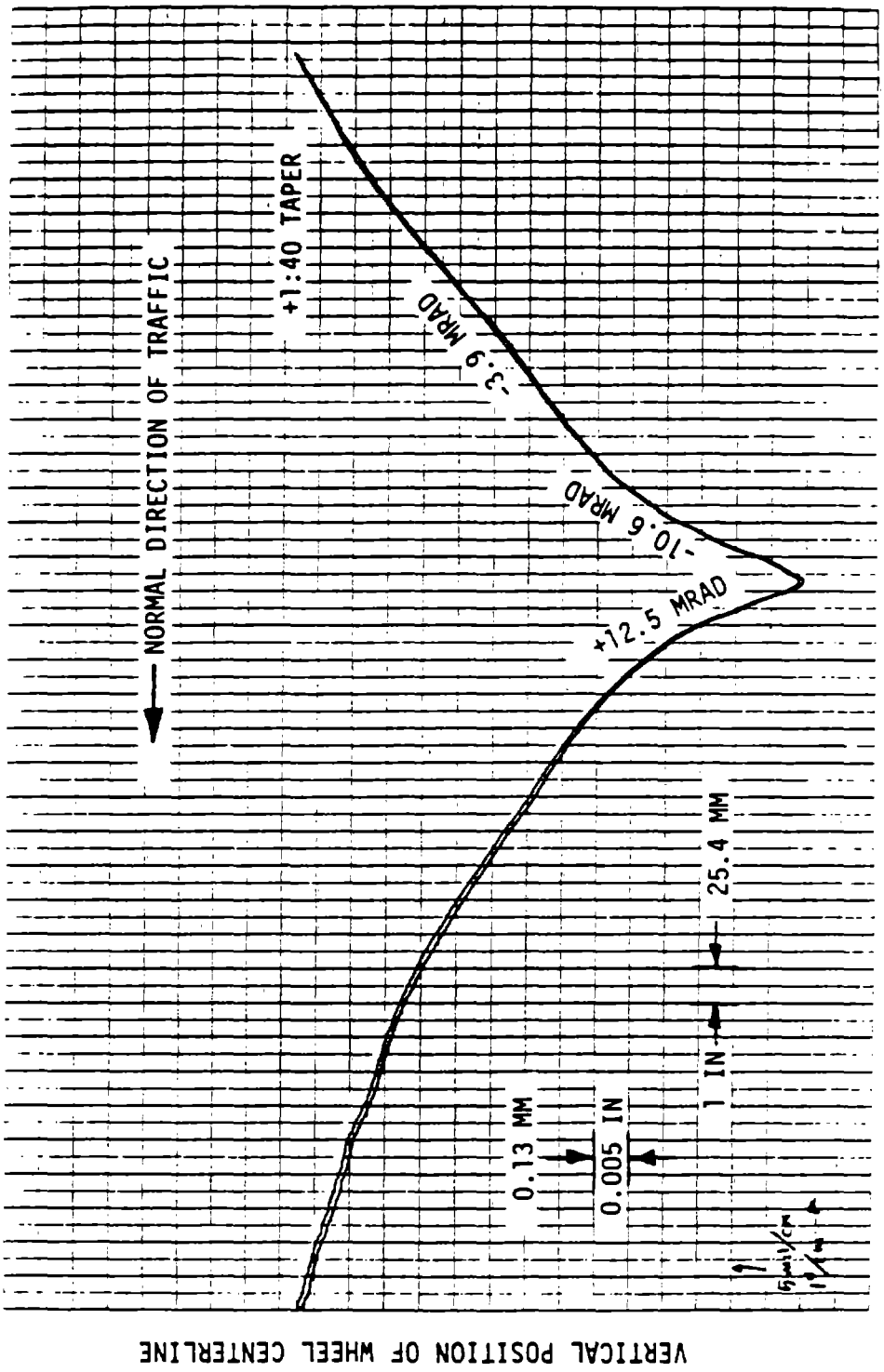

FIGURE 5-5. MEASURED RAIL RUNNING-SURFACE PROFILE NEAR BATTERED ENGINE BURN

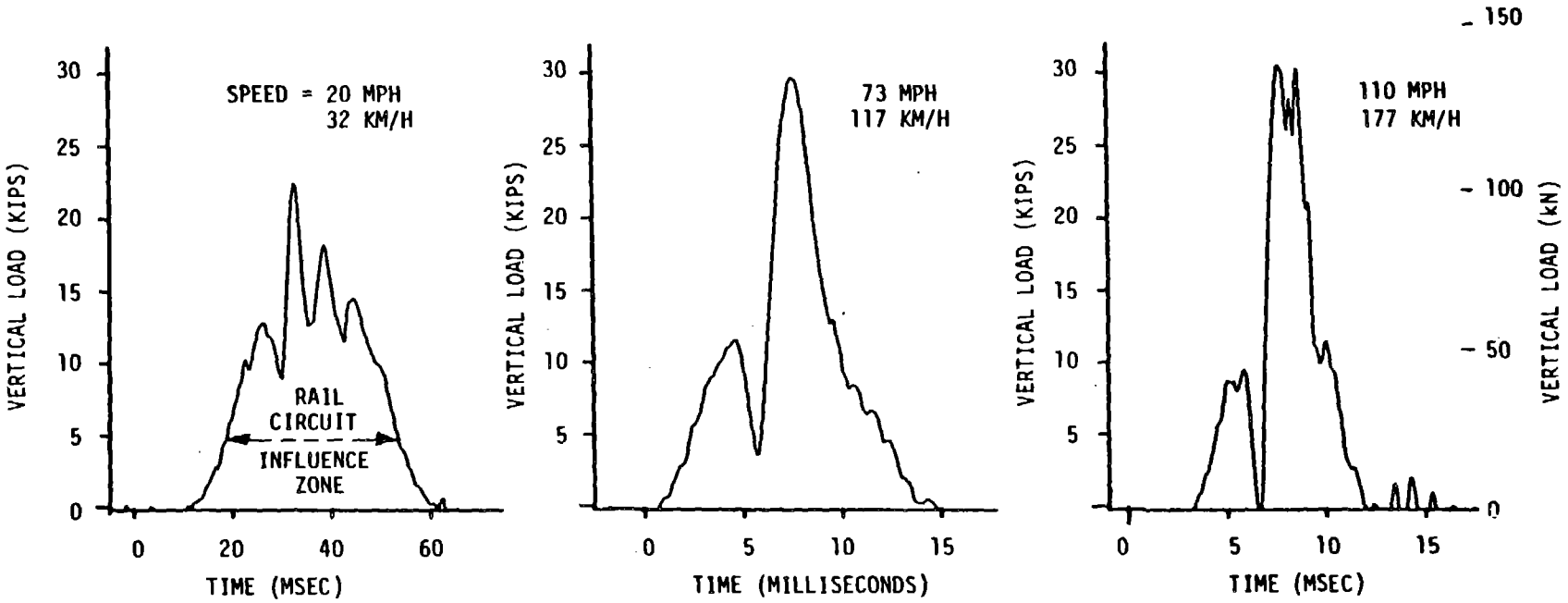

FIGURE 5-6. MEASURED LOAD RESPONSE UNDER AMCOACH WHEEL OVER THE EDGEWOOD IMPACT DETECTOR SITE RAIL SURFACE DEFECT

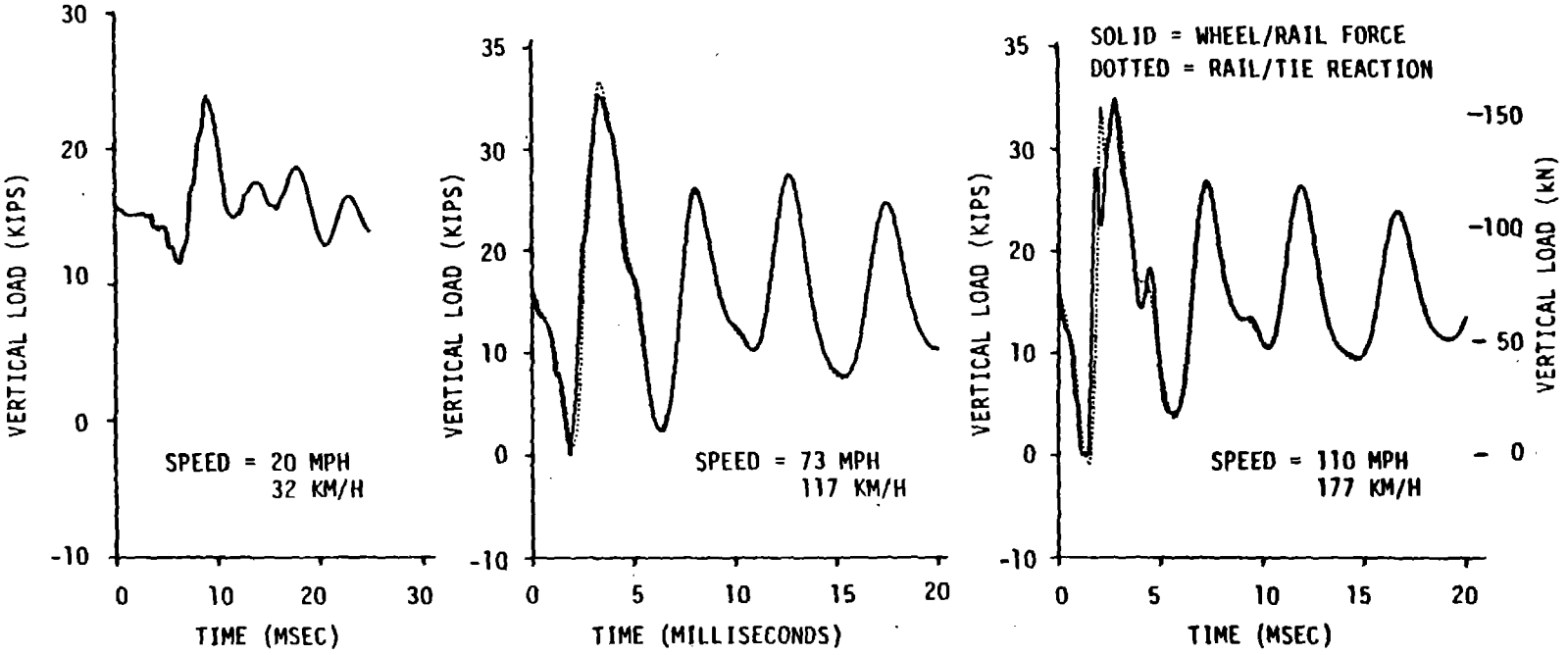

FIGURE 5-7. PREDICTED LOAD RESPONSE FOR AMCOACH WHEEL OVER EDGEWOOD RAIL SURFACE PROFILE DEFECT

One of the more interesting aspects of the study was the calculation of the energy dissipated by worn wheel profiles. Since a time-integration solution was used in the program, it was a simple matter to calculate the damping forces and relative displacements for each time-step, and to sum these for the vehicle and the track, separately, over the total solution time. This typically ran 20 milliseconds, or 20 to 30 in. (0.5 to 0.75 m) of the wheel circumference. Typical values are given in Table 5-1 for three of the four wheel profiles of Figure 5-2. Just the larger of the two measured divots on Axle #19 is considered in this table. For a wheel rough around its whole circumference (such as Axle #20, and probably Axle #19), the energy consumed by wheel roughness can easily exceed 20 hp (15 kW) per wheel. In terms of the Davis equation for calculating drawbar resistance, Axle 19 would apply roughly 150 lb (667 N) of drag at 74 mph (119 km/h), or 2 lb/ton (8 N/tonne) per wheelset. This assumes that the second divot dissipates about two-thirds the energy that the larger divot dissipates, and that both wheel profiles are the same. It is of interest to note that only about 10 percent of the energy is dissipated in the vehicle suspension, the rest in the track structure.

5.2 MODEL PREDICTIONS

With confidence gained in the model by comparing measured and predicted response to measured wheel and rail profiles, the model can then be used to predict loads for other wheel and rail conditions. As an example, wheel vertical loads were predicted for one of the measured engine burns with a depth of 0.090 in. (2.29 mm) over roughly a 60 in. (1.52 m) wavelength, shown in Figure 5-5. Rail clip fallout and loosening inserts were noted at the tie nearest the engine burn. Predicted vertical load response under a passenger car wheel at 120 mph (193 km/h), the current track speed, is shown in Figure 5-8. A peak load of 66 kips (194 kN) with an impact factor of 4.1 is predicted.

Little is known at this time about the actual shape of wheel profiles on freight cars. The traditional slid-flat or battered slid-flat profile error has been used in past studies, both experimental and analytical. It is to this type of defect that the Association of American Railroads inspection and condemning limits are addressed. The longer-wavelength runout type defect has been measured for as-manufactured freight car wheels[33], but there has yet been no study of worn freight car profiles addressing the longer wavelengths now known to exist on passenger car wheels.

TABLE 5-1. ENERGY DISSIPATED BY TYPICAL ROUGH WHEEL PROFILES

	Speed		Vehicle		Track		Average Power Over Divot		Average Power Over Wheel***	
Axle*	(mph)	(km/h)	(ft-lb)	(Joules)	(ft-lb)	(Joules)	(hp)	(kw)	(hp)	(kw)
7	65	105	25	34	214	290	22	16	4.4	3.3
9	71	114	33	45	270	366	28	21	6.1	4.6
19**	74	119	38	52	356	483	36	27	8.3	6.2

*See Figure 5-2.
**Larger profile error only.
***Remainder of wheel circumference assumed smooth.

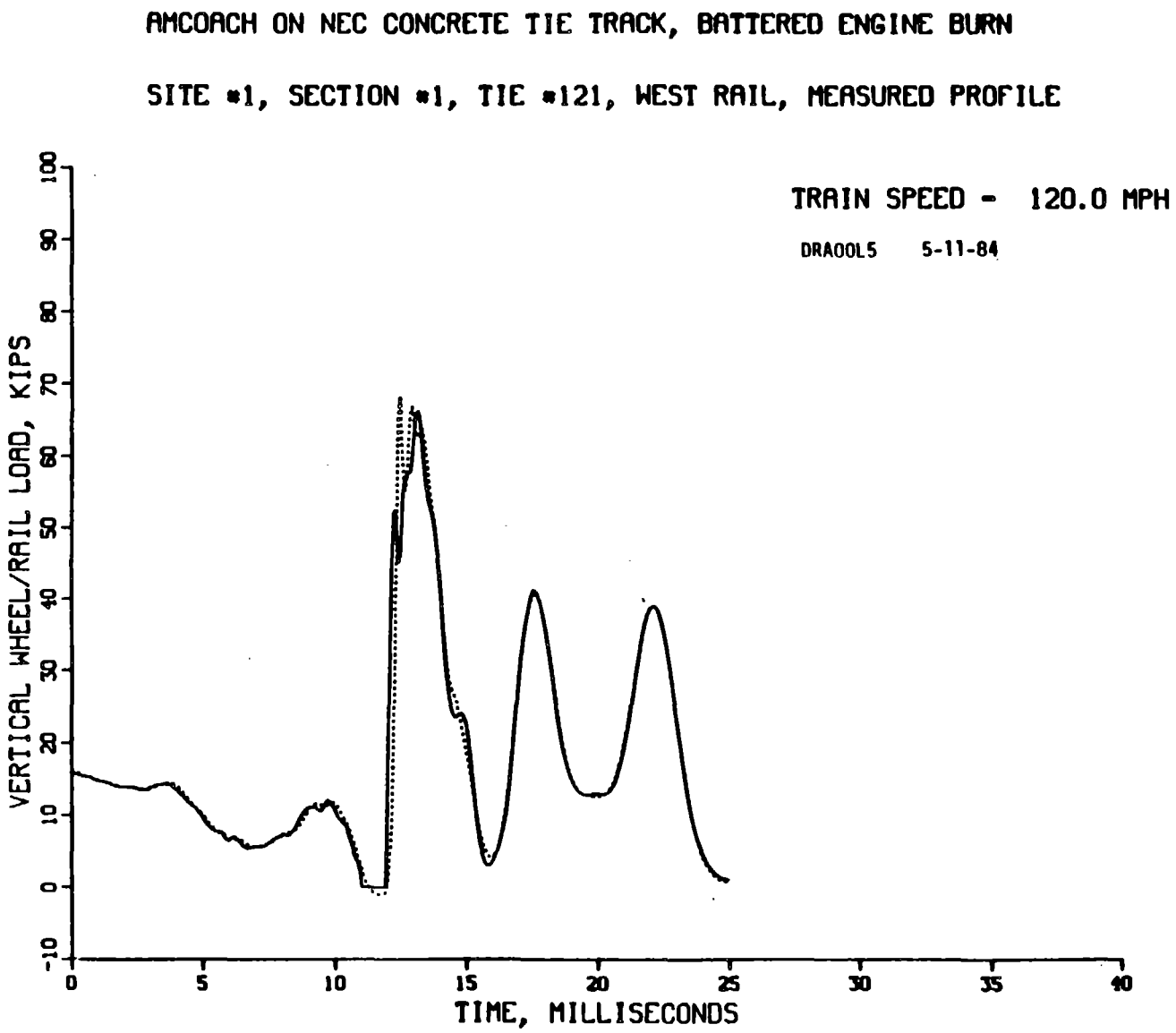

FIGURE 5-8. PREDICTED DYNAMIC VERTICAL WHEEL LOAD AT BATTERED ENGINE BURN UNDER HIGH-SPEED PASSENGER CAR

Load exceedances detected by the Edgewood impact detector have shown that about 100 freight car wheelsets per week passing the detector site generate loads in excess of 75 kips (334 kN), with several of these loads per week reaching the 102-kip (454 kN) digital saturation limit of the detector. Laboratory tests have shown that wheel impact loads in the 75-85 kip (334-378 kN) range will initiate concrete tie rail seat cracks with the current tie design and stiff EVA tie pads.

6. SUMMARY AND CONCLUSIONS

Both the rail and the tie are, in reality, complex distributed structures and can be modeled only crudely as lumped masses. A dynamic finite-element model can be used to model the track structure in greater detail. However, the cost of development of a detailed, dynamic finite-element model and the computation costs for exercising such a model can be formidable. While the computer model, Program IMPACT, provides a good simulation of the moving vertical load along the rail running surface, it does not provide an understanding of the detailed rail stress response under this load. As stated earlier, British Rail currently employs an analytical model of the wheel/rail system represented as a Timoshenko beam on discrete elastic supports[12], with the rail normal modes of vibration handled as a Fourier series. Good correspondence between measured and calculated rail strains are cited in Reference (12).

As shown in this review, the larger-amplitude, lower frequency flat wheel impact loads are transmitted vertically with little attenuation through the rail to the ties. The higher-frequency impact loads are of lower amplitude and (even though attenuated in the rail) are of less concern. Therefore, it is recommended that static analysis be employed to investigate stresses in the rail, with the peak dynamic load from Program IMPACT applied at the rail running surface, and the appropriate reaction forces applied at the rail/tie interfaces. Higher frequency dynamic effects between reaction points can then be neglected without seriously compromising the accuracy of results.

REFERENCES

(1) American Railway Engineering Association Committee on Rail, "Test of Rail Joint Impact Effects on the Chicago and North Western," Proc. American Railway Engineering Association, Vol. 57, 1956, pp. 865-883.

(2) Gilchrist, A. O., "Results of a Survey of Rail Joint Irregularity Using Motion," British Rail Research Dept., Report DYN/15, 1965.

(3) Prause, R. H., and H. D. Harrison, "Data Analysis and Instrumentation Requirements for Evaluating Rail Joints and Rail Fasteners on Urban Tracks," DOT Report UMTA-NA-06-0025-78-8, 1975.

(4) Jenkins, H. H., et al., "The Effect of Track and Vehicle Parameters on Wheel/Rail Vertical Dynamic Forces," Railway Engineering Journal, 3, No. 1 (Jan. 1974), pp. 2-26.

(5) Radford, R. W., "Wheel/Rail Vertical Forces in High-Speed Railway Operation," ASME Journal of Eng. for Ind., Trans. ASME, Nov. 1977, pp. 849-858.

(6) Ahlbeck, D. R., et al., "Evaluation of Analytical and Experimental Methodologies for the Characterization of Wheel/Rail Loads," Report No. FRA/OR&D-76-276, NTIS PB272 063 Nov. 1976.

(7) Hadden, J. A., et al., "Influence of Unsprung Mass on Rail Vehicle/Track Performance," Review Paper, DOT/FRA Improved Passenger Equipment Evaluation Program (IPEEP), Jan. 29, 1980.

(8) Joint Committee on Relation Between Track and Equipment, "Effect of Flat Wheels on Track and Equipment," AAR Report No. MR-113, May 1951.

(9) Satoh, Y., "Dynamic Effect of a Flat Wheel on Track Deformation," Bulletin of the Permanent Way Society of Japan, 12, No. 7 (July 1964), pp. 14-22.

(10) Frederick, C. O., D. P. Cannon, and S. G. Newton, "Dynamic Rail Stresses Due to Wheel Flat Impact," AIT Symposium on Railway Dynamics, Madrid, 1977.

(11) Lyon, D., "The Calculation of Track Forces Due to Dipped Rail Joints, Wheel Flats and Rail Welds," British Rail Research Dept., Tech. Note TS.2, Feb. 1972.

(12) Newton, S. G., and R. A. Clark, "An Investigation into the Dynamic Effects on the Track of Wheel Flats on Railway Vehicles," Journal Mechanical Engineering Science, IMechE 1979, 21, No. 4, 1979.

(13) Ahlbeck, D. R., et al., "Measurements of Wheel/Rail Loads on Class 5 Track," Report No. FRA/ORD-80/19, NTIS PB80-196868, Feb. 1980.

(14) Lipson, C., and J. S. Narendra, Statistical Design and Analysis of Engineering Experiments (New York, McGraw-Hill), 1972.

(15) Ahlbeck, D. R., F. E. Dean, and R. H. Prause, "A Methodology for Characterization of the Wheel/Rail Load Environment -- A Pilot Application," Battelle-Columbus Laboratories, January 1984.

(16) Ahlbeck, D. R., "Predicting the Load Environment on Railroad Track," ASME Paper No. 80-RT-7, April 1980.

(17) Ver, I. L., and C. I. Holmer, "Interaction of Sound Waves with Solid Structures," In: Noise and Vibration Control, ed. L. L. Beranek (New York, McGraw-Hill, 1971), Chapter 2, pp. 270-357.

(18) Ibid., p 272.

(19) Meirovitch, L. E., Analytical Methods in Vibrations (New York: MacMillan Co., 1967), pp. 352-360.

(20) Sato, Y., and S. Kosuge, "Evaluation of Rail Head Surface Configuration Viewed from Wheel Load Variation," Quarterly Reports (RTRI), Vol. 24, No. 2, 1983, pp. 68-71.

(21) Newton, S. G. and Clark, R. A., "An Investigation into the Dynamic Effects on the Track of Wheelflats on Railway Vehicles," Journal Mechanical Engineering Science, IMechE, Vol. 21, No. 4, 1979, pp. 287-297.

(22) Mair, R. I., "Aspects of Railroad Track Dynamics (Part I: Vertical Response)," BHP Melbourne Research Labs, Report MRL 81/3 (BHPMNM/RDC/74/017), Feb. 1974.

(23) Mair, R. I., "Natural Frequency of Rail Track and Its Relationship to Rail Corrugation," Civil Engineering Transactions 1977, Inst. of Engineers, Australia, pp. 6-11.

(24) Ahlbeck, D. R., "An Investigation of Impact Loads Due to Wheel Flats and Rail Joints," ASME Paper 80-WA/RT-1, 1980.

(25) Dean, F. E., et al., "Effect of Tie Pad Stiffness on the Impact Loading of Concrete Ties," Proc., Second International Heavy Haul Railway Conference, Sept. 1982, Paper 82-HH-41, pp. 442-458.

(26) Third Quarterly Progress Report, "Development of Safety Criteria for Evaluating Concrete Tie Track in the Northeast Corridor," Battelle's Columbus Laboratories to DOT/FRA, Contract DTFR53-83-C-00009, March 2, 1984.

(27) Thomson, W. T., Vibration Theory and Application, Prentice-Hall, 1963, pp. 305-311.

(28) Springfield, J. F., "Optimization of Parameters of a Vibrating Beam Mounted on Damped, Flexible End Supports", MS Thesis, U. of Virginia, Jan. 1961.

(29) Sewall, J. L., Parrish, R. V., and Darling, B. J., "Dynamic Responses of Railroad Car, Models to Vertical and Lateral Rail Inputs," NASA TN D-6375, Nov. 1971.

(30) Ver, I. L., C. S. Ventres, and M. M. Myles, "Wheel/Rail Noise - Part III: Impact Noise Generation by Wheel and Rail Discontinuities," Journal of Sound and Vibration, 46, No. 3, pp. 395-417.

(31) Third Quarterly Progress Report, "Development of Safety Criteria for Evaluating Concrete Tie Track in the Northeast Corridor," Battelle Columbus Laboratories to DOT/FRA, Contract DTFR53-83-C-00009, March 2, 1984.

(32) Ahlbeck, D. R., and H. D. Harrison, "Techniques for Measurement of Wheel-Rail Forces," The Shock and Vibration Digest, 12, No. 10 (October 1980), pp. 31-41.

90 copies